On the Performance Analysis of Digital Communication Systems Perturbed by Non-Gaussian Noise and Interference

Dissertation By

Hamza Soury

In Partial Fulfillment of the Requirements

For the Degree of

Doctor of Philosophy

King Abdullah University of Science and Technology, Thuwal

Kingdom of Saudi Arabia

The dissertation of Hamza Soury is approved by the examination committee

Committee Chairperson: Professor Mohamed-Slim Alouini

External Committee Member: Professor Abdelhak M. Zoubir

Committee Member: Professor Tareq Al-Naffouri

Committee Member: Professor Taous-Meriem Laleg-Kirati

to my parents, my wife, and my family

ABSTRACT

On the Performance Analysis of Digital Communication Systems Perturbed by Non-Gaussian Noise and Interference

Hamza Soury

The Gaussian distribution is typically used to model the additive noise affecting communication systems. However, in many cases the noise cannot be modeled by a Gaussian distribution. In this thesis, we investigate the performance of different communication systems perturbed by non-Gaussian noise. Three families of noise are considered in this work, namely the generalized Gaussian noise, the Laplace noise/interference, and the impulsive noise that is modeled by an α-stable distribution. More specifically, in the first part of this thesis, the impact of an additive generalized Gaussian noise is studied by computing the average symbol error rate (SER) of one dimensional and two dimensional constellations in fading environment. We begin by the simple case of two symbols, i.e. binary phase shift keying (BPSK) constellation. From the results of this constellation, we extended the work to the average SER of an M pulse amplitude modulation (PAM). The first $2-D$ constellation is the M quadrature amplitude modulation (QAM) (studied for two geometric shapes, namely square and rectangular), which is the combination of two orthogonal PAM signals (in-phase and quadrature phase PAM). In the second part, the system performance of a circular constellation, namely M phase shift keying (MPSK) is studied in conjunction with a Laplace noise with independent

noise components. A closed form and an asymptotic expansion of the SER are derived for two detectors, maximum likelihood and minimum distance detectors. Next, we look at the intra cell interference of a full duplex cellular network which is shown to follow a Laplacian distribution with dependent, but uncorrelated, complex components. The densities of that interference are expressed in a closed form in order to obtain the SER of several communication systems (BPSK, PAM, QAM, and MPSK). Finally, we study the statistics of the α-stable distribution. Those statistics are expressed in closed form in terms of the Fox H function and used to get the SER of BPSK, PAM, and QAM constellations. An approximation and an asymptotic expansion for high signal to noise ratio are presented also and their efficiency is proved using Monte Carlo simulations. It is worth mentioning that all the error rates presented in this work are averaged over a generalized flat fading, namely the extended generalized $\mathcal{K}$, which has the ability to capture most of the known fading distribution. Many special cases are treated and simpler closed form expressions of the probability of error are derived and compared to some previous reported results.

ACKNOWLEDGMENTS

I would like to express my sincere appreciation and gratitude to my supervisor, Prof. Mohamed-Slim Alouini for his support, continuous guidance, and encouragement throughout the course of this work. He has been a great source of knowledge and has inspired me with precious ideas. His enthusiasm and valuable feedback for research made my study enjoyable, exciting, and ultimately fruitful with rich experience. I am very grateful to Prof. Karim Abed-Meriam (Polytech'Orleans, France), Prof. Faouzi Bader (CentraleSuplec, Campus of Rennes, France), Dr. Ferkan Yilmaz (Vodafone, Turkey), and Dr. Hesham ElSawy (KAUST) for their enormous technical support. It was a true honor to work and share ideas with them. I would like also to thank our research group members at KAUST for providing support and resources for this thesis. Additionally, I would like to thank my friends at KAUST; we made great moments together.

Finally, I am very thankful to my parents and my wife for their continuous encouragement and for bearing with me for my negligence towards them during this journey and their deep moral support at all times. To them, I dedicate this work.

TABLE OF CONTENTS

LIST OF ABBREVIATIONS

Symbol	**Meaning**
GN	Gaussian Noise
MSE	Mean Square Error
RV	Random Variable
CLT	Central Limit Theorem
GGD	Generalized Gaussian Distribution
LN	Laplace Noise
MAI	Multiple Access Interference
TH	Time Hopping
UWB	Ultra-Wide Bandwidth
PDF	Probability Density Function
FSO	Free-Space Optics
CDF	Cumulative Distribution Function
GG	Generalized Gaussian
GGN	Generalized Gaussian Noise
GGRV	Generalized Gaussian Random Variable
BER	Bit Error Rate
BPSK	Binary Phase Shift Keying
AWGN	Additive White Gaussian Noise
SER	Symbol Error Rate
ASER, $\overline{SER}$	Average Symbol Error Rate
EGK	Extended Generalized-$\mathcal{K}$
SNR	Signal-to-Noise Ratio
MUI	Multi User Interference
MCA	Middleton Class A
MPSK	M-ary Phase Shift Keying
PAM	Pulse Amplitude Modelation
QAM	Quadrature Amplitude Modulation

Symbol	**Meaning**
AWGGN	Additive White Generalized Gaussian
CCDF	Complementary Cumulative Density Function
FHF	Fox H Function
MGF	Meijer's G Function
dB	Decibel
SISO	Single Input Single Output
ML	Maximum Likelihood
ABER	Average Bit Error Rate
BFHF	Bivariate Fox H Funcation
GNM	Generalized Nakagami-m
GK	Generalized-K
BMGF	Bivariate Meijer G Function
AWLN	Additive White Laplace noise
MD	Minimum Distance
MAP	Maximum a Posteriori
QPSK	4-PSK
3NT	3-Node Topology
FD	Full Duplex
UE	Users Equipment
HD	Half Duplex
SI	Self Interference
BS	Base Stations
BW	Bandwidth
NLOS	Non-Line Of Sight
CHF	Characteristic Function
SIR	Signal-to-Interference Ratio
MIMO	Multiple Input Multiple Output
INR	Interference-to-Noise-power-Ratio
SINR	Signal to Interference plus Noise Ratio
SGG	Sum of independent GGRV
MOGF	Moment Generation Function
CGF	Cumulant Generation Function
PE	Probability of Error

LIST OF SYMBOLS

Symbol	**Meaning**
α	Noise parameter
N_0	Power spectral density
σ^2	Variance
$\mathcal{N}$	Noise
μ	Mean of RV
Λ,Λ_0	Normalization coefficients
$\mathbb{E}[\cdot]$	Expected value, mean
$\Gamma(\cdot)$	Gamma function
$Q_\alpha(\cdot)$	Complementary CDF of generalized Gaussian noise
$\Gamma(\cdot,\cdot)$	Upper incomplete Gamma function
$\mathcal{H}$	Fading envelope
$m,\ m_s$	Fading and shadowing figure
$\xi,\ \xi_s$	Fading and shadowing shaping factor
β	$\Gamma(m+1/\xi)/\Gamma(m)$
β_s	$\Gamma(m_s+1/\xi_s)/\Gamma(m_s)$
Ω	$\mathbb{E}[\mathcal{H}]$
$\Gamma(\cdot,\cdot,\cdot,\cdot)$	Extended incomplete Gamma function
γ	SNR
$E_{\mathcal{S}}$	Average energy per symbol
$\mathcal{S}$	Transmitted signal
$\mathcal{R}$	Received signal
$\overline{\gamma}$	Average SNR
$p_X(x),\ f_X(x)$	PDF of random variable X
$f_{XY}(x,y)$	Joint PDF of random variables (X,Y)

Symbol	**Meaning**
$\mathrm{H}_{\cdot,\cdot}^{\cdot,\cdot}[\ \cdot\ ]$	Fox H function
$\mathrm{G}_{\cdot,\cdot}^{\cdot,\cdot}[\ \cdot\ ]$	Meijer's G Function
$\Pr(A)$	Probability of event A
e	Error event
$\Pr(e\|\gamma)$	Conditional probability of error over γ
$P_{PAM}(e),\ P_{QAM}(e),\ P_{PSK}(e)$	Probability of error of PAM, QAM, and PSK
M	Constellation size
d	Decision distance
$\mathcal{I}(x)$	$\int_0^\infty Q_\alpha(xh)p_{\mathcal{H}}(h)dh$
$M_I,\ M_Q$	In phase and quadrature phase symbols size
$d_I,\ d_Q$	In phase and quadrature phase decision distances
A_I	$\frac{d_I}{2\sigma}$
A_Q	$\frac{d_Q}{2\sigma}$
τ	$\frac{d_I}{d_Q}$, in phase to quadrature phase ratio
$\mathcal{J}$	$\int_0^\infty Q_\alpha(A_Ih)Q_\alpha(A_Qh)p_{\mathcal{H}}(h)dh$
$\mathrm{H}_{\cdot,\cdot,\cdot,\cdot,\cdot,\cdot}^{\cdot,\cdot,\cdot,\cdot,\cdot,\cdot}[\ \cdot\ ,\ \cdot\ ]$	Bivariate Fox H function
$\mathrm{G}_{\cdot,\cdot,\cdot,\cdot,\cdot,\cdot}^{\cdot,\cdot,\cdot,\cdot,\cdot,\cdot}[\ \cdot\ ,\ \cdot\ ]$	Bivariate Meijer's G function
$\tan(\cdot)$	Tangent function
$\tan^{-1}(\cdot),\ \arctan(\cdot)$	Inverse tangent function
$\mathcal{L}(\mu,\sigma)$	Laplace distribution with mean μ and variance σ^2
I, Q	In phase and quadrature phase components
$n_I,\ n_Q$	In phase and quadrature phase noise components
$s_I,\ s_Q$	In phase and quadrature phase signal components
I_2	Identity matrix of order 2
θ	$\frac{\pi}{M}$, rotation angle
ϕ, ϕ_k	$\frac{2k\pi}{M}$, phase angle
$\|\|\cdot\|\|_1$	L_1 norm
c_x	$\cos(x)$
s_x	$\sin(x)$
(X, Y)	Rotation axis
P_c	Probability of correct detection
δ	$\sin\theta$
$\det(A)$	Determinant of matrix A
$g(k,\gamma),\ F(k),\ G(k)$	Generic functions
$\mathcal{L}(x)$	$\int_0^\infty p_\gamma(\gamma)e^{-x\sqrt{\gamma}}d\gamma$

Symbol	Meaning
$\mathcal{L}_1(x)$	$\int_0^\infty \sqrt{\gamma} p_\gamma(\gamma) e^{-x\sqrt{\gamma}} d\gamma$
$\mathcal{L}'(x)$	Derivative of $\mathcal{L}(x)$
$U(\cdot,\cdot,\cdot)$	Tricomi confluent hypergeometric function
$\mathcal{R}(x)$, x_r	Real part of x
$\mathcal{I}(x)$, x_i	Imaginary part of x
$\rho(x)$	$1-\frac{1}{x}$
P_d	Downlink transmit power
$\mathcal{A}_d$	Downlink large scale power attenuation
P_u	Interfering transmit power
$\mathcal{A}_u$	Interference large scale power attenuation
j	$j^2=-1$, complex number
Z	Intra cell interference
$\varphi_X(\cdot)$	Characteristic function of X
$F_X(\cdot)$	CDF of X
$\bar{F}_X(\cdot)$	CCDF of X
$K_0(\cdot)$	0-th order of the modified Bessel function of second kind
$K_1(\cdot)$	1-st order of the modified Bessel function of second kind
ℓ_k	Maximum likelihood criteria
R	$\sqrt{I^2+Q^2}$
ψ	$\arctan(Q/I)$
$Q(\cdot,\cdot,\cdot)$	Two dimensional Gaussian Q function
$\overline{SER}$	Average SER
$\mathcal{T}$	Throughput
B	Bandwidth
$S\alpha S$	Symmetric α-stable
$sign(x)$	Signum of x
$\psi_\alpha(\cdot)$	CCDF of $S\alpha S$
$\Psi_\alpha(\cdot)$	$\int_0^\infty \psi_\alpha(\gamma) p_\gamma(\gamma) d\gamma$
$\Delta(k,b)$	$\frac{b}{k}, \frac{b+1}{k}, \cdots, \frac{b+k-1}{k}$
$p\Psi q(\cdot)$	Fox-Wright generalized hypergeometric function
$M_\alpha(t)$	Moment generation function of $S\alpha S$
$m_n(X)$	n-th moment of RV X
$K_X(t),\ K_\alpha$	Cumulative generation function of $S\alpha S$
$k_n(X)$	n-th cumulant of RV X
$Kurt(X)$	Kurtosis of RV X

LIST OF FIGURES

LIST OF TABLES

Chapter 1

Introduction

1.1 Motivation

The performance of digital communication systems has been extensively studied in the presence of a Gaussian noise and flat fading [1, 2, 3, 4, 5]. Actually the additive Gaussian noise (GN) model is widely used in the performance analysis of most of the communication systems because its quadratic form makes the minimization of the mean square error (MSE) as the best criteria to find filters and estimate system parameters. In digital communication, the quadratic form of Gaussian distribution reduces the maximum likelihood detector to the minimum distance detector using the euclidian distance which is commonly used. Furthermore, it is known that the Gaussian distribution is the limit of the arithmetic mean of independent random variable (RV) according to the central limit theorem (CLT) which makes the Gaussian noise a suitable choice in the presence of many additive perturbations in the channel. However, this theorem is valid only within particular conditions that are not always satisfied and the sum of RVs may not be very large to reach the normal distribution. The limitation of the CLT and the real characteristics of the noises has pushed researchers to deal with another type of noise, namely non-Gaussian noise [6]. Many families of non-Gaussian noise are available in the literature. Three families of them are considered in this thesis, namely the

generalized Gaussian [7, 8, 9], Laplacian distribution [10, 11], and the so called α stable family [12, 13, 14, 15].

In several communication systems, it has been suggested that the noise follows a generalized Gaussian distribution (GGD)[7, 8, 9]. For instance, in [7], the GGD was used to model the noise for an underwater communication channel. In addition, in [8] and [9] the GGD was used to model the additive noise for sensor network and local spectrum sensing applications. On the other hand, it has been widely reported that the GGD can model different type of noise. For instance, the Gaussian, uniform, and Laplace distributions, which are special cases of the GGD [8, 9].

The second non-Gaussian perturbation, viz Laplace, has pinched research interest for a long time for its properties. It is widely used and is indeed quite popular in signal processing, signal detection, and communication studies to model impulsive noise/interference. Many communication systems, in which the Laplace noise (LN) is applicable, can be found in the literature. Indeed, studies of multiple access interference (MAI) in time hopping (TH) ultra-wide bandwidth (UWB), with Laplacian perturbation, were conducted in [16, 17, 18, 19, 20, 21, 22, 23, 24]. In [18], an accurate evaluation of the multiple access performance in TH-PPM and TH-UWB systems was conducted. Actually, the probability density function (PDF) of the sum of the interference and the Gaussian noise in the discrete time model was established. The results of [20] show that this PDF can not be a Gaussian distribution (see [18, Fig.2 and Fig.3]). An approximation of that PDF was made in [16, 17], where Beaulieu *et al.* proved that the cumulative MAI in the discrete time model can be modeled as a Laplacian distribution for TH-UWB systems. In fact in [16, Fig.2], the authors have shown that the PDF of the multiple interference, coming form the multi-user, can be approximated by the Laplacian PDF. More specifically, the tail of the simulated PDF is near the Laplacian PDF tail. Moreover, in [17], the authors proved that the MAI in discrete time model can be modeled as

an additive noise which can not be a Gaussian distribution. Actually they tried three types of distributions, one of them is the Laplacian distribution, which was shown to offer a better fit than the Gaussian approximation for the MAI as described in [17, Fig.1]. On the other hand, in the UWB wireless systems, the multi-user interference can be modeled also by the Laplace distribution [10, 11]. In addition, the LN is studied in the free-space optics (FSO) communication context as a non Gaussian additive noise [25]. Besides its use as an additive noise, the Laplace distribution can also model the interference in full-duplex networks operating over Rayleigh fading channels.

Another motivation to deal with non Gaussian perturbation is the impulsive character of such noise/interference. More specifically, in real life applications, severe impairments and perturbations may have an impulsive nature [26, 15]. These perturbations can deteriorate the performance of many communication systems. The impulsive noise can be modeled by many distributions such as α-stable [27, 28, 29, 15, 30]. In fact, in [30], the α-stable distribution has been firstly studied by Feller after it was defined the first time by Lévy [31]. Since then the α-stable, considered as the generalization of stable distribution, has motivated researchers to analyze its behavior in communication systems because of its properties and ability to model different kind of perturbations. Indeed, Cardieri presented a nice survey in [29] about the interference models used in wireless ad hoc networks and the used models to describe the interference, one of this model is the α-stable distribution. Also in [13], the authors have modeled the noise (which also can be considered as additive interference/perturbation) by an α-stable model. Therewith, some other works were proposed in the literature to solve the problem of filtering in impulsive noise environment that can be modeled by α-stable distribution [32, 33, 34, 35, 36, 37]. In fact these works proposed a full rank adaptive filters which are built by optimizing an objective function that contains a combination of

L_1 and L_2 norms.

Though its widely use in wireless communication, the PDF and the cumulative distribution function (CDF), of the α-stable distribution, have a closed-form only for three special cases, say, Gaussian ($\alpha = 2$), Cauchy ($\alpha = 1$), and Pearson ($\alpha = \frac{1}{2}$) [38], which motivates the investigation of the statistics of the α-stable distribution. Subsequently, the performance analysis of communication systems subject to an α stable perturbation (noise, interference,...) can be also studied using the obtained results.

1.2 Related Work

As mentioned above, the generalized Gaussian (GG) noise is used in sensor networks, sensing applications, and UWB communication systems. In addition, due to its generic character, it is used to model several types of noise. One of these noises could be the impulsive noise, uniform or Laplace which has many applications in digital communication and signal processing. For instance, in [21] the multi user interference in UWB was modeled as GG noise (GGN). In addition, Fiorina introduced in [21] a method to estimate the distribution parameter α using an estimation of the kurtosis of the GGD that depends only on the second and fourth moments. Moreover, a recent work studied the properties of the sum of two independent GG random variables (GGRV) [39]. Indeed, Zhao *et al.* studied in [39] the properties of the PDF of the sum of two GGRVs. They proved that such PDF has the same properties of the PDF of GGD (symmetry, convexity, monotonicity...) but they did not compute the PDF of the sum. On the other hand, they gave an approximation of the PDF of the sum of two identically independent distributed (i.i.d.) GGDs.

Beside the GGD, the Laplace distribution, which appears as a special case of the

GGD, is also well studied in the literature. For example in the UWB wireless systems, the multi-user interference can be modeled by the Laplacian distribution [17, 18, 21, 22, 23, 10, 11, 24]. Furthermore, the LN was studied by Kamboj *et al.* [25] in an FSO communication context as a non Gaussian additive noise. In another area of research, Beaulieu *et al.* designed an optimal detector for LN [40, 41], and studied some properties of the LN by computing the bit error rate of binary data [42]. Finally, work in [43] dealt with detection problems in LN environment, while in [44] the authors were focusing on the discrete-time detection of a time-varying LN. More specifically, most of those previous works were dealing with the bit error rate (BER) of binary phase shift keying (BPSK) constellation for different system models. In addition, Beaulieu and Young studied some optimal detectors in LN using different filter structure for UWB systems. In fact, the intention was to find the best optimal filter (either matched filter or other filter) to get the lower bit error rate for a BPSK constellation in this environment. On the other hand, Kamboj *et al.* focused on getting the probability of false alarm in FSO systems in presence of slow Rayleigh fading.

Furthermore, several works studied the performance of systems perturbed by noise/interference modeled by α-stable distribution [12, 13, 14, 15]. Some of these works were focusing on the detection in presence of α-stable distribution. In fact a near optimal detection has been investigated in [15], while a multi user detection using filtering in impulsive noise is described in [12]. In addition, the authors in [14] studied the deductibility matter in a sensor network where the noise is assumed to be impulsive α-stable by approximating its PDF to obtain the detection probability. On the other hand, the α-stable process has been used to model impulsive perturbation to build a particle filter for acoustic source [27], and to study a reduced rank adaptive filter in the same environment [45]. Moreover, the estimation of the stable parameter α, known also as the characteristic parameter, seems interesting to

researchers, which can be confirmed by looking into [28, 46, 47]. Moreover, several works investigated the PDF of the α-stable distribution without obtaining a closed form [29]. In [14] an approximation of the PDF has been used for performance analysis of the used system. In addition, it has been claimed in [48] that optimal processing cannot be done if the perturbation PDF is not analytically expressed. Another area of research is considered in this thesis which is the computation of the probability of error for different $1-D$ and $2-D$ constellations perturbed by non Gaussian noise. Many works dealt with the average symbol error probability of different digital communication systems in the presence of a Gaussian noise [1, 2, 3, 4, 5]. Furthermore, the performance analysis of such systems over generalized fading channels subject to additive white Gaussian noise (AWGN) has been extensively studied [49, 50, 51, 52] to obtain the probability of error of those communication systems. In addition, several expressions including integral forms and approximations of the symbol error rate (SER) were derived in [53].

1.3 Summary of Contributions

In this work, we investigate the performance of different communication systems by computing the average probability of error of different shapes of constellations applied to communication systems perturbed by non Gaussian noise (in particular GGN, LN, and α stable type of noise) over generalized flat fading. In fact, we couple a one dimensional $(1-D)$ and two dimensional $(2-D)$ constellations with the used perturbation distribution to get the average SER (ASER) over generalized flat fading. More specifically, we consider a system with an input signal generated according to a given constellation fed to a channel with an Extended Generalized-K (EGK) fading envelope [54], and subject to non Gaussian noise or/and interference. Hence the goal is to obtain a generic expression for the probability of error of the

system under consideration and then to simplify this expression as much as possible for different values of the fading and noise parameters. Since the deployed noise and fading families are general distribution that can cover several special cases of the well known distribution, only some selected special cases are investigated in this thesis to obtain simpler closed form of the analyzed error rates.

On the other hand, note that in the derivation of the average symbol error probability of a $2-D$ modulation in the standard Gaussian case, the challenge consists of solving an integral involving the product of two traditional Gaussian Q functions [1, 3, 2, 4]. Here, in the presence of other type of noise, the problem is more complicated because we have to derive an integral of the product of two CDFs of the deployed non Gaussian perturbation. Such integral expression appears when we consider the ASER over EGK fading. In the $1-D$ case, the problem is less complex because we need to evaluate an integral involving one CDF. Moreover, the EGK distribution is a versatile fading envelope model that describes signal fluctuations in received signal-to-noise ratio (SNR) due to multi-path, shadowing, or a mixture of such processes in the environment. Indeed, it has five parameters and includes most of the well-known fading distributions in the literature as either special or limit cases as shown in Table A.1. The major contribution of this work is to express the derived ASER in a closed form in terms of a family of special functions defined by the Mellin contour integrals [55]. However, before proceeding to the mathematical analysis, the discrete time model in non Gaussian noise should be defined and investigated.

1.4 Discrete Time Model

In [19, 20] Dhibi *et al.* studied the impulsiveness of the multi user interference (MUI) in UWB systems. In [19], they presented a mathematical proof of the

impulsiveness of the MUI after filtering [19, Eq. 18]. Actually they showed that the PDF of the MUI describes the so-called Middleton Class A (MCA) noise, which is an impulsive noise distribution. In our model, one may replace the MCA distribution by a non Gaussian distribution. Therefore, the works [16, 17, 18, 19, 20, 21] have studied the discrete time model of an UWB system with MUI. They proved that the MAI (or the MUI), in discrete time model, can be modeled as a non Gaussian noise and that the thermal noise component (Gaussian noise) can be neglected. These previous studies were made for UWB systems. Nevertheless, our model is applicable for any system using the same discrete time model and is as such not limited to UWB systems.

It is worth noting that the linear filter is no longer optimal in presence of non Gaussian noise in general, and Laplacian noise in particular as proved in [56], where in [56, Fig.5 and Fig.6] the optimal filter has better performance than the linear filter. Actually, the superiority of the soft limiting receiver, built in [16], over the matched filter is intuitive, as mentioned in [16].

1.5 Outline of Thesis

According to the description given above, the remaining of this thesis is organized as follows. In Chapter 2, the probability of error is computed and expressed in a closed form for communication systems, mapped using BPSK, pulse amplitude modulation (PAM), and quadrature amplitude modulation (QAM) constellations, perturbed by GG noise through an EGK channel. The probability of error of the M-ary phase shift keying (MPSK) constellation cannot be expressed in closed form in the presence of GGN, so its error rates are described through a Laplace noisy channel with independent components in Chapter 3. Continuing with the Laplace perturbation, the intra cell interference in a full duplex network is studied in

Chapter 4 where it is proved to be Laplacian with dependent, uncorrelated components. Furthermore, the probability of error of the user in the full duplex network are investigated through an EGK fading. The last family of noise distribution (α stable) is analyzed in Chapter 5 where the statistics of such distribution are studied and the probability of error of some digital communication systems is studied as an application. Finally, some concluded remarks and further possible extensions are provided in Chapter 6.

Chapter 2

Error Performance Over Generalized Gaussian Noise

One of the most known non-Gaussian noise families is the GGN [7, 8, 9] where its PDF is defined later. In this chapter, the probability of error of several digital communication systems perturbed by GGN is analyzed. For instance, the BER of BPSK and the SER of PAM, square QAM, and rectangular QAM constellations are studied and derived in closed form. Moreover, these error rates are derived in terms of the instantaneous SNR, so an average expressions of them are investigated in the presence of a versatile fading distribution, such as the EGK distribution.

2.1 Noise and Fading Distributions

2.1.1 Generalized Gaussian

In many communications systems the noise is typically considered as an AWGN, but in this part we assume that the noise is an additive white GGN (AWGGN) with zero mean and variance $N_0/2$. More specifically, the PDF of the AWGGN noise is

given in [57, Eq. (6.2)], that is

$$p_{\mathcal{N}}\left(n \,|\, \mu, \sigma, \alpha\right) = \frac{\alpha\,\Lambda}{2\Gamma\left(1/\alpha\right)} \exp\left(-\Lambda^{\alpha}|n-\mu|^{\alpha}\right), \tag{2.1}$$

defined over $n \in \mathbb{R}$, where the parameters $\alpha \in \mathbb{R}^{+}$ and $\mu \in \mathbb{R}$ denote the shaping parameter and the mean, respectively. Moreover, the coefficient Λ, which is considered to normalize the noise PDF, is defined as

$$\Lambda = \frac{\Lambda_0}{\sigma} = \sqrt{\frac{2\Gamma(3/\alpha)}{N_0\Gamma(1/\alpha)}}, \tag{2.2}$$

where $\Lambda_0 = \sqrt{\Gamma(3/\alpha)/\Gamma(1/\alpha)}$ is the normalizing coefficient with respect to the shaping parameter α, and the parameter $\sigma^2 = \mathbb{E}[\mathcal{N}^2] - \mu^2 = N_0/2$ denotes the variance of the AWGGN noise. Furthermore, in (2.1) (i.e., also seen in (2.2)), $\Gamma(\cdot)$ denotes the Gamma function defined in [58, Eq. (6.1.1)]. Note that the distribution of the AWGGN random variable strictly depends on its shaping parameter α. As such, the AWGGN distribution demonstrates a superior fit to the measured noise data over a wide range of physical channel conditions. In other words, most of the common noise types can be shown to be special cases of the GGN. For example, it simplifies to the well-known Gaussian noise for $\alpha = 2$, and Laplacian noise for $\alpha = 1$. In addition, the statistical properties of the AWGGN have been studied in [59] for $\alpha = \frac{1}{2}$ and $\alpha = \frac{1}{3}$, and specific simulation techniques were developed for these values. Table 2.1 illustrates some special cases of the GGN. Furthermore, the PDF of the GGD is plotted in Fig. 2.1 of some values of the shape parameter α. In order to compute the average probability of error in a AWGGN channel and simplify integrals arising in the derivation steps, we present the generalized Q-function $Q_{\alpha}(\cdot)$, namely also the complementary CDG (CCDF) of GGD, which is

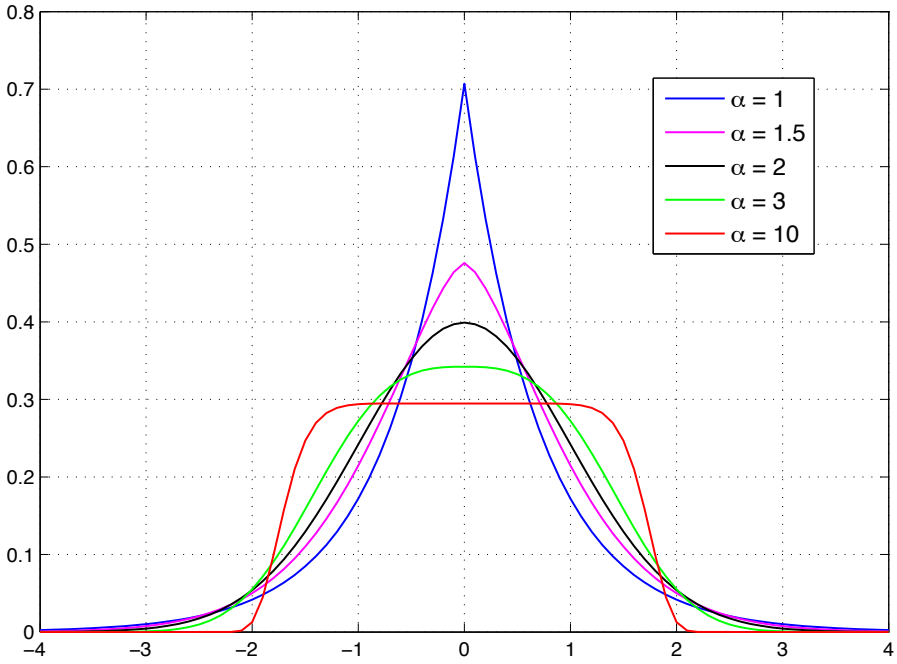

Figure 2.1: Representation of the generalized Gaussian noise for different values of α, with zero mean and unit variance.

Table 2.1: Some Special Cases of Generalized Gaussian Distribution

Noise Distribution	$\boldsymbol{\alpha}$
Impulsive	0
Laplace	1
Gaussian	2
Uniform	∞

given by

$$Q_\alpha(x) = \frac{\alpha\Lambda_0}{2\Gamma(1/\alpha)} \int_x^\infty \exp\left(-\Lambda_0^\alpha |u|^\alpha\right) du, \tag{2.3}$$

defined over $x \geq 0$, where Λ_0 is defined in (2.2). It is useful to note that for $x \leq 0$ we can use the following identity

$$Q_\alpha(x) = 1 - Q_\alpha(-x). \tag{2.4}$$

In addition, by a simple change of variable, the generalized Q-function $Q_\alpha(\cdot)$ can also be written as

$$Q_\alpha(x) = \frac{1}{2\Gamma(1/\alpha)} \int_{\Lambda_0^\alpha x^\alpha}^{\infty} u^{1/\alpha - 1} \exp(-u)\, du, \tag{2.5}$$

$$= \frac{1}{2\Gamma(1/\alpha)} \Gamma(1/\alpha, \Lambda_0^\alpha x^\alpha), \tag{2.6}$$

where $\Gamma(a, x)$ is the upper incomplete gamma function defined in [58, Eq. (6.5.3)].

2.1.2 EGK Distribution

In the present thesis, we assume that the fading envelope, $\mathcal{H}$, follows an EGK distribution which is a versatile fading envelope model that generalizes many of commonly used statistical models that describe signal fluctuations in the received SNR due to multi-path, shadowing, or a mixture of such processes in the environment[54]. It has five parameters and includes most of the well-known fading distribution in the literature as either special or limit cases as shown in Table A.1. With the EGK model, the PDF of the fading envelope $\mathcal{H}$ is given in [54, Eq. (2)], as

$$p_{\mathcal{H}}(h) = \frac{2\xi}{\Gamma(m_s)\Gamma(m)} \left(\frac{\beta_s \beta}{\Omega}\right)^{m\xi} h^{2m\xi - 1} \Gamma\left(m_s - m\frac{\xi}{\xi_s}, 0, \left(\frac{\beta_s \beta}{\Omega}\right)^{m\xi} h^{2\xi}, \frac{\xi}{\xi_s}\right), \tag{2.7}$$

defined over $h \in (0, \infty)$, where the parameters m $(0.5 \leq m < \infty)$ and ξ $(0 \leq \xi < \infty)$ represent the fading figure (diversity severity / order) and the fading shaping factor, respectively, while m_s $(0.5 \leq m_s < \infty)$ and ξ_s $(0 \leq \xi_s < \infty)$ represent the shadowing severity and the shadowing shaping factor (inhomogeneity), respectively. In addition, the parameter $\beta = \Gamma(m + 1/\xi)/\Gamma(m)$ and $\beta_s = \Gamma(m_s + 1/\xi_s)/\Gamma(m_s)$, while $\Omega = \mathbb{E}[\mathcal{H}^2]$ $(0 \leq \Omega < \infty)$. In (2.7), $\Gamma(\cdot, \cdot, \cdot, \cdot)$ is the extended incomplete Gamma

function defined in [57, Eq. (6.2)] as

$$\Gamma(a, x, b, \beta) = \int_x^{\infty} r^{a-1} \exp\left(-r - br^{-\beta}\right) dr, \tag{2.8}$$

where $a, \beta, b \in \mathbb{C}$ and $x \in \mathbb{R}^+$.

$\mathcal{H}$ is not practicable to use in computation of the probability of error, instead of it we are using the SNR γ. In fact, γ denotes the received SNR for the symbols distorted by non-Gaussian noise/interference at the receiver and can be defined as

$$\gamma = \frac{\mathbb{E}[\mathcal{R}]^2}{\mathbb{E}[\mathcal{R}^2] - \mathbb{E}[\mathcal{R}]^2} = \frac{\mathcal{H}^2 E_{\mathcal{S}}}{N_0}, \tag{2.9}$$

where $E_{\mathcal{S}}$ denotes the average power of the transmitted symbols $\mathcal{S}$, $(E_{\mathcal{S}} = \mathbb{E}[\mathcal{S}^2] < \infty)$, $\mathcal{R}$ is the received signal, and N_0 represents the noise variance. Then, starting from (2.7) and using a standard transformation of RV, we can write the PDF of γ as [54, Eq. (3)]

$$p_\gamma(\gamma) = \frac{\xi}{\Gamma(m_s)\Gamma(m)} \left(\frac{\beta_s \beta}{\overline{\gamma}}\right)^{m\xi} \gamma^{m\xi - 1} \Gamma\left(m_s - m\frac{\xi}{\xi_s}, 0, \left(\frac{\beta_s \beta}{\overline{\gamma}}\right)^{m\xi} \gamma^{\xi}, \frac{\xi}{\xi_s}\right), \tag{2.10}$$

where $\overline{\gamma} = \mathbb{E}[\gamma] = \mathbb{E}[\mathcal{H}^2] E_{\mathcal{S}}/N_0$ is the average SNR per symbol.

2.1.3 Alternative Expressions of $Q_\alpha(\cdot)$ and $p_\gamma(\cdot)$

In order to simplify the computation in the next steps, we express the generalized Q function and the PDF of EGK distribution alternatively in terms of the Fox H function (FHF), $\mathrm{H}_{p,q}^{m,n}[\ \cdot\ ]$, whose definition is given by [55, Eq. (1.1.1)] and [60] as

$$\mathrm{H}_{p,q}^{m,n}\left[z \middle| \begin{matrix}(a_i, \alpha_i)_{1,p} \\ (b_j, \beta_j)_{1,q}\end{matrix}\right] = \frac{1}{2\pi i} \int_{\mathcal{C}} \frac{\prod_{j=1}^{m} \Gamma(b_j + \beta_j s) \prod_{i=1}^{n} \Gamma(1 - a_i - \alpha_i s)}{\prod_{j=n+1}^{p} \Gamma(a_i + \alpha_i s) \prod_{j=m+1}^{q} \Gamma(1 - b_j - \beta_j s)} z^{-s} ds, \tag{2.11}$$

where $\mathcal{C}$ denotes Mellin-Barnes contour. The FHF can be efficiently computed using MATHEMATICA® [61, Appendix].

Actually, an explicit relation between the incomplete Gamma function and the Meijer's G function (MGF) [55, Eq. (2.9.1)] is given in [60, Eq. (8.4.16/2)]. In addition, the MGF appears as a special case of the FHF [55, Eq. (2.9.1)] and it is a built in function in MATHEMATICA®. Thus by using [60, Eq. (8.3.2/21)] in (2.6), we obtain a new expressions of $Q_\alpha(\cdot)$ in terms of the FHF, that is

$$Q_\alpha(x) = \frac{1}{2\Gamma(1/\alpha)} \mathrm{H}_{1,2}^{2,0}\left[\Lambda_0^\alpha |x|^\alpha \,\middle|\, \begin{matrix}(1,1)\\(\frac{1}{\alpha},1),(0,1)\end{matrix}\right]. \tag{2.12}$$

On the other hand, the PDF of the SNR could be expressed in terms of the FHF. Indeed we utilize the identities [57, Eq. (6.22)] and [55, Eqs. (2.1.4), (2.1.5), and (2.1.11)] to express (2.10) in terms of the Fox's H function, as

$$p_\gamma(\gamma) = \frac{1}{\Gamma(m_s)\Gamma(m)\gamma} \mathrm{H}_{0,2}^{2,0}\left[\frac{\beta_s\beta}{\overline{\gamma}}\gamma \,\middle|\, \begin{matrix}\overline{\qquad}\\(m_s,\frac{1}{\xi_s}),(m,\frac{1}{\xi})\end{matrix}\right]. \tag{2.13}$$

Once all the mathematic tools are defined, a general expression for the conditional probability of error is studied in what follows assuming a fixed fading coefficient. Subsequently, as a result of that, we average these expressions over the PDF of the channel fading distribution. A general expression is obtained whose special cases are highlighted in order to check analytical correctness.

2.2 Bit Error Rate of BPSK System

Let us consider a typical BPSK communication system which consists of a transmitter, a channel, and a receiver. The signal transmission in this system is termed a single input single output (SISO) transmission whose well-known

mathematical model is given by[5]

$$\mathcal{R} = \mathcal{H}\,\mathcal{S} + \mathcal{N}, \tag{2.14}$$

where $\mathcal{S} \in \{S_+, S_-\}$ represents the transmitted BPSK symbol, $S_+ = -S_- = \sqrt{E_{\mathcal{S}}}$, and $E_{\mathcal{S}}$ is the energy of the symbol (i.e., energy per bit in this case). Moreover, $\mathcal{R} \in \mathbb{R}$ denotes the received signal in which the transmitted symbol $\mathcal{S}$ is multiplied by the channel fading coefficient $\mathcal{H} \in \mathbb{R}^+$ and added to some additive GG noise $\mathcal{N} \in \mathbb{R}$.

2.2.1 Conditional BER

Referring to the mathematical model given in (2.14), the received signal $\mathcal{R}$ can be modeled for each symbol transmission as a AWGGN random variable with mean $\mu = \mathcal{H}S_\pm$ and variance N_0. Consequently, assuming that the channel fading envelope $\mathcal{H}$ is flat (i.e., slowly changes during symbol transmission), and then utilizing (2.9), the conditional PDFs, $p_{\mathcal{R}}(r|S_\pm, \gamma)$, for two signals can be obtained as

$$p_{\mathcal{R}}(r|S_\pm, \gamma) = \frac{\alpha\Lambda}{2\Gamma(1/\alpha)} \exp\left(-\Lambda^\alpha \left| r - \sqrt{\tfrac{N_0}{E_{\mathcal{S}}}\gamma}\, S_\pm \right|^\alpha\right). \tag{2.15}$$

Since the AWGGN distribution is symmetric around its mean and the transmitted BPSK symbols $S_\pm$ have the same a-priori probability of occurrence (i.e., $\Pr\{S_+\} = \Pr\{S_-\} = 1/2$), the maximum likelihood (ML) detector decides $S_\pm$ if $p_{\mathcal{R}}(r|S_\pm, \gamma) \geq p_{\mathcal{R}}(r|S_\mp, \gamma)$. After some algebraic manipulations, the ML decision rule can be simplified to

$$\text{Decide } \mathrm{S}_\pm \text{ if } \left| \mathcal{R} - \sqrt{\frac{\mathrm{N}_0}{\mathrm{E}_{\mathcal{S}}}\gamma}\, \mathrm{S}_\pm \right| \leq \left| \mathcal{R} - \sqrt{\frac{\mathrm{N}_0}{\mathrm{E}_{\mathcal{S}}}\gamma}\, \mathrm{S}_\mp \right|. \tag{2.16}$$

The resulting conditional error probability $\Pr(e|\gamma)$ in AWGGN channel can be written as $\Pr(e|\gamma) = (1/2)\Pr(\mathcal{R} < 0|S_+) + (1/2)\Pr(\mathcal{R} > 0|S_-)$. Using (2.15), the conditional BER $\Pr(e|\gamma)$ is found to be given by

$$\Pr(e|\gamma) = \frac{\alpha\Lambda}{2\Gamma(1/\alpha)} \int_0^\infty \exp\left(-\Lambda^\alpha \left| r - \sqrt{N_0\gamma}\right|^\alpha\right) dr, \tag{2.17}$$

which can be re-written as

$$\Pr(e|\gamma) = Q_\alpha\left(\sqrt{2\gamma}\right). \tag{2.18}$$

The definition of the generalized Gaussian Q-function will help us in the following subsection computing the average BER (ABER) of BPSK signalling in AWGGN channel subjected to EGK fading.

2.2.2 Average Error Probability

The ABER can be, in general, written as

$$\Pr(e) = \int_0^\infty \Pr(e|\gamma)\, p_\gamma(\gamma)\, d\gamma, \tag{2.19a}$$

$$= \int_0^\infty Q_\alpha\big(\sqrt{2\gamma}\,\big) p_\gamma(\gamma)\, d\gamma, \tag{2.19b}$$

where $p_\gamma(\gamma)$ represents the PDF of the instantaneous SNR γ given in (2.10). Substituting both (2.13) and (2.12) into (2.19b), the ABER over EGK fading channel can be expressed as

$$\Pr(e) = \frac{1}{2\Gamma(1/\alpha)\Gamma(m_s)\Gamma(m)} \int_0^\infty \frac{1}{\gamma}\, \mathrm{H}_{1,2}^{2,0}\left[\left(\sqrt{2\gamma}\,\Lambda_0\right)^\alpha \middle| \begin{matrix}(1, \frac{1}{\alpha}) \\ (\frac{1}{\alpha}, \frac{1}{\alpha}), (0, \frac{1}{\alpha})\end{matrix}\right] \times \mathrm{H}_{0,2}^{2,0}\left[\frac{\beta_s\beta}{\overline{\gamma}}\gamma \middle| \begin{matrix}\overline{\qquad} \\ (m_s, \frac{1}{\xi_s}), (m, \frac{1}{\xi})\end{matrix}\right] d\gamma. \tag{2.20}$$

Using the identity [55, Eq.(2.8.4)] to solve the integral of the product of two FHFs

$$\begin{aligned}&\int_0^\infty t^{\eta-1}\mathrm{H}_{p,q}^{m,n}\left[zt^\sigma\left|\begin{matrix}(a_i,\alpha_i)_{1,p}\\(b_j,\beta_j)_{1,q}\end{matrix}\right.\right]\mathrm{H}_{P,Q}^{M,N}\left[wt\left|\begin{matrix}(c_i,\gamma_i)_{1,P}\\(d_j,\delta_j)_{1,Q}\end{matrix}\right.\right]dt\\ &= w^{-\eta}\mathrm{H}_{p+Q,q+P}^{m+N,n+M}\left[zw^{-\sigma}\left|\begin{matrix}(a_i,\alpha_i)_{1,n},(1-d_j-\eta\delta_j,\sigma\delta_j)_{1,Q},(a_i,\alpha_i)_{n+1,p}\\(b_j,\beta_j)_{1,m},(1-c_j-\eta\gamma_j,\sigma\gamma_j)_{1,P},(b_j,\beta_j)_{m+1,q}\end{matrix}\right.\right],\end{aligned}\tag{2.21}$$

and after some algebraic manipulations, (2.20) simplifies to

$$\Pr(e)=\frac{1}{\alpha\Gamma(1/\alpha)\Gamma(m_s)\Gamma(m)}\mathrm{H}_{2,3}^{2,2}\left[\frac{\beta_s\beta}{2\Lambda_0^2\overline{\gamma}}\left|\begin{matrix}(1-\frac{1}{\alpha},\frac{2}{\alpha}),(1,\frac{2}{\alpha})\\(m_s,\frac{1}{\xi_s}),(m,\frac{1}{\xi}),(0,\frac{2}{\alpha})\end{matrix}\right.\right].\tag{2.22}$$

For the purpose of checking this closed-form result, it is necessary, as a preliminary matter, to note that (2.22) is a general expression for the ABER of BPSK signaling over AWGGN channel subjected to an EGK fading distribution. As such, we will discuss, in the following, some special cases of noise and fading yielding more simplified expressions.

2.2.3 Special Cases

2.2.3.1 EGK Fading over Gaussian Noise

For standard additive Gaussian noise, setting $\alpha=2$ in (2.22) and using the fact that $\Gamma(1/2)=\sqrt{\pi}$ and $\Gamma(3/2)=\sqrt{\pi}/2$, we can readily simplify (2.22) to

$$\Pr(e)=\frac{1}{2\sqrt{\pi}\Gamma(m_s)\Gamma(m)}\mathrm{H}_{2,3}^{2,2}\left[\frac{\beta_s\beta}{\overline{\gamma}}\left|\begin{matrix}(\frac{1}{2},1),(1,1)\\(m_s,\frac{1}{\xi_s}),(m,\frac{1}{\xi}),(0,1)\end{matrix}\right.\right],\tag{2.23}$$

which is in agreement with the expression given in [54, Eq.(34)] for $b=\frac{1}{2}$ and $a=1$, as expected.

2.2.3.2 EGK Fading in Additive Laplace Noise Channel

The Laplace noise is obtained for $\alpha = 1$. As such, substituting $\alpha = 1$ in (2.22) results in the ABER in additive Laplace noise channel subjected to the EGK Fading channel, i.e.

$$\Pr(e) = \frac{1}{\Gamma(m_s)\Gamma(m)} \mathrm{H}_{2,3}^{2,2}\left[\frac{\beta_s \beta}{4\overline{\gamma}} \middle| \begin{matrix} (0,2),(1,2) \\ (m_s, \frac{1}{\xi_s}),(m, \frac{1}{\xi}),(0,2) \end{matrix}\right]. \tag{2.24}$$

Using the identity [55, Eq.(2.1.1)], and noticing that the first argument of the FHF is equal to the last argument of the second row of parameters, $(0,2)$, we can re-write (2.24) in a simple form as

$$\Pr(e) = \frac{1}{\Gamma(m_s)\Gamma(m)} \mathrm{H}_{1,2}^{2,1}\left[\frac{\beta_s \beta}{4\overline{\gamma}} \middle| \begin{matrix} (1,2) \\ (m_s, \frac{1}{\xi_s}),(m, \frac{1}{\xi}) \end{matrix}\right]. \tag{2.25}$$

It may be of interest to mention that, in additive Laplace noise channel, we can derive more special cases by setting ξ and ξ_s in the general formula (2.25) to the desired values. For example, for the special case of $\xi = 1$ and $\xi_s = 1$, the fading distribution is reduced to the generalized-K fading. Then, as a result of substituting $\xi = 1$ and $\xi_s = 1$ into (2.25), the average error probability $\Pr(e)$ for the Generalized-K fading yields

$$\Pr(e) = \frac{1}{\Gamma(m_s)\Gamma(m)} \mathrm{H}_{1,2}^{2,1}\left[\frac{m_s\, m}{4\overline{\gamma}} \middle| \begin{matrix} (1,2) \\ (m_s,1),(m,1) \end{matrix}\right]. \tag{2.26}$$

In addition, if we set $\xi_s = 1$ and let $m_s \to \infty$, we have a generalized Nakagami-m fading model. A limit property of the FHF can be shown, using the well-known relation $\lim\limits_{m\to\infty} \frac{m^{-s}\Gamma(m+s)}{\Gamma(m)} = 1$ in the Mellin-Barnes representation of the FHF [55, Eq.(1.1.1) and Eq.(1.1.2)], as

$$\mathrm{H}_{p,q}^{m,n}\left[z \middle| \begin{matrix} (a_i,\alpha_i)_{1,p} \\ (b_j,\beta_j)_{1,q} \end{matrix}\right] = \lim_{m\to\infty} \frac{1}{\Gamma(m)} \mathrm{H}_{p,q+1}^{m+1,n}\left[m\, z \middle| \begin{matrix} (a_i,\alpha_i)_{1,p} \\ (m,1),(b_j,\beta_j)_{1,q} \end{matrix}\right]. \tag{2.27}$$

Replacing the values of ξ_s and m_s in (2.25), and using the result given in (2.27), we can derive a compact closed-form expression for the generalized Nakagami-m fading, that is

$$\Pr(e) = \frac{1}{\Gamma(m)} \mathrm{H}_{1,1}^{1,1}\left[\frac{\beta}{4\overline{\gamma}}\middle|\begin{matrix}(1,2)\\(m,\frac{1}{\xi})\end{matrix}\right]. \tag{2.28}$$

2.2.3.3 Nakagami-m Fading in AWGGN Channel

It helps to remember that the Nakagami-m fading is obtained by substituting the shadowing severity $m_s \to \infty$, shadowing shaping factor $\xi_s \to 1$ and fading shaping factor $\xi \to 1$ into (2.22), and then utilizing the identity given in (2.27).
Consequently, we have a new closed-form result for the ABER in AWGGN channel subject to the Nakagami-m fading given by

$$\Pr(e) = \frac{1}{\alpha\Gamma(1/\alpha)\Gamma(m)} \mathrm{H}_{2,2}^{1,2}\left[\frac{m}{2\Lambda_0^2\overline{\gamma}}\middle|\begin{matrix}(1-\frac{1}{\alpha},\frac{2}{\alpha}),(1,\frac{2}{\alpha})\\(m,1),(0,\frac{2}{\alpha})\end{matrix}\right]. \tag{2.29}$$

2.2.4 Numerical Results

In this section, we study the behavior of BPSK signalling for different values of the noise parameter α.
The numerical results obtained using (2.29) are illustrated in Fig. 2.2 for two values of shape factor m and different values of the GGD parameter α, these numerical results are compared with the simulation results. It is shown that the numerical results and simulations are in perfect agreement. Furthermore, it is worth mentioning that the system has better performance for high value of the fading figure (diversity order) m of the channel fading and high value of shape parameter α of the AWGGN noise. For lower m (i.e. $m = 1$), the fading dominates the error. However, as m increases, the error tends to be mostly due to the additive noise.
As another numerical example, note that the generalized-K fading is obtained by setting the fading shaping factor ξ and the shadowing severity ξ_s to one (i.e.

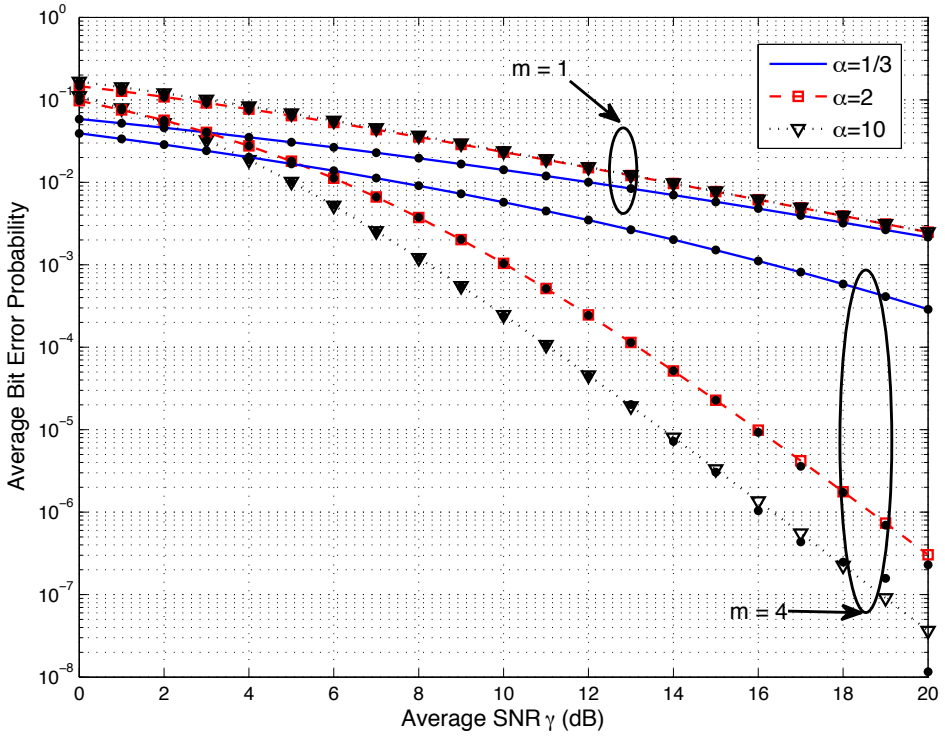

Figure 2.2: ABER of BPSK over Nakagami-m fading (the dot markers denote simulation results while dashed and solid lines represent analytical results).

$\xi = 1, \xi_s = 1$) in (2.22). In this case the ABER can be re-written as

$$\Pr(e) = \frac{1}{\alpha\Gamma(1/\alpha)\Gamma(m_s)\Gamma(m)} \mathrm{H}_{2,3}^{2,2}\left[\frac{m_s m}{2\Lambda_0^2\overline{\gamma}}\middle|\begin{matrix}(1-\frac{1}{\alpha},\frac{2}{\alpha}),(1,\frac{2}{\alpha})\\(m_s,1),(m,1),(0,\frac{2}{\alpha})\end{matrix}\right]. \tag{2.30}$$

For the ABER of generalized-K fading, numerical results, obtained by (2.30), and simulations are drawn in Fig. 2.3 for different values of AWGGN shaping factor α, channel fading figure m, and shadowing fading severity m_s, and are shown to be in perfect agreement.

In this section, we analyzed the average bit error probability of binary coherent signaling when transmitted over a AWGGN channel subjected to extended generalized-K fading. Some numerical results were presented to illustrate the mathematical formalism and to show the impact of the GGD and fading parameters

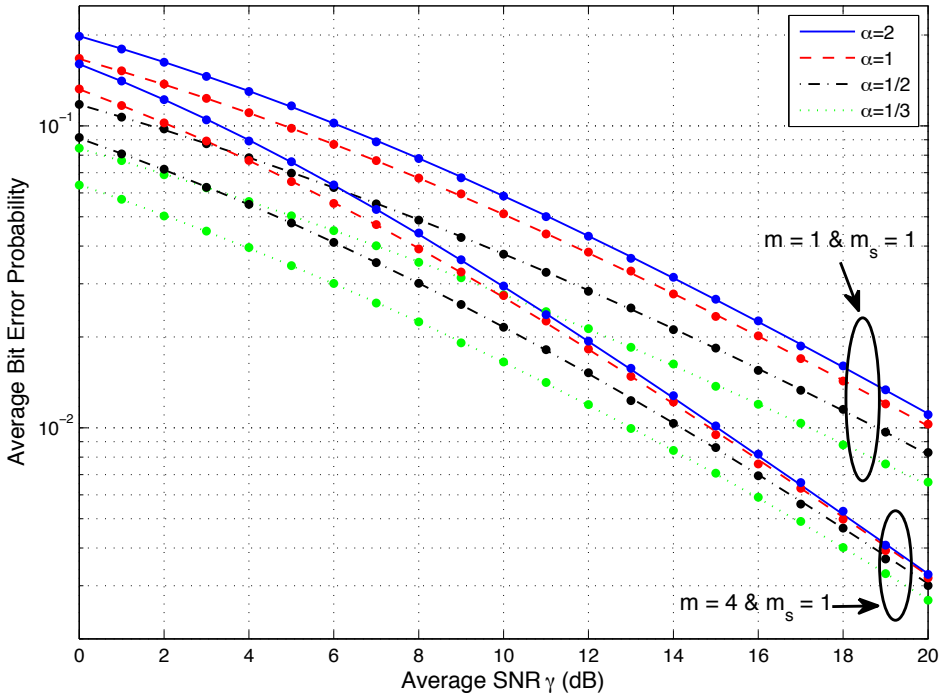

Figure 2.3: ABER of BPSK over generalized-K fading (the dot markers denote simulation results while lines represent analytical results).

on the average probability of error. In the next sections, PAM and QAM constellations are taking into consideration to get the probability of error.

2.3 Symbol Error Rate of M-PAM

In pulse amplitude modulation, PAM, the information is conveyed by the amplitude of the pulse. In this section we investigate the closed form of the average symbol error rate ASER for MPAM in the presence of GGN and EGK fading. The PAM case can be analyzed using the BPSK results of previous section. Actually, we consider the same system model used in previous section (2.14), where the transmitted signal $\mathcal{S}$ is multiplied by a channel fading envelope $\mathcal{H}$ that has a generalized flat fading characteristics and the resulting signal is then corrupted at

the receiver end by an AWGGN $\mathcal{N}$ with zero mean, variance σ^2, and shaping parameter α (2.14). Indeed the transmitted signal $\mathcal{S}$ is mapped according to an M-PAM constellation. In [5], the probability of error of the system above is well studied for the Gaussian noise case, and the resulting SER was shown to be given by [5, Eq. (8.3.5)] for the PAM constellation.

Since the generalized Gaussian distribution and the Gaussian distribution have the same symmetry properties, the SER of the MPAM signalling over an AWGGN channel can be easily written as

$$P_{PAM}(e) = 2\left(1 - \frac{1}{M}\right) Q_\alpha\left(\frac{d}{2\sigma}\right), \tag{2.31}$$

where d is the decision distance.

Before proceeding to the proof, we remember the expression of the conditional BER of the BPSK constellation that is given in (2.18) as

$$P_{BPSK} = Q_\alpha\left(\frac{d}{2\sigma}\right), \tag{2.32}$$

for d is the decision distance and σ^2 is the noise variance.

It appears from (2.16) that the decision region is based on the euclidian distance between the received signal and the constellation symbols. In the present case, consider an MPAM constellation with decision distance d. The probability of error for the PAM is divided into two terms, one for the outermost points (2 points) and the other for the remaining $M-2$ points. The first term is similar for both points and is equal to the error between one outermost point and its closest neighbor which is equal to the error of BPSK with decision distance d, so $P_{outer} = Q_\alpha\left(\frac{d}{2\sigma}\right)$. On the other hand, each of the remaining $M-2$ points has two neighbors from both sides, so the probability of error is twice the probability of error between two symbols $P_{inter} = 2\ Q_\alpha\left(\frac{d}{2\sigma}\right)$. By the end, since all symbols are equiprobable, the total

probability of error of the MPAM is given by

$$P_{PAM}(e) = \underbrace{2\frac{1}{M}Q_\alpha\left(\frac{d}{2\sigma}\right)}_{\text{Two outermost points}} + \underbrace{2(M-2)\frac{1}{M}Q_\alpha\left(\frac{d}{2\sigma}\right)}_{\text{The remaining } M-2 \text{ points}} = 2\left(1-\frac{1}{M}\right)Q_\alpha\left(\frac{d}{2\sigma}\right). \tag{2.33}$$

In the presence of a slow fading channel, the ASER is given by averaging the conditional SER (2.31) over the PDF of the fading envelope $\mathcal{H}$ (2.7), $p_{\mathcal{H}}(h)$, yielding

$$\mathrm{Pr}_{PAM}(e) = 2\left(1-\frac{1}{M}\right)\mathcal{I}\left(\frac{d}{2\sigma}\right), \tag{2.34}$$

where we define

$$\mathcal{I}(x) = \int_0^\infty Q_\alpha(hx)\, p_{\mathcal{H}}(h)\, dh \tag{2.35}$$

with x takes the value $\frac{d}{2\sigma}$ in (2.35). This definition will be helpful in the following sections.

Now let us consider an EGK fading environment with average fading power $\Omega = \mathbb{E}[\mathcal{H}^2]$. Thereby, $\mathcal{I}(x)$ reduces to the mean of a generalized Q function over an EGK distribution which has been already solved in (2.22)

$$\mathcal{I}(x) = \frac{1}{\alpha\Gamma(1/\alpha)\Gamma(m_s)\Gamma(m)}\mathrm{H}_{2,3}^{2,2}\left[\frac{\beta_s\beta}{x^2\Lambda_0^2\,\Omega}\,\middle|\,\begin{matrix}(1-\frac{1}{\alpha},\frac{2}{\alpha}),(1,\frac{2}{\alpha})\\(m_s,\frac{1}{\xi_s}),(m,\frac{1}{\xi}),(0,\frac{2}{\alpha})\end{matrix}\right]. \tag{2.36}$$

2.4 Symbol Error Rate of QAM Constellation

In this section, we consider a rectangular QAM mapping for the transmitted signal $\mathcal{S}$. Actually, the QAM constellation is formed by two independent and orthogonal M-ary PAM signals, such that the in-phase and quadrature phase constellations. More specifically, M_I-ary PAM and M_Q-ary PAM, where $M = M_I M_Q$.

2.4.1 Conditional SER

In [1], the probability of error of the system is well studied for the Gaussian noise case, and the resulting SER was shown to be given by [1, Eq. (10)] for the QAM constellation. By replacing the Q function by the previously defined Q_α, the SER of the M-QAM can be written as

$$\begin{aligned} P_{QAM}(E) = 2\left(1-\frac{1}{M_I}\right)Q_\alpha\left(A_I\right) + 2\left(1-\frac{1}{M_Q}\right)Q_\alpha\left(A_Q\right) \\ -4\left(1-\frac{1}{M_I}\right)\left(1-\frac{1}{M_Q}\right)Q_\alpha\left(A_I\right)Q_\alpha\left(A_Q\right), \end{aligned} \tag{2.37}$$

where $A_I = \frac{d_I}{2\sigma}$, $A_Q = \frac{d_Q}{2\sigma}$, d_I and d_Q are the in-phase and quadrature phase decision distances, respectively. According to these notations the average energy per symbol E_S can be expressed as

$$\begin{aligned} E_S &= \frac{1}{12}\left(d_Q^2(M_Q^2-1) + d_I^2(M_I^2-1)\right) \\ &= \frac{1}{12}d_I^2\left(\tau^2(M_Q^2-1) + (M_I^2-1)\right) \\ &= \frac{1}{3}A_I^2\sigma^2\left(\tau^2(M_Q^2-1) + (M_I^2-1)\right), \end{aligned} \tag{2.38}$$

where $\tau = d_Q/d_I = A_Q/A_I$ is the in-phase-to-quadrature-phase decision ratio. If we denote by Ω the average fading power $\Omega = \mathbb{E}[\mathcal{H}^2]$, the average SNR can be written as

$$\overline{\gamma} = \frac{1}{6}A_I^2\Omega\left(\tau^2(M_Q^2-1) + (M_I^2-1)\right). \tag{2.39}$$

The results found in (2.47) can be proven even without using the similarity of the distributions of each noise. In fact, from (2.33) the SER of the in-phase M_I-PAM

and the quadrature phase M_Q-PAM are given by

$$P_I = 2\left(1 - \frac{1}{M_I}\right) Q_\alpha\left(\frac{d_I}{2\sigma}\right), \tag{2.40}$$

$$P_Q = 2\left(1 - \frac{1}{M_Q}\right) Q_\alpha\left(\frac{d_Q}{2\sigma}\right). \tag{2.41}$$

Furthermore, a correct reception of the QAM symbol appears only when we have a correct reception in the in-phase signals and the quadrature phase signals. Since both constellations are independent, the probability of correct symbol reception for the rectangular M-QAM system is given by

$$P_c = (1 - P_I(e))(1 - P_Q(e)),$$

and the SER is obtained as

$$P_S = 1 - Pc = 1 - (1 - P_I)(1 - P_Q) = P_I + P_Q - P_I P_Q. \tag{2.42}$$

Using (2.40) and (2.41) in (2.42), we get

$$\begin{aligned} P_S = {} & 2\left(1 - \frac{1}{M_I}\right) Q_\alpha\left(A_I\right) + 2\left(1 - \frac{1}{M_Q}\right) Q_\alpha\left(A_Q\right) \\ & -4\left(1 - \frac{1}{M_I}\right)\left(1 - \frac{1}{M_Q}\right) Q_\alpha\left(A_I\right) Q_\alpha\left(A_Q\right). \end{aligned} \tag{2.43}$$

The ASER is obtained by averaging the conditional SER (2.43) over the PDF of the slow fading $\mathcal{H}$, yielding

$$\mathrm{Pr}_{QAM}\left(e\right) = 2\left(1 - \frac{1}{M_I}\right)\mathcal{I}(A_I) + 2\left(1 - \frac{1}{M_Q}\right)\mathcal{I}(A_Q) - 4\left(1 - \frac{1}{M_I}\right)\left(1 - \frac{1}{M_Q}\right)\mathcal{J}, \tag{2.44}$$

where $\mathcal{I}(\cdot)$ is defined in (2.35), and $\mathcal{J}$ is defined as follows

$$\mathcal{J} = \int_0^\infty Q_\alpha\left(hA_I\right) Q_\alpha\left(hA_Q\right) p_{\mathcal{H}}(h)\, dh. \tag{2.45}$$

It is important to note that this closed-form result (2.44) is a new generic expression for the ASER of rectangular M-QAM signaling perturbed by GGN.

2.4.2 Conditional SER of Square QAM

The square QAM modulation is obtained from the rectangular QAM studied in the previous section by setting $M_I = M_Q = \sqrt{M}$ and $d_I = d_Q = d$ (i.e. $A_I = A_Q = A$). According to these setting, the decision distance can be written in terms of the average energy per symbol, E_S, as $d = \sqrt{\frac{6E_S}{M-1}}$ and so $A = \sqrt{\frac{6E_S}{(M-1)4\sigma^2}} = \sqrt{\frac{3E_S}{(M-1)N_0}}$. Thus the conditional SER is derived from (2.43) as

$$P_S(E) = 4\left(1 - \frac{1}{\sqrt{M}}\right) Q\left(\sqrt{\frac{3E_S}{N_0(M-1)}}\right) - 4\left(1 - \frac{1}{\sqrt{M}}\right)^2 Q^2\left(\sqrt{\frac{3E_S}{N_0(M-1)}}\right). \tag{2.46}$$

Conditioning on the channel, the SER is expressed in terms of the instantaneous SNR as

$$\Pr(e|\gamma) = 4\left(1 - \frac{1}{\sqrt{M}}\right) Q_\alpha\left(\sqrt{\frac{3\gamma}{M-1}}\right) - 4\left(1 - \frac{1}{\sqrt{M}}\right)^2 Q_\alpha^2\left(\sqrt{\frac{3\gamma}{M-1}}\right), \tag{2.47}$$

where $\gamma = \frac{\mathcal{H}^2 E_{\mathcal{S}}}{N_0}$ is the instantaneous SNR per symbol at the receiver. In what follows, only the quantities $\mathcal{I}(\cdot)$ and $\mathcal{J}$ are studied for different fading models. The square QAM case can be deduced easily from these expressions.

2.4.3 Average SER over EGK Fading

As mentioned previously, $\mathcal{H}$ is following an EGK PDF (Sec. 2.1.2), with average fading power $\Omega = \mathbb{E}[\mathcal{H}^2]$. $\mathcal{I}(\cdot)$ is already investigated in the previous section. However, $\mathcal{J}$ is difficult to compute using the classical expressions of the EGK distribution and the GGD. Thereby, we use the alternative expressions of $Q_\alpha(\cdot)$ and $p_{\mathcal{H}}(h)$ given in Sec. 2.1.3, in order to derive a closed-form expressions for $\mathcal{J}$ and, as a result, for the ASER. More specifically, $\mathcal{J}$ can written as an integral involving the product of three FHFs (product of two Q_α functions and $p_{\mathcal{H}}(h)$). Such integral can be solved using the identity [62, Eq. (2.3)] that involves the product of three FHFs

$$\begin{aligned}\int_0^\infty x^{\lambda-1}\mathrm{H}_{p,q}^{m,0}\left[ax\left|\begin{matrix}(a_i,\alpha_i)_{1,p}\\(b_j,\beta_j)_{1,q}\end{matrix}\right.\right]\mathrm{H}_{p_2,q_2}^{m_2,n_2}\left[\beta x^h\left|\begin{matrix}(c_i,r_i)_{1,p_2}\\(d_j,\delta_j)_{1,q_2}\end{matrix}\right.\right]\mathrm{H}_{p_3,q_3}^{m_3,n_3}\left[\delta x^k\left|\begin{matrix}(e_i,E_i)_{1,p_3}\\(f_j,F_j)_{1,q_3}\end{matrix}\right.\right]dx\\ = a^{-\lambda}\mathrm{H}_{p,q;p_2,q_2;p_3,q_3}^{0,m;m_2,n_2;m_3,n_3}\left[\frac{\beta}{a^h},\frac{\delta}{a^k}\left|\begin{matrix}(1-b_j-\lambda\beta_j;h\beta_j,k\beta_j)_{1,q}\\(1-a_i-\lambda\alpha_i;h\alpha_i,k\alpha_i)_{1,p}\end{matrix}\right.\left|\begin{matrix}(c_i,r_i)_{1,p_2}\\(d_j,\delta_j)_{1,q_2}\end{matrix}\right.\left|\begin{matrix}(e_i,E_i)_{1,p_3}\\(f_j,F_j)_{1,q_3}\end{matrix}\right.\right].\end{aligned} \tag{2.48}$$

Using (2.48), $\mathcal{J}$ can be expressed in terms of the FHF of two variables defined in [62], also known as the Bivariate Fox H-function (BFHF) $\mathrm{H}_{\cdot,\cdot;\cdot,\cdot;\cdot,\cdot}^{\cdot,\cdot;\cdot,\cdot;\cdot,\cdot}[\cdot,\cdot]$ and whose MATLAB implementation is outlined in[63]. Finally a closed form of $\mathcal{J}$ is found as

$$\begin{aligned}\mathcal{J} = &\frac{1}{2\alpha\Gamma(1/\alpha)^2\Gamma(m_s)\Gamma(m)}\\ &\times\mathrm{H}_{2,1;0,2;1,2}^{0,2;2,0;2,0}\left[\frac{\beta_s\beta}{A_I^2\Lambda_0^2\Omega},\tau^\alpha\left|\begin{matrix}(1-\frac{1}{\alpha};\frac{2}{\alpha},1),(1;\frac{2}{\alpha},1)\\(0;\frac{2}{\alpha},1)\end{matrix}\right.\left|\begin{matrix}\text{——}\\(m_s,\frac{1}{\xi_s}),(m,\frac{1}{\xi})\end{matrix}\right.\left|\begin{matrix}(1,1)\\(\frac{1}{\alpha},1),(0,1)\end{matrix}\right.\right].\end{aligned} \tag{2.49}$$

To conclude this section, a closed-form of the ASER of QAM is obtained using (2.36) and (2.49) in (2.44). This closed-form is a general expression of the ASER of rectangular and square QAM in arbitrary EGK fading subject to AWGGN, and holds as such for a considerable range of noise and fading parameters.

At this stage, the ASER of either PAM or QAM is totally expressed in terms of $\mathcal{I}(\cdot)$ and $\mathcal{J}$. In the next section we are focusing on some special cases of noise and fading

to simplify their closed form.

2.4.4 Special Cases of Noise and Fading

2.4.4.1 EGK Fading with Additive Laplace Noise

The first special case of the generalized Gaussian noise appears when α equals to 1 (i.e. Laplace noise). Using the properties and the special cases of the FHF [55], and BFHF functions [62], The quantities $\mathcal{I}(\cdot)$ (2.36) and $\mathcal{J}$ (2.49) can be re-written as

$$\mathcal{I}(x) = \frac{1}{\Gamma(m_s)\Gamma(m)} \mathrm{H}_{1,2}^{2,1}\left[\frac{\beta_s \beta}{2x^2\,\Omega}\middle| \begin{matrix}(1,2)\\ (m_s, \frac{1}{\xi_s}), (m, \frac{1}{\xi})\end{matrix}\right] \tag{2.50}$$

$$\mathcal{J} = \frac{1}{2\Gamma(m_s)\Gamma(m)} \mathrm{H}_{1,0;0,2;0,1}^{0,1;2,0;1,0}\left[\frac{\beta_s \beta}{2A_I^2\Omega}, \tau \middle| \begin{matrix}(1;2,1)\\ \text{——}\end{matrix}\middle| \begin{matrix}\text{——}\\ (m_s, \frac{1}{\xi_s}), (m, \frac{1}{\xi})\end{matrix}\middle| \begin{matrix}\text{——}\\ (0,1)\end{matrix}\right]. \tag{2.51}$$

In fact, $\mathcal{J}$ can be expressed in terms of $\mathcal{I}(\cdot)$ for the LN. Indeed using the Mellin definition of the BHFH [62, Eq. (1.1)], we re-write $\mathcal{J}$ as

$$\mathcal{J} = \frac{1}{2\Gamma(m_s)\Gamma(m)} \frac{1}{(2\pi i)^2} \int_{L_1}\int_{L_2} \Gamma(-2s-t)\Gamma(m_s + s/\xi_s)\Gamma(m + s/\xi)\Gamma(t) \times \left(\frac{\beta_s \beta}{2A_I^2\Omega}\right)^{-s} \tau^{-t} dt\; ds. \tag{2.52}$$

Using the inverse Mellin transform of the extended incomplete Gamma function $\Gamma(\cdot,\cdot,\cdot,\cdot)$ [57, Eq. (6.29)], and its special case presented in [57, Eq. (6.42)], we get

$$\frac{1}{2\pi i}\int_{L_2} \Gamma(-2s-t)\Gamma(t)\tau^{-t} dt = \Gamma(-2s, 0, \tau, -1) = \Gamma(-2s)\,(1+\tau)^{2s}\,. \tag{2.53}$$

Replacing (2.53) in (2.52)

$$\begin{aligned}\mathcal{J} &= \frac{1}{2\Gamma(m_s)\Gamma(m)}\frac{1}{2\pi i}\int_{L_1}\Gamma(m_s+s/\xi_s)\Gamma(m+s/\xi)\Gamma(-2s)\left(\frac{\beta_s\beta}{2\left(A_I+A_Q\right)^2\Omega}\right)^{-s}ds \\ &= \frac{1}{2\Gamma(m_s)\Gamma(m)}\mathrm{H}_{1,2}^{2,1}\left[\frac{\beta_s\beta}{2(A_I+A_Q)^2\,\Omega}\middle|\begin{matrix}(1,2)\\(m_s,\frac{1}{\xi_s}),(m,\frac{1}{\xi})\end{matrix}\right] \\ &= \frac{1}{2}\mathcal{I}(A_I+A_Q). \end{aligned} \tag{2.54}$$

Hence, in the presence of LN, the ASER is totally characterized by $\mathcal{I}(\cdot)$. The expression (2.50) contains also the FHF but with a lower rank than the general expressions given in (2.36), which means that it can be computed with a reduced complexity of evaluation. Since the LN is an interesting case of study, it is also of interest to study other special cases of fading in conjunction with the LN.

2.4.4.2 Generalized Nakagami-m Fading with Laplace Noise

A special case of the previous studied case is to couple the generalized Nakagami-m (GNM) fading with Laplace noise. The GNM fading is obtained by setting $\xi_s = 1$ and $m_s \to \infty$ in (2.50). Therefore $\mathcal{I}(\cdot)$ simplifies to

$$\mathcal{I}(x) = \frac{1}{\Gamma(m)}\mathrm{H}_{1,1}^{1,1}\left[\frac{\beta}{2x^2\,\Omega}\middle|\begin{matrix}(1,2)\\(m,\frac{1}{\xi})\end{matrix}\right]. \tag{2.55}$$

Re-writing the expression of the FHF, using some changes of variable, and the identity [57, Eq. (6.29)], a new expression of $\mathcal{I}(\cdot)$ can be obtained as

$$\mathcal{I}(x) = \frac{\xi}{\Gamma(m)}\left(\frac{\beta}{2x^2\,\Omega}\right)^{m\xi}\Gamma\left(2m\xi, 0, \left(\frac{\beta}{2x^2\,\Omega}\right)^{\xi}, -2\xi\right). \tag{2.56}$$

Recall that $\mathcal{J} = \frac{1}{2}\mathcal{I}(A_I + A_Q)$. Thus the ASER of QAM is well defined according to (2.44).

2.4.4.3 Rayleigh Fading with Laplace Noise

Keeping an additive LN, the Rayleigh fading case is obtained by setting $m = 1$ and $\xi = 1$ in (2.56). From (2.56) and with a simple manipulation of $\Gamma(\cdot,\cdot,\cdot,\cdot)$, it can be shown that $\mathcal{I}$ is equivalent to

$$\begin{aligned}
\mathcal{I}(x) &= \frac{1}{2x^2\,\Omega}\Gamma\left(2, 0; \frac{1}{2x^2\,\Omega}; -2\right) \\
&\overset{[57,Eq.\ (6.2)]}{=} \frac{1}{2x^2\,\Omega}\int_0^\infty te^{-t-\frac{t^2}{2x^2\,\Omega}}dt \\
&\overset{u=\frac{t}{\sqrt{2x^2\Omega}}+\frac{\sqrt{2x^2\Omega}}{2}}{=} \frac{e^{\frac{x^2\Omega}{2}}}{\sqrt{2x^2\,\Omega}}\int_{\sqrt{\frac{x^2\Omega}{2}}}^\infty \left(\sqrt{2x^2\Omega}u - x^2\Omega\right)e^{-u^2}du \\
&= e^{\frac{x^2\Omega}{2}}\int_{\sqrt{\frac{x^2\Omega}{2}}}^\infty ue^{-u^2}du - \frac{e^{\frac{x^2\Omega}{2}}\sqrt{2x^2\,\Omega}}{2}\int_{\sqrt{\frac{x^2\Omega}{2}}}^\infty e^{-u^2}du \\
&= \frac{1}{2} - \frac{x}{2}\sqrt{2\pi\Omega}e^{\frac{\Omega x^2}{2}}Q\left(x\sqrt{\Omega}\right), \qquad (2.57)
\end{aligned}$$

which is a very simple expression involving only the standard Gaussian Q function (i.e. $Q(x) = Q_2(x)$). To the best of the author's knowledge, the expression of the ASER with additive LN and Rayleigh fading in (2.57) is a new expression that has not been reported previously.

2.4.4.4 Generalized K Fading with Gaussian Noise

The last two special cases will focus on the classical Gaussian noise with different fading distributions. The first example deals with the performance of M-QAM over a Generalized-K (GK) fading subjected to an AWGN channel. This case is obtained by setting $\alpha = 2$, $\xi = 1$, and $\xi_s = 1$. With these settings, the main integrals in (2.36) and (2.49) can be reduced to

$$\mathcal{I}(x) = \frac{1}{2\sqrt{\pi}\Gamma(m_s)\Gamma(m)}\mathrm{G}_{2,3}^{2,2}\left[\frac{2m_s m}{x^2\,\Omega}\,\middle|\,\begin{matrix}\frac{1}{2}, 1\\ m_s, m, 0\end{matrix}\right]. \qquad (2.58)$$

$$\mathcal{J} = \frac{1}{4\pi\Gamma(m_s)\Gamma(m)} \mathrm{G}_{2,1;0,2;1,2}^{0,2;2,0;2,0} \left[\frac{2m_s m}{A_I^2\Omega}, \tau^2 \left| \begin{matrix} \frac{1}{2}, 1 \\ 0 \end{matrix} \right| \begin{matrix} - \\ m, m_s \end{matrix} \left| \begin{matrix} 1 \\ \frac{1}{2}, 0 \end{matrix} \right. \right], \tag{2.59}$$

where $\mathcal{J}$ is expressed in terms of the bivariate Meijer G-function (BMGF) whose MATHEMATICA® implementation is given in [64, Table II].

2.4.4.5 Rayleigh Fading with Gaussian Noise

The Rayleigh fading is a special case of the GK distribution by simply setting $m = 1$ and tending $m_s \to \infty$. In this case, the main integrals, $\mathcal{I}(\cdot)$ and $\mathcal{J}$ in (2.58) and (2.59), respectively, reduce to

$$\mathcal{I}(x) = \frac{1}{2\sqrt{\pi}} \mathrm{G}_{2,2}^{1,2} \left[\frac{2}{x^2\,\Omega} \left| \begin{matrix} \frac{1}{2}, 1 \\ 1, 0 \end{matrix} \right. \right]. \tag{2.60}$$

$$\mathcal{J} = \frac{1}{4\pi} \mathrm{G}_{2,1;0,1;1,2}^{0,2;1,0;2,0} \left[\frac{2}{A_I^2\Omega}, \tau^2 \left| \begin{matrix} \frac{1}{2}, 1 \\ 0 \end{matrix} \right| \begin{matrix} - \\ 1 \end{matrix} \left| \begin{matrix} 1 \\ \frac{1}{2}, 0 \end{matrix} \right. \right], \tag{2.61}$$

The expressions in (2.60) and (2.61) involve reduced rank MGF and BMGF functions in comparison with (2.58) and (2.59). However, it is interesting to note that these formulas are numerically equivalent to

$$\begin{aligned} \mathcal{I}(x) &= \frac{1}{2} - \frac{1}{2}\sqrt{\frac{x^2\Omega}{2 + x^2\Omega}} \\ \mathcal{J} &= \frac{1}{4} - \frac{1}{2\pi} \left[\sqrt{\frac{A_I^2\Omega}{2 + A_I^2\Omega}} \tan^{-1}\left(\frac{A_I}{A_Q} \sqrt{\frac{2 + A_I^2\Omega}{A_I^2\Omega}} \right) \right. \\ &\quad \left. + \sqrt{\frac{A_Q^2\Omega}{2 + A_Q^2\Omega}} \tan^{-1}\left(\frac{A_Q}{A_I} \sqrt{\frac{2 + A_Q^2\Omega}{A_Q^2\Omega}} \right) \right], \end{aligned} \tag{2.62}$$

where $\tan^{-1}(.)$ is the inverse tangent function, in agreement with the known expressions of Beaulieu [1, Eq. (5)] of the ASER of M-QAM over Rayleigh fading through an AWGN channel.

It is worth mentioning that in these special cases, we are not just setting the

parameters in the general expression (2.36) and (2.49). Rather, in each case, we offered simplified closed-form expressions of the main parts of the ASER with reduced computational complexity. In fact, from the definition of the FHF [55, Eq.(1.1.1)], the complexity of evaluating the Mellin integral is based on the rank of the FHF, which is reduced in these special cases. In what follows some selected numerical results and simulations are analyzed for square and rectangular QAM in different communication schemes/scenarios.

2.4.5 Simulation Results for Square 16-QAM

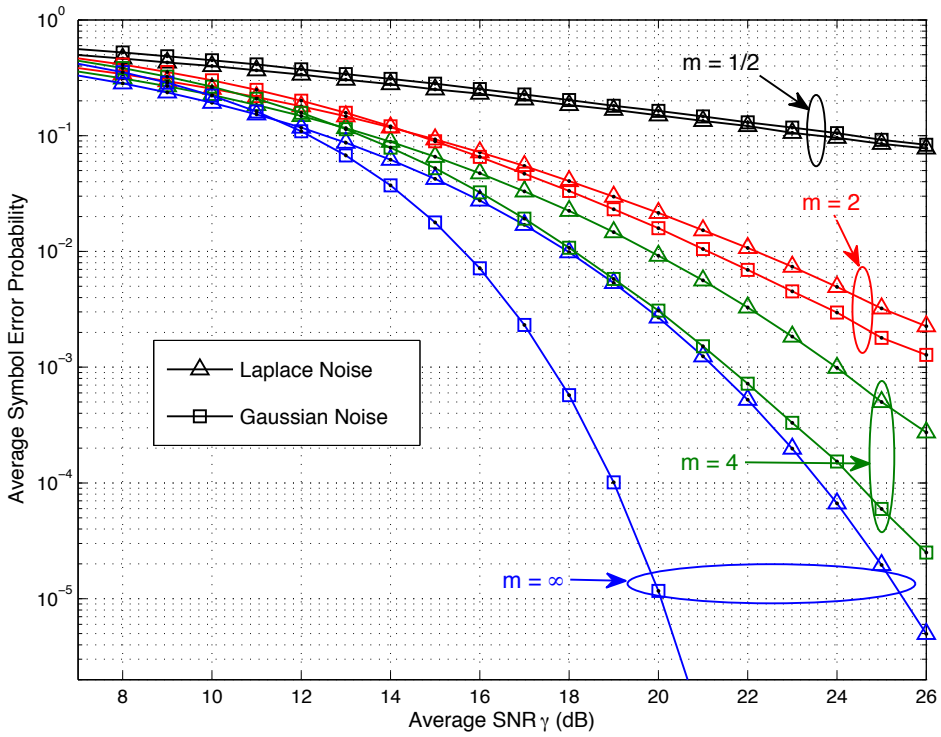

Figure 2.4: ASER of 16-QAM over Nakagami-m fading subject to Laplace noise and Gaussian noise. The markers denote simulation results while solid lines represent analytical results.

In this section, we plot the ASER of 16-QAM signaling for different type of noise (i.e. different values of α), and fading (i.e. different values of m, m_s, ξ, and ξ_s). As

a first numerical example, we look into Gaussian and Laplace noise in conjunction with Nakagami-m fading. The numerical results of this example are presented in Fig. 2.4 for four values of the Nakagami-m fading parameter, namely $m = \frac{1}{2}, 2, 4,$ and ∞. The numerical results obtained from the main formula (2.44) are compared to computer-based Monte-Carlo simulation results. It is clear that the numerical results and simulation results match perfectly as a validation of our analytical results. In both noise cases, the ASER improves as the fading parameter m increases, as expected. In addition, for a high amount of fading (i.e. $m = \frac{1}{2}$), the ASER for the Laplace case is better than the ASER for the Gaussian case. However, for a low amount of fading (i.e. $m \geq 2$), we note that there are two regimes. The first regime is for low SNR ($\overline{\gamma} \leq 12$ dB) in which the Laplace noise has better performance than the Gaussian noise, and in second regime, for high SNR ($\overline{\gamma} > 12$dB) in which ASER for the Gaussian case is better than the ASER for the Laplace case.

In Fig. 2.5, we look into the Rayleigh fading case and vary the noise parameter α. Note again, from Fig. 2.5, that the simulation results match perfectly the analytical results obtained from (2.44). In this case of Rayleigh fading, it is worth mentioning that the system has better performance by decreasing the noise parameter α, which confirms the result found in the previous example when the Laplace noise has better performance than the Gaussian noise for high amount of fading. At high SNR ($\overline{\gamma} > 28$dB), the performance of the system converges essentially to one curve for different values of noise parameter.

Finally, in order to see the impact of the fading parameter, we draw the ASER for the case of Nakagami-4 fading and the same values of the noise parameter in Fig. 2.6. Similar to what happened in the first example, we have also in this case two regions. For low SNR the ASER decreases with the noise parameter. However, for high SNR, the system performance gets better by increasing α.

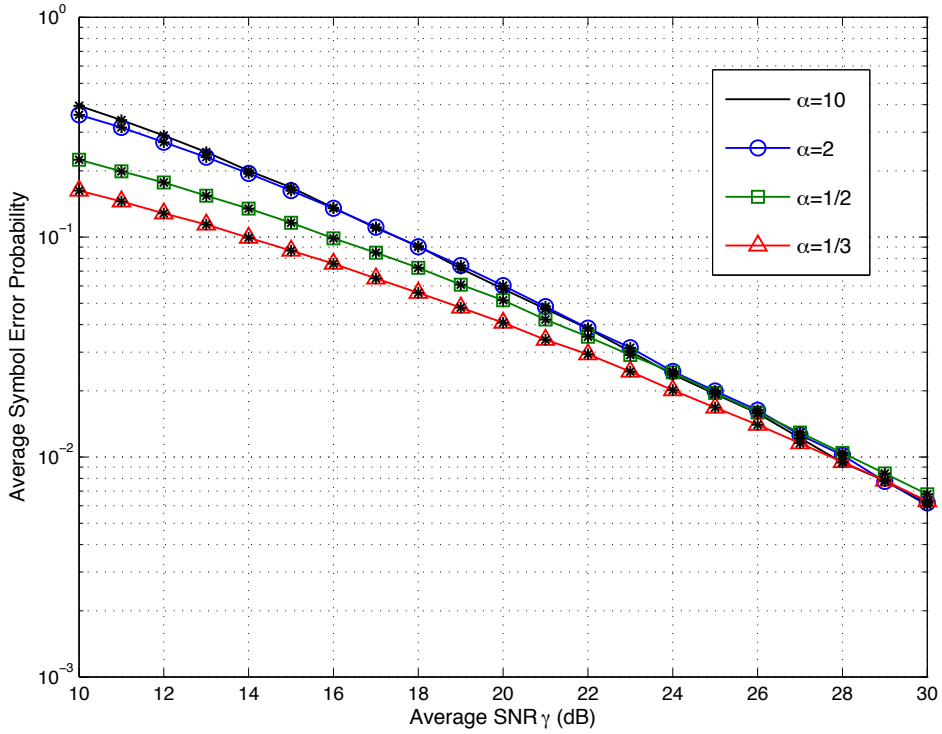

Figure 2.5: ASER of 16-QAM over Rayleigh fading subject to generalized Gaussian noise (the markers denote simulation results while solid lines represent analytical results).

Another illustration is presented in the next section for a rectangular QAM constellation.

2.4.6 Simulation Results for 8×4 -QAM

Let us consider a 32-QAM system (i.e. 8×4-QAM), and investigate the system performance as a function of the SNR for different type of noise (i.e. different values of α), and fading (i.e. different set of values of m, m_s, ξ, and ξ_s). From (2.39), the average SNR can be written as $\overline{\gamma} = 0.5 A_I^2 \Omega \left(5\tau^2 + 21\right)$. Thereby $A_I^2\Omega = \frac{2\overline{\gamma}}{5\tau^2+21}$ and $A_Q^2\Omega = \frac{2\tau^2\overline{\gamma}}{5\tau^2+21}$. For instance, τ is fixed ($\tau = (21/5)^{1/2}$), so the average energies of the in-phase and quadrature phase signals are equal.

The first studied case is a comparison between the Gaussian and Laplace noises in

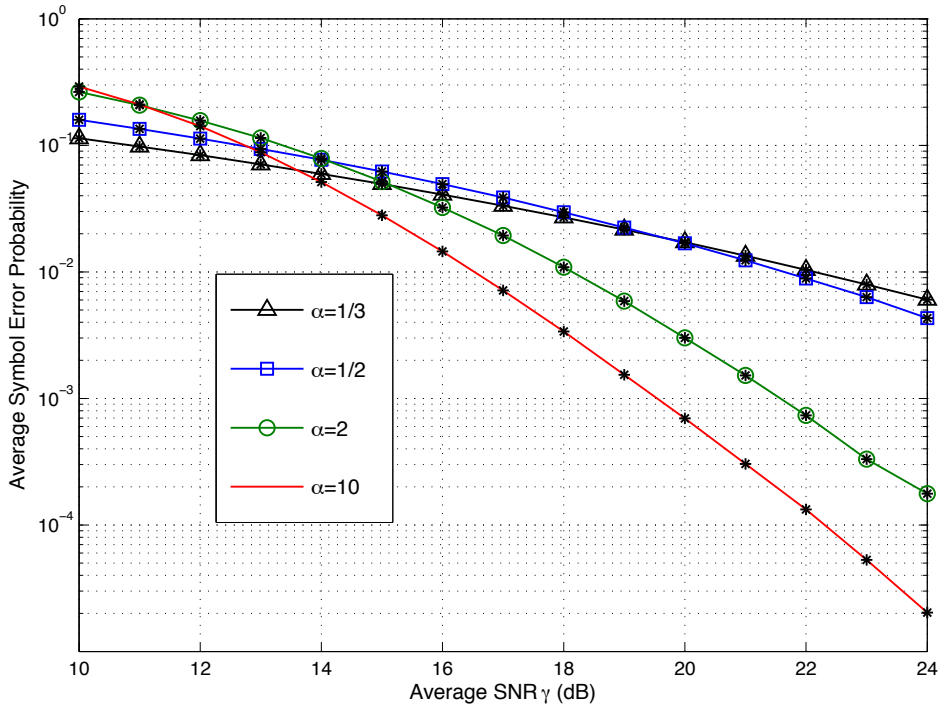

Figure 2.6: ASER of 16-QAM over Nakagami-4 fading subject to generalized Gaussian noise (the markers denote simulation results while solid lines represent analytical results).

conjunction with Nakagami-m fading. Note that the Nakagami-m fading is obtained by setting the fading shaping factor $\xi = 1$ in (2.56) for the LN. Fig. 2.7 shows the ASER as a function of the average SNR per symbol $\overline{\gamma}$ for both cases Gaussian and Laplace and for four values of the fading parameter, namely $m = \frac{1}{2}, 2, 4$, and ∞. A comparison between the analytical results, presented in this section, and a computer-based Monte-Carlo simulations results are presented also. The simulation results match perfectly the analytical results derived previously. A general look at the figure shows us that the performance of the system is improved by increasing the fading parameter m, as expected. In addition, for lower SNR (i.e. SNR$<$ 15 dB), we note that the ASER of the LN is better than the ASER of the Gaussian noise. The situation reverse for high SNR and low amount of fading ($m \geq 2$) since the Gaussian

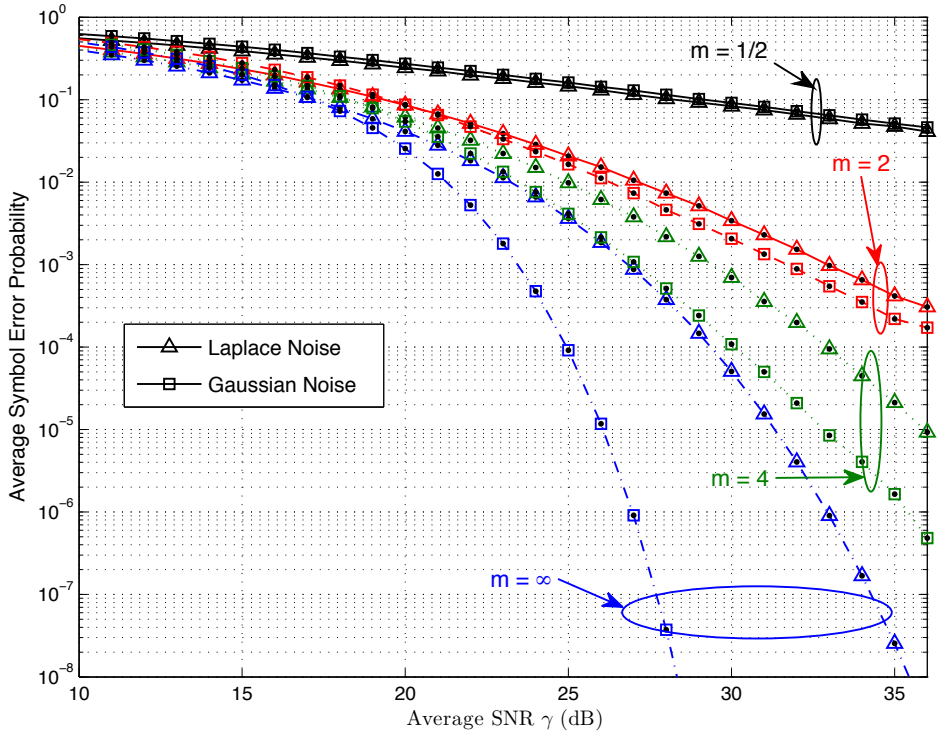

Figure 2.7: ASER of 8×4-QAM over Nakagami-m fading subject to Laplace noise and Gaussian noise. The dots denote simulation results while the lines represent analytical results.

noise yields better results than LN. However for high amount of fading, such as for example $m = 1/2$, the performance in LN is better than in the Gaussian noise case. In the second numerical example, we compare the Rayleigh fading and the Nakagami-4 fading. For instance, in Fig. 2.8, we draw the ASER in function of the SNR per QAM symbol for different values of α. Note again that the simulation results match perfectly the analytical results obtained from (2.36) and (2.49). In Rayleigh fading case, it is worth mentioning that the system has better performance by decreasing the noise parameter α, which confirm the result found in the previous example when the LN had better performance than the Gaussian noise for high amount of fading. However, the situation becomes different for lower amount of fading (i.e. when $m = 4$), and we get two regions. For low SNR the ASER decreases

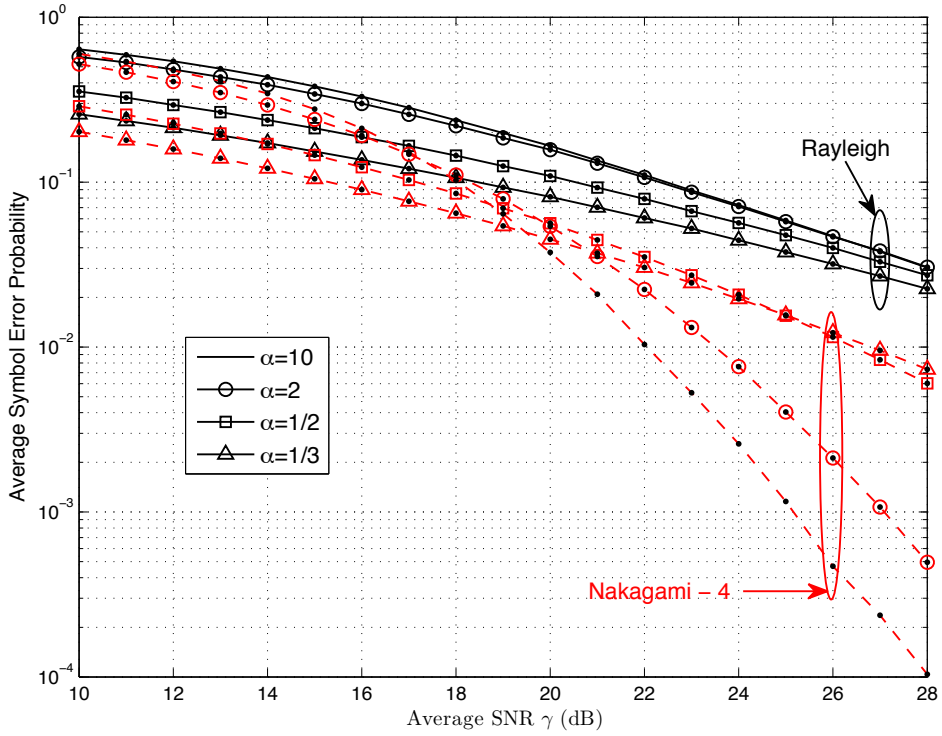

Figure 2.8: ASER of 8×4-QAM over Rayleigh and Nakagami-4 fading subject to generalized Gaussian noise. The dots denote simulation results while the lines represent analytical results.

with the noise parameter, and for high SNR it gets better by increasing α. A similar results to those studied in the square 16-QAM scenario.

A new parameter appears on the energy expression, which is the ratio τ, and in this numerical example we want to see the effect of τ on the system performance. Therefore Fig. 2.9 draws the ASER of the system described above (32-QAM with different values of τ) as a function of the SNR and for different values of the in-phase-to-quadrature decision distance ratio. It is clear that the best case is when the in-phase and quadrature distance are equal (i.e. $\tau = 1$) for both cases of noise. For equal energy between the in-phase and quadrature signal (i.e. $\tau = (21/5)^{1/2}$), the system looses in performance but in small amount (about 1 dB for $SER = 6 \times 10^{-4}$). However, the loss is more important when the quadrature signal

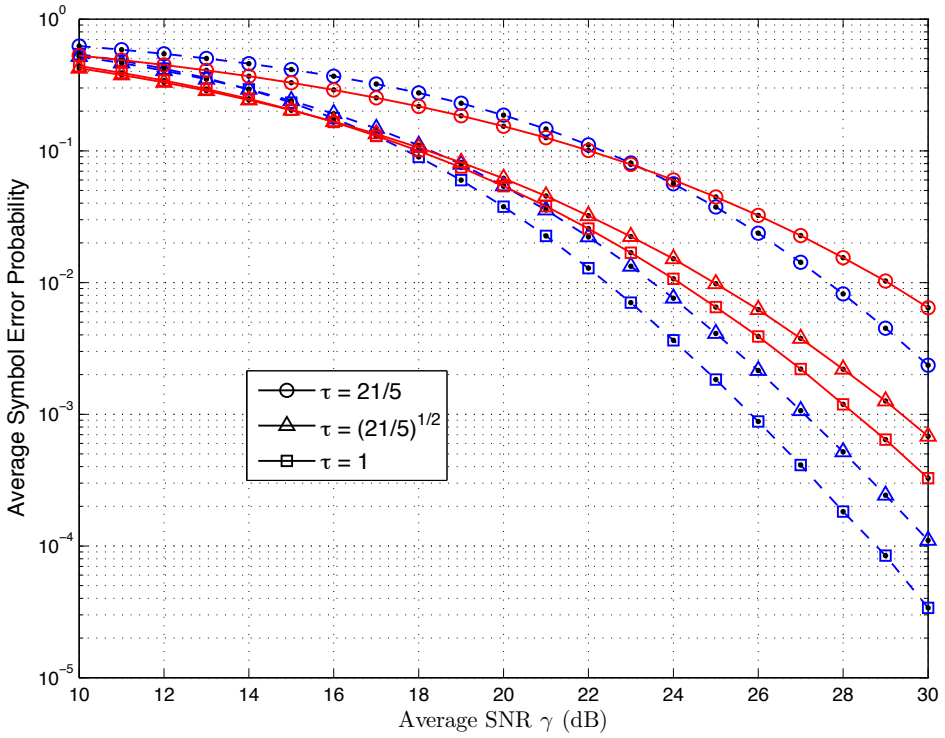

Figure 2.9: ASER of 8×4-QAM over Nakagami-4 fading subject to Laplace and Gaussian noise. The dots denote simulation results, the solid lines (red) represent the Laplace noise case, and the dashed lines (blue) represent Gaussian noise case.

has 21/5 times the average energy of the in-phase signal (i.e. $\tau = 21/5$), since it incurs a loss of about 4 dB for $SER = 6 \times 10^{-3}$, relative to the case where $\tau = 1$.

2.5 Conclusion

In this chapter, we studied the average symbol error probability of different modulations schemes such as the BPSK, PAM, square QAM, and rectangular QAM. These digital communication systems are assumed to be perturbed by an additive GGN over a generalized fading ditribution, namely EGK channel. A closed form of the ASER was derived in terms of the FHF and BFHF. Furthermore, several special cases of the noise, covered by the selected noise family, and different type of fading

included in the EGK family. By the end an illustration of the mathematical formalism is presented. Actually, some selected numerical results are described for the Nakagami-m fading and Rayleigh fading in conjunction with the Gaussian, Laplace noise, and other type of noise. In the next chapter, we study another constellation, viz MPSK modulation when it is perturbed by a Laplace noise.

Chapter 3

Error Rate of MPSK Over Laplace Noise

In this chapter, we consider a channel with additive white Laplace noise (AWLN). In this case, the ML detector differs from the minimum distance (MD) detector. As such, we present the decision regions corresponding to both MD detector and ML detector and derive the SER of M-PSK using both detectors (ML and MD). That decision regions should help to get the conditional SER. Besides the additive noise, it is assumed that the communication is affected also by a multiplicative noise that behaves as a flat fading, which is modeled by an EGK distribution.

3.1 Detection Regions in Laplace Noise

3.1.1 System Model

Let us consider a SISO communication system. $\mathcal{S}$, the transmitted signal, is mapped according to an MPSK constellation, where M is a power of 2. The symbols are distributed uniformly over the circle with radius $\sqrt{E_S}$, defined as the energy per symbol, all symbols are equal likely. The mathematical model of the system was given in (2.14), where $\mathcal{S}$ is multiplied by a channel fading coefficient

$\mathcal{H} \in \mathbb{R}^+$ and added to a Laplace noise $\mathcal{N}$. In (2.14), $\mathcal{R}$ denotes the received signal. $\mathcal{S}$, $\mathcal{N}$, and $\mathcal{R}$ have two components (in-phase and quadrature phase components). The noise is considered as Laplace noise with zero mean and one side power spectral density $\sigma^2 = N_0/2$. More specifically, the PDF of a Laplace random variable is defined as [43, 44, 42]

$$X \sim \mathcal{L}(\mu, \sigma) \quad , \quad f_X(x; \mu, \sigma) = \frac{1}{\sqrt{2}\sigma} e^{-\sqrt{2}\frac{|x-\mu|}{\sigma}}, \tag{3.1}$$

where μ represents the location parameter and is equal to the mean, while σ is the variance.

In the following analysis of the detection regions, the system performance is conditioned over the instantaneous received SNR γ, which is defined as (2.9) $\gamma = \frac{\mathcal{H}^2 E_{\mathcal{S}}}{N_0}$. Without loss of generality, we normalize $\mathcal{S}$ in (2.14) by dividing it by $\mathcal{H}\sqrt{E_S}$. The resulting normalized system model is given by

$$r = s + n, \tag{3.2}$$

where s has a unit energy per symbol and n has a variance equal to $\frac{1}{\gamma}$.

The in-phase component is indexed by I, while the quadrature phase component is indexed by Q in all signals. Indeed, (s_I, s_Q) are the components of s, (n_I, n_Q) are the components of n, and (I, Q) are the received components. The components of the normalized system model can be re-written as

$$\begin{cases} I &= s_I + n_I \\ Q &= s_Q + n_Q. \end{cases} \tag{3.3}$$

Note that n_I and n_Q are independent random variables that follow a Laplace distribution with zero mean and variance $\frac{1}{2\gamma}$ each. Therefore, (I, Q) can be modeled as two independent Laplace random variables with mean (s_I, s_Q) and covariance

matrix $\frac{1}{2\gamma}I_2$ (I_2 denote the identity matrix of order 2). From (3.1), the joint PDF of (I, Q) can thus be written as

$$f_{IQ}(I,Q) = \gamma e^{-2\sqrt{\gamma}\left(|I-s_I|+|Q-s_Q|\right)},\ \forall\ I,\ Q\ \in \mathbb{R}. \tag{3.4}$$

3.1.2 Maximum Likelihood Detector

The transmitted symbols are distributed uniformly over the unit circle, which means that $(s_I^k, s_Q^k) = (\cos(\phi), \sin(\phi))$, where $\phi = \frac{2k\pi}{M}$ and $k \in \{0, 1, \ldots M-1\}$. Consider two equal likely symbols $s^\phi = (s_I^\phi, s_Q^\phi)$ and $s^\theta = (s_I^\theta, s_Q^\theta)$ with angles ϕ and θ. In what follows, we will refer to the angles instead of the signal to mention the desired symbol. Since the angles are equal likely, the maximum a posteriori (MAP) probability detector coincide with the ML detector. Thereby, the detector decides ϕ if $f_{IQ}(I, Q|\phi, \gamma) > f_{IQ}(I, Q|\theta, \gamma)$. In other words the following condition should be satisfied to decide ϕ instead of θ

$$|I - \cos(\phi)| + |Q - \sin(\phi)| < |I - \cos(\theta)| + |Q - \sin(\theta)|\,. \tag{3.5}$$

This condition can be also re-written using the L_1 norm as

$$\| r - s^\phi \|_1 < \| r - s^\theta \|_1\ .$$

It is obvious that this condition is similar to the known minimum euclidian distance condition (in particular in the Gaussian noise case). However instead of using the euclidian distance, the rule deploys the L_1 norm distance to detect the better angle (symbol).

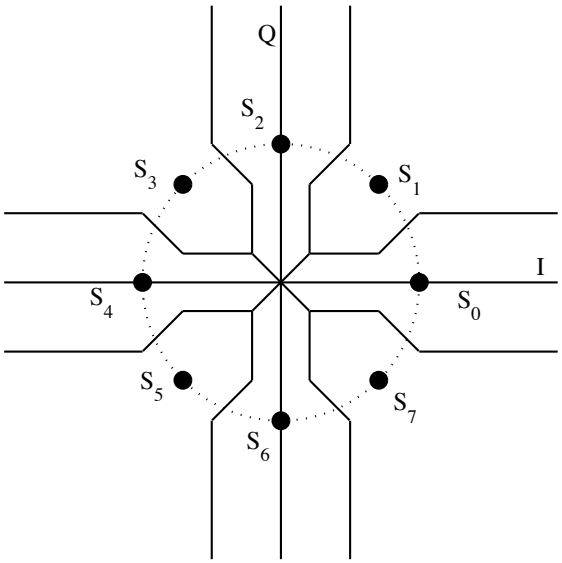

Figure 3.1: Signal constellation and decision regions using the ML rule for 8-PSK.

3.1.2.1 Decision Regions for 8-PSK

Consider for example an 8-PSK constellation as shown in Fig. 3.1. In this example, we will produce the decision regions of the 8-PSK and draw it. Considering the symmetric properties of the PDF of the received signal $f_{IQ}(I, Q)$, we can focus only on the quarter of the plan lying between the I axis and the Q axis, where $\phi \in [0, \frac{\pi}{2}]$. Afterwards, we are focusing on the decision boundaries between s_0, s_1, and s_2. From (3.5), we decide $\phi = 0$ (instead of $\phi = \frac{\pi}{4}$) when

$$|I - 1| + |Q| < \left| I - \frac{\sqrt{2}}{2} \right| + \left| Q - \frac{\sqrt{2}}{2} \right|. \tag{3.6}$$

To solve this inequality, three intervals appear according to the value of I, which are $I < \frac{\sqrt{2}}{2}$, $\frac{\sqrt{2}}{2} \leq I < 1$, and $1 \leq I$. The same analysis appears when dealing with the decision boundaries between $\phi = \frac{\pi}{4}$ and $\phi = \frac{\pi}{2}$, but the intervals appear according to the value of Q. Note that the region near the origin $(0, 0)$ is a conflict zone between

$\phi = 0$ and $\phi = \frac{\pi}{2}$ which needs to be studied separately. Near the origin, (3.5) can be simplified, and we decide $\phi = 0$ when $Q < I$. Finally, the decision boundaries between $\phi = 0$, $\phi = \frac{\pi}{4}$, and $\phi = \frac{\pi}{2}$, can be summarized in Table 3.1. The symmetric

Table 3.1: Decision Regions of 8PSK using ML detector in Laplace noise

$I \in$	$[0, \frac{\sqrt{2}-1}{2}]$	$[\frac{\sqrt{2}-1}{2}, \frac{1}{2}]$	$[\frac{1}{2}, \frac{\sqrt{2}}{2}]$	$[\frac{\sqrt{2}}{2}, 1]$	$[1, +\infty[$
$\phi = 0$	$Q < I$	$Q < \frac{\sqrt{2}-1}{2}$	$Q < \frac{\sqrt{2}-1}{2}$	$Q < I - \frac{1}{2}$	$Q < \frac{1}{2}$
$\phi = \frac{\pi}{4}$	$\varnothing$	$\frac{\sqrt{2}-1}{2} \leq Q < I + \frac{1}{2}$	$\frac{\sqrt{2}-1}{2} \leq Q$	$I - \frac{1}{2} \leq Q$	$\frac{1}{2} \leq Q$
$\phi = \frac{\pi}{2}$	$Q \geq I$	$I + \frac{1}{2} \leq Q$	$\varnothing$	$\varnothing$	$\varnothing$

of these decision boundaries relative to the I axis and Q axis, constructs the decision regions of the remaining 3 quarters of the plan to get the decision boundaries for all symbols. These boundaries are drawn in Fig. 3.1.

3.1.2.2 General MPSK

The analysis of the decision boundaries in the general case of MPSK is more complicated. To simplify the procedure, we can find first the decision region of an angle ϕ and its complementary angle $\frac{\pi}{2} - \phi$ together (for example (S_0 and S_4) and (S_1 and S_3) in Fig. 3.3). Then the boundary between these two angle is the first bisector (line with equation $Q = I$). More specifically, it is easier to begin by finding the decision boundary between two adjacent angles ϕ and θ lying between 0 and $\frac{\pi}{4}$ with $\phi > \theta$. Hence to decide ϕ, condition (3.5) should be satisfied. In more details

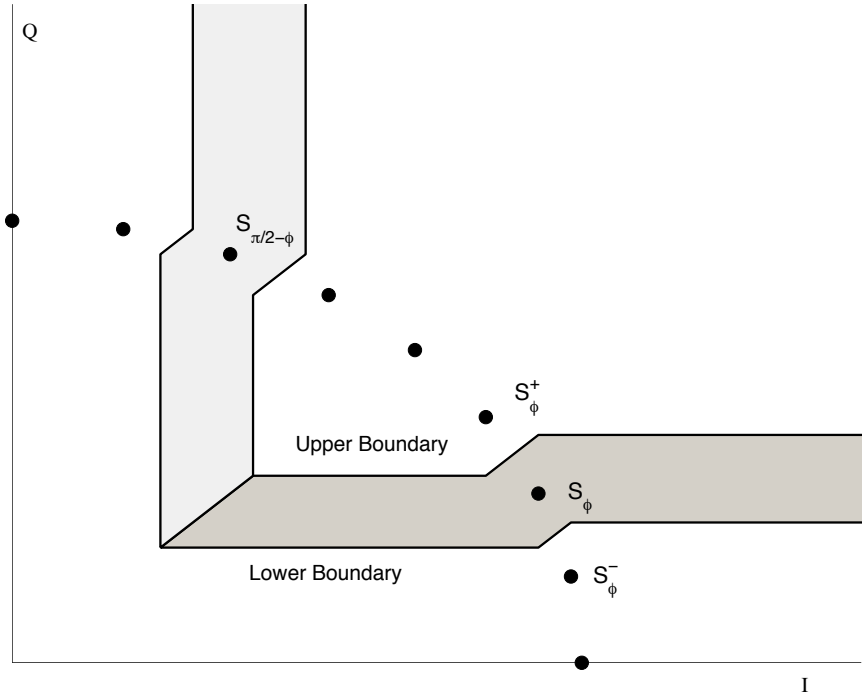

Figure 3.2: Decision regions of two complementary angles ϕ and $\frac{\pi}{2} - \phi$.

the decision between ϕ and θ can be summarized as follows

$$\begin{cases} \text{If} \quad I \in [\frac{c_\phi + s_\phi + s_\theta - c_\theta}{2}, c_\phi] & \begin{cases} \theta \text{ if} \quad Q < \frac{c_\phi + s_\phi + s_\theta - c_\theta}{2} \\ \phi \text{ if} \quad Q \geq \frac{c_\phi + s_\phi + s_\theta - c_\theta}{2} \end{cases} \\ \text{if} \quad I \in [c_\phi, c_\theta] & \begin{cases} \theta \text{ if} \quad Q < I + \frac{s_\theta + s_\phi - c_\theta - c_\phi}{2} \\ \phi \text{ if} \quad Q \geq I + \frac{s_\theta + s_\phi - c_\theta - c_\phi}{2} \end{cases} \\ \text{if} \quad I \in [c_\theta, +\infty[& \begin{cases} \theta \text{ if} \quad Q < \frac{s_\theta + c_\theta + s_\phi - c_\phi}{2} \\ \phi \text{ if} \quad Q \geq \frac{s_\theta + c_\theta + s_\phi - c_\phi}{2} \end{cases} \end{cases}, \tag{3.7}$$

where $c_x = \cos(x)$ and $s_x = \sin(x)$ for any angle x.

Given the previous analysis, the decision boundaries of ϕ and $\frac{\pi}{2} - \phi$ are described in Fig. 3.2. In fact, in Fig. 3.2 the lower boundary (between S^-_ϕ with angle ϕ^- and S^+_ϕ

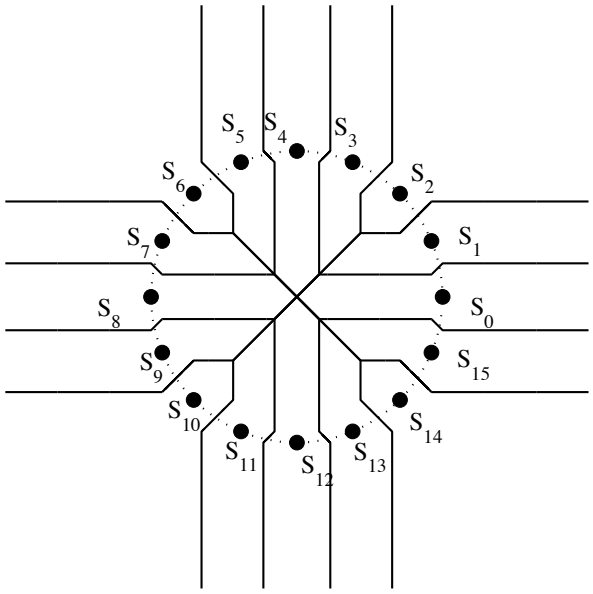

Figure 3.3: Signal constellation and decision regions using the ML rule for 16-PSK.

with angle ϕ^+) is obtained with substituting θ by ϕ^- in (3.7), where the upper boundary is obtained with replacing ϕ by ϕ^+ and θ by ϕ in (3.7). In addition, the image of the lower and the upper boundaries by the axial symmetry, with axe the first bisector, represent the decision boundaries corresponding to $\frac{\pi}{2} - \phi$. A full illustration of 16-PSK is presented in Fig. 3.3.

As shown in the previous example (8-PSK), the construction of the decision boundaries in L_1 norm is complicated, especially for higher M $(16, 32, 64...)$ which of course leads to more complications in the SER calculation. However, the usual minimum euclidian distance presents a simple detector which leads to less complicated SER computations and final expressions.

3.1.3 Detection with L_2 Norm

When the receivers assume that the additional noise is Gaussian, while it is Laplace in reality, the receiver uses the minimum euclidian distance detector instead of the L_1 norm detector. Therefore, it is necessary to study the behavior of the model presented above using the MD detector (L_2 norm detector) and compare the system performance of both detectors in presence of additive Laplace noise.

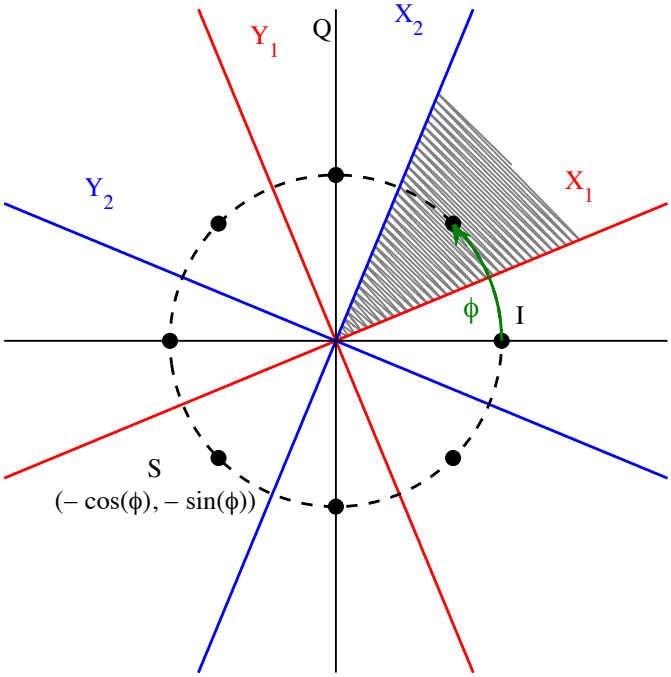

Figure 3.4: Signal constellation and decision regions using the L_2 norm for 8-PSK.

To get the decision regions of an MPSK constellation using L_2 norm, we go back to (3.5) and replace the L_1 norm by the L_2 norm. In this case, decide ϕ if

$$|I - \cos(\phi)|^2 + |Q - \sin(\phi)|^2 < |I - \cos(\theta)|^2 + |Q - \sin(\theta)|^2 . \tag{3.8}$$

The decision region of ϕ lies in the part of the plan between the two angles $\phi - \frac{\pi}{M}$

and $\phi + \frac{\pi}{M}$. Fig.3.4 presents the detection zones for an example of 8-PSK. It is clear that these detection zones are less complex than those presented in Fig.3.1. The axis (X_1, Y_1) and (X_2, Y_2) are a rotational transformation of (I, Q) and are used in the next section.

3.2 Conditional SER of M-PSK

As the previous section, we will compute the conditional SER using both detectors.

3.2.1 SER using L_1 Norm Detector

3.2.1.1 SER of 8-PSK

From the general analysis given in Sec. 3.1.2 and the decision boundaries presented in Table 3.1, the SER can be obtained from the probability of correct detection. In fact the probability of correct detection of ϕ can be evaluated as

$$\mathrm{P_c}(\phi|\gamma) = \int_{\text{Detection zone of } \phi} f_{IQ}(I, Q|\phi, \gamma) dI dQ. \tag{3.9}$$

Replace the detection zone and PDF of (I, Q), we get the probability of correct detection of each symbol. The total probability of error can be obtained as

$$\begin{aligned} \Pr(e|\gamma) &= 1 - \mathrm{P_c}(\gamma) = 1 - \frac{1}{8}\sum_{k=0}^{7} \mathrm{P_c}\left(\frac{2k\pi}{8}\middle|\,\gamma\right) \\ &= \frac{1}{8}\left[4\left(2 + (\sqrt{2}-1)\sqrt{\gamma}\right)\mathrm{e}^{-\sqrt{\gamma/2}} + \left(-1 + (2-\sqrt{2})\sqrt{\gamma}\right)\mathrm{e}^{-\sqrt{2\gamma}}\right]. \end{aligned} \tag{3.10}$$

A generalization of this result is developed in the next subsection.

3.2.1.2 SER of General M-PSK

To compute the SER for general MPSK constellation ($M \geq 8$), we proceed like in the previous special case by computing first the probability of correct detection and the probability of error of each symbol. The total SER is then obtained as the mean of all of the probability of error per symbol. As the decision regions are symmetric relative to the first bisector, we can limit our interest to the symbols with angles lie between 0 and $\frac{\pi}{4}$. The two limit cases, such that 0 and $\frac{\pi}{4}$, can be treated separately since their angles are known. Hence, using the decision region presented in subsection 3.1.2.2, the probability of error of $\phi = 0$ can be evaluated as

$$P_e(0,\gamma) = 1 - 2\gamma \left(\int_0^t \int_0^I e^{-2\sqrt{\gamma}(1-I+Q)} dQdI + \int_t^{\cos(2\theta)} \int_0^t e^{-2\sqrt{\gamma}(1-I+Q)} dQdI \right.$$
$$\left. + \int_{\cos(2\theta)}^1 \int_0^{I+t-\cos(2\theta)} e^{-2\sqrt{\gamma}(1-I+Q)} dQdI + \int_1^\infty \int_0^{t+1-\cos(2\theta)} e^{-2\sqrt{\gamma}(I-1+Q)} dQdI \right), \tag{3.11}$$

where $t = \frac{1}{2}\left(\cos(2\theta) + \sin(2\theta) - 1\right)$, and $\theta = \pi/M$.

In the same way, for $\phi = \frac{\pi}{4}$ the PDF of (I, Q) is defined by

$$f_{IQ}(I,Q) = \gamma e^{-2\sqrt{\gamma}\left(|I-\frac{\sqrt{2}}{2}|+|Q-\frac{\sqrt{2}}{2}|\right)}.$$

Thus the probability of error of $\phi = \frac{\pi}{4}$ can be expressed as

$$\begin{aligned} P_e(\phi = \frac{\pi}{4}, \gamma) = 1 - \gamma \Bigg(& \int_{\frac{\sqrt{2}-u+v}{2}}^{\frac{\sqrt{2}}{2}} \int_{\frac{\sqrt{2}-u+v}{2}}^{\frac{\sqrt{2}}{2}} e^{2\sqrt{\gamma}\left(I+Q-\sqrt{2}\right)} dQdI \\ & + \int_{\frac{\sqrt{2}-u+v}{2}}^{\frac{u+v}{2}} \int_{\frac{\sqrt{2}}{2}}^{I+\frac{u-v}{2}} e^{2\sqrt{\gamma}(I-Q)} dQdI + \int_{\frac{u+v}{2}}^{\frac{\sqrt{2}}{2}} \int_{\frac{\sqrt{2}}{2}}^{+\infty} e^{2\sqrt{\gamma}(I-Q)} dQdI \\ & + \int_{\frac{\sqrt{2}}{2}}^{u} \int_{I+\frac{v-u}{2}}^{\frac{\sqrt{2}}{2}} e^{2\sqrt{\gamma}(Q-I)} dQdI + \int_{u}^{+\infty} \int_{\frac{u+v}{2}}^{\frac{\sqrt{2}}{2}} e^{2\sqrt{\gamma}(Q-I)} dQdI \\ & + \int_{\frac{\sqrt{2}}{2}}^{+\infty} \int_{\frac{\sqrt{2}}{2}}^{+\infty} e^{-2\sqrt{\gamma}(I+Q)-\sqrt{2}} dQdI \Bigg), \end{aligned} \tag{3.12}$$

where $u = \cos(\frac{\pi}{4} - \frac{2\pi}{M})$ and $v = \sin(\frac{\pi}{4} - \frac{2\pi}{M})$. Finally, evaluating the above integrals and using algebraic simplifications and trigonometric formulas, (3.11) and (3.12) can be simplified to

$$\begin{aligned} P_e(0,\gamma) = & \sqrt{\gamma} \sin\left(\frac{\pi}{M}\right) \cos\left(\frac{\pi}{M} + \frac{\pi}{4}\right) \mathrm{e}^{-\sqrt{2\gamma}} \\ & + \left(1 + \sqrt{2\gamma} \sin\left(\frac{\pi}{M}\right)^2\right) \mathrm{e}^{-2\sin(\frac{\pi}{M})\cos\left(\frac{\pi}{M}-\frac{\pi}{4}\right)\sqrt{\gamma}} \\ P_e\left(\frac{\pi}{4}, \gamma\right) = & -\frac{1}{4} \mathrm{e}^{-2\sin(\frac{2\pi}{M})\sqrt{\gamma}} \\ & + \left(1 + \sqrt{2\gamma} \sin\left(\frac{\pi}{M}\right) \cos\left(\frac{\pi}{M} + \frac{\pi}{4}\right)\right) \mathrm{e}^{-\sin(\frac{2\pi}{M})\sqrt{\gamma}}. \end{aligned} \tag{3.13}$$

On the other hand, the probability of error of other symbols is more complicated. For a general symbol i.e. angle $\phi = \frac{2k\pi}{M}$, lies between $\frac{2(k-1)\pi}{M}$ and $\frac{2(k+1)\pi}{M}$ for $1 \leq k \leq \frac{M}{8} - 1$, the probability of error can be expressed in terms of cosine and sine of these angles. For that let us define the series $c_k = \cos(\frac{2k\pi}{M})$, and $s_k = \sin(\frac{2k\pi}{M})$. A simple integration of the PDF of the received signal (I, Q) over the decision region

of ϕ gives the expression in (3.14)

$$\begin{aligned}
P_e(\frac{2k\pi}{M},\gamma) = & \int_{\frac{c_k+s_k+s_{k-1}-c_{k-1}}{2}}^{s_k} \int_{\frac{c_k+s_k+s_{k-1}-c_{k-1}}{2}}^{I} e^{2\sqrt{\gamma}(I-c_k+Q-s_k)} dQdI \\
& + \int_{s_k}^{c_k} \int_{\frac{c_k+s_k+s_{k-1}-c_{k-1}}{2}}^{s_k} e^{2\sqrt{\gamma}(I-c_k+Q-s_k)} dQdI \\
& + \int_{s_k}^{\frac{c_{k+1}+s_{k+1}+s_k-c_k}{2}} \int_{s_k}^{I} e^{2\sqrt{\gamma}(I-c_k-Q+s_k)} dQdI \\
& + \int_{\frac{c_{k+1}+s_{k+1}+s_k-c_k}{2}}^{c_k} \int_{s_k}^{\frac{c_{k+1}+s_{k+1}+s_k-c_k}{2}} e^{2\sqrt{\gamma}(I-c_k-Q+s_k)} dQdI \\
& + \int_{c_{k+1}}^{c_k} \int_{\frac{c_{k+1}+s_{k+1}+s_k-c_k}{2}}^{I+\frac{s_{k+1}-c_{k+1}+s_k-c_k}{2}} e^{2\sqrt{\gamma}(I-c_k-Q+s_k)} dQdI \\
& + \int_{c_k}^{c_{k-1}} \int_{I+\frac{s_k-c_k+s_{k-1}-c_{k-1}}{2}}^{\frac{s_k-c_k+s_{k-1}+c_{k-1}}{2}} e^{2\sqrt{\gamma}(-I+c_k+Q-s_k)} dQdI \\
& + \int_{c_k}^{+\infty} \int_{\frac{s_k-c_k+s_{k-1}+c_{k-1}}{2}}^{s_k} e^{2\sqrt{\gamma}(-I+c_k+Q-s_k)} dQdI \\
& + \int_{c_k}^{+\infty} \int_{s_k}^{\frac{c_k+s_k+s_{k+1}-c_{k+1}}{2}} e^{2\sqrt{\gamma}(-I+c_k-Q+s_k)} dQdI. \qquad (3.14)
\end{aligned}$$

By computing these integrals and making some algebraic and trigonometric operation, P_e can be written in a simpler closed form

$$\begin{aligned}
P_e(\tfrac{2k\pi}{M},\gamma) = & \quad \frac{1}{2}\left[\mathrm{e}^{-2\delta\cos\left((2k-1)\theta-\frac{\pi}{4}\right)\sqrt{\gamma}}\left(1+\sqrt{2\gamma}\delta\sin\left((2k-1)\theta\right)\right)\right. \\
& \left. +\mathrm{e}^{-2\delta\cos\left((2k+1)\theta-\frac{\pi}{4}\right)\sqrt{\gamma}}\left(1+\sqrt{2\gamma}\delta\sin\left((2k+1)\theta\right)\right)\right] \\
& +\frac{1}{8}\left[\mathrm{e}^{-2\cos\left(2k\theta+\frac{\pi}{4}\right)\sqrt{\gamma}}\left(1+4\sqrt{\gamma}\delta\cos\left((2k+1)\theta+\frac{\pi}{4}\right)\right)\right. \\
& \left. -\mathrm{e}^{-2\cos\left(2(k-1)\theta+\frac{\pi}{4}\right)\sqrt{\gamma}}\right], \qquad (3.15)
\end{aligned}$$

where $\delta = \sin(\theta)$.

Assembling those expressions, the total symbol error rate is the average of the

probability of error of all symbols which can be written as

$$\Pr(e|\gamma) = \frac{4}{M}\left[P_e(0,\gamma) + 2\sum_{k=1}^{\frac{M}{8}-1} P_e\left(2k\theta,\gamma\right) + P_e\left(\frac{\pi}{4},\gamma\right)\right]. \tag{3.16}$$

Note that the SER of the previous special case (8-PSK) is included in this generic expression and equal to

$$\Pr(e|\gamma) = \frac{1}{2}\left[P_e(0,\gamma) + P_e\left(\frac{\pi}{4},\gamma\right)\right]. \tag{3.17}$$

The expression given in (3.16) does not cover the special cases of QPSK (4-PSK) and BPSK (2-PSK) because the decision region analysis, presented above, is constructed for $M \geq 8$. These two cases are very simple to deal because the decision region using L_1 norm is the same as the decision region using L_2 norm. Therefore, the SER of these special cases are presented in the next subsection which focuses on the SER of M-PSK using the L_2 norm detector.

3.2.2 SER using L_2 Norm Detector

The general analysis of SER of MPSK constellation in Gaussian noise environment was presented in [52]. We use, in what follows, a similar analysis to compute the SER of MPSK in LN environments. Assume that $s = (s_I, s_Q) = (-\cos(\phi), -\sin(\phi))$ is sent. The objective is to compute the probability of error detection of s for general ϕ. To do so, consider two rotation of coordinates, i.e. rotation transformation from (I, Q) to (X_1, Y_1) with rotation angle $\phi - \theta$, and from (I, Q) to (X_2, Y_2) with rotation angle $\phi + \theta$ (see Fig.3.4). Using two transformation matrices,

we get the new basis from the initial basis as

$$\begin{bmatrix} X_1 \\ Y_1 \end{bmatrix} = \begin{bmatrix} \cos(\phi-\theta) & \sin(\phi-\theta) \\ -\sin(\phi-\theta) & \cos(\phi-\theta) \end{bmatrix} \begin{bmatrix} I \\ Q \end{bmatrix}, \tag{3.18}$$

and

$$\begin{bmatrix} X_2 \\ Y_2 \end{bmatrix} = \begin{bmatrix} \cos(\phi+\theta) & \sin(\phi+\theta) \\ -\sin(\phi+\theta) & \cos(\phi+\theta) \end{bmatrix} \begin{bmatrix} I \\ Q \end{bmatrix}. \tag{3.19}$$

From Fig.3.4, the SER can be expressed as

$$Pe(\phi,\gamma) = \Pr(Y_1 \geq 0) + \Pr(Y_2 \leq 0) - \Pr(Y_1 \geq 0, Y_2 \leq 0). \tag{3.20}$$

Thus, to compute the SER for MPSK, we have to find the PDF of Y_1 and Y_2 separately and also their joint PDF. From (3.18) and (3.19), Y_1 and Y_2 appear as the sum of two independent Laplace random variables with means $\mathbb{E}[Y_1] = -\sin\theta$, $\mathbb{E}Y_2] = \sin\theta$, and variances $\sigma^2_{Y_1} = \sigma^2_{Y_2} = \frac{1}{2\gamma}$, respectively.

Let us consider two independent Laplace random variables

$(Z_1, Z_2) \sim (\mathcal{L}(0,\sigma_1), \mathcal{L}(0,\sigma_2))$, and suppose $Y = Z_1 + Z_2$. The PDF of Y is given in [**?**, Eq. (3.3.23)] as

$$f_Y(y) = \begin{cases} \frac{1}{2\sigma}\left(\frac{1}{\sqrt{2}} + \frac{|y|}{\sigma}\right) e^{-\sqrt{2}\frac{|y|}{\sigma}} & \text{if } \sigma = \sigma_1 = \sigma_2 \\ \frac{1}{\sqrt{2}(\sigma_1^2 - \sigma_2^2)}\left(\sigma_1 e^{-\sqrt{2}\frac{|y|}{\sigma_1}} - \sigma_2 e^{-\sqrt{2}\frac{|y|}{\sigma_2}}\right) & \text{if } \sigma_1 \neq \sigma_2. \end{cases} \tag{3.21}$$

This property can be extended to the non zero mean case by a centralization of the random variable $Y' = Y - \mathbb{E}[Y]$. Consequently, the PDF of Y_1 and Y_2 can be

obtained as follows

$$\begin{aligned} f_{Y_1}(y) &= \frac{\sqrt{\gamma}}{\cos 2(\phi-\theta)}\left(|\cos(\phi-\theta)|e^{-\frac{2\sqrt{\gamma}|y+sin\theta|}{|\cos(\phi-\theta)|}} - |\sin(\phi-\theta)|e^{-\frac{2\sqrt{\gamma}|y+sin\theta|}{|\sin(\phi-\theta)|}}\right) \\ f_{Y_2}(y) &= \frac{\sqrt{\gamma}}{\cos 2(\phi+\theta)}\left(|\cos(\phi+\theta)|e^{-\frac{2\sqrt{\gamma}|y-sin\theta|}{|\cos(\phi+\theta)|}}|\sin(\phi+\theta)|e^{-\frac{2\sqrt{\gamma}|y-sin\theta|}{|\sin(\phi+\theta)|}}\right). \end{aligned} \tag{3.22}$$

Using (3.22), the probabilities $\Pr(Y_1 \geq 0)$ and $\Pr(Y_2 \leq 0)$ in (3.20) can be easily obtained as

$$\begin{aligned} \Pr(Y_1 \geq 0) &= \int_0^\infty f_{Y_1}(y_1)dy_1 \qquad (3.23) \\ &= \frac{1}{2\cos 2(\phi-\theta)}\left(\cos^2(\phi-\theta)e^{\frac{-2\sin\theta}{|\cos(\phi-\theta)|}\sqrt{\gamma}} - \sin^2(\phi-\theta)e^{\frac{-2\sin\theta}{|\sin(\phi-\theta)|}\sqrt{\gamma}}\right) \\ \Pr(Y_2 \leq 0) &= \int_0^\infty f_{Y_2}(y_2)dy_2 \qquad (3.24) \\ &= \frac{1}{2\cos 2(\phi+\theta)}\left(\cos^2(\phi+\theta)e^{\frac{-2\sin\theta}{|\cos(\phi+\theta)|}\sqrt{\gamma}} - \sin^2(\phi+\theta)e^{\frac{-2\sin\theta}{|\sin(\phi+\theta)|}\sqrt{\gamma}}\right). \end{aligned}$$

Now, we have to evaluate the probability $\Pr(Y_1 \geq 0, Y_2 \leq 0)$ in (3.20) and this represents the probability of the shaded region in Fig.3.4. First we have to find the joint PDF of (Y_1, Y_2). From (3.18) and (3.19), (Y_1, Y_2) can be written as a linear transformation of (I, Q) as

$$\begin{bmatrix} Y_1 \\ Y_2 \end{bmatrix} = \begin{bmatrix} -\sin(\phi-\theta) & \cos(\phi-\theta) \\ -\sin(\phi+\theta) & \cos(\phi+\theta) \end{bmatrix} \begin{bmatrix} I \\ Q \end{bmatrix} = A \begin{bmatrix} I \\ Q \end{bmatrix} \tag{3.25}$$

Using this change of variable, the joint PDF of (Y_1, Y_2) can be obtained from the joint PDF of (I, Q) (3.4) using the transformation formula

$$\begin{aligned} f_{Y_1Y_2}(y_1, y_2) &= \frac{1}{\det(A)} f_{IQ}(A^{-1}[y_1, y_2]^t) \\ &= \frac{\gamma}{\sin 2\theta} e^{-\frac{2\sqrt{\gamma}}{\sin 2\theta}T}, \end{aligned} \tag{3.26}$$

where

$$\begin{aligned} T &= |\cos(\phi+\theta)(y_1+\sin\theta)-\cos(\phi-\theta)(y_2-\sin\theta)| \\ &+|\sin(\phi+\theta)(y_1+\sin\theta)-\sin(\phi-\theta)(y_2-\sin\theta)|. \end{aligned}$$

Once we obtain $f_{Y_1Y_2(y_1,y_2)}$, the probability $\Pr(Y_1 \geq 0, Y_2 \leq 0)$ can be easily obtained as

$$\begin{aligned} \Pr(Y_1 \geq 0, Y_2 \leq 0) &= \int_0^{\infty}\int_{-\infty}^{0} f_{Y_1Y_2}(y_1,y_2)dy_2dy_1 \\ &= \begin{cases} \frac{\sin\theta}{2(\cos\theta+\sin\theta)}e^{-2\sqrt{\gamma}} \text{ if } \phi = 0 \\ \\ \frac{\sin 2\theta}{4(\cos 2\theta+\sin 2\phi)}e^{-2\sqrt{\gamma}(\cos\phi+\sin\phi)} \text{ if } \phi > 0. \end{cases} \end{aligned} \tag{3.27}$$

At this point, by substituting (3.23),(3.24), and (3.27) into (3.20), we get the probability of error of $s = (-\cos\phi, -\sin\phi)$ for general $\phi \in [0, \frac{\pi}{2}[$, $Pe(\gamma,\phi)$

$$\begin{cases} Pe\,(\gamma,0) &= \frac{1}{1-\tan(\theta)^2}e^{-\tan(\theta)\sqrt{2\gamma}} - \frac{\tan(\theta)}{2(1-\tan(\theta))}e^{-\sqrt{2\gamma}} \\ Pe\,(\gamma,\phi) &= \frac{1}{2\cos 2(\phi-\theta)}\left(\cos^2(\phi-\theta)e^{\frac{-2\sin\theta}{\cos(\phi-\theta)}\sqrt{\gamma}}\right. \\ &\quad \left. -\sin^2(\phi-\theta)e^{\frac{-2\sin\theta}{\sin(\phi-\theta)}\sqrt{\gamma}}\right) \\ &\quad +\frac{1}{2\cos 2(\phi+\theta)}\left(\cos^2(\phi+\theta)e^{\frac{-2\sin\theta}{\cos(\phi+\theta)}\sqrt{\gamma}}\right. \\ &\quad \left. -\sin^2(\phi+\theta)e^{\frac{-2\sin\theta}{\sin(\phi+\theta)}\sqrt{\gamma}}\right) \\ &\quad -\frac{\sin 2\theta}{4(\cos 2\theta+\sin 2\phi)}e^{-2(\cos\phi+\sin\phi)\sqrt{\gamma}}. \end{cases} \tag{3.28}$$

As the symbols are equiprobable and distributed uniformly on the unit circle and from the symmetric properties of the PDF of Laplacian random variable, we can limit ourselves to the symbols lying between 0 and $\frac{\pi}{2}$ so $0 \leq \phi < \frac{\pi}{2}$. In addition, ϕ can take the values $\phi = \frac{2k\pi}{M}$, for $k = 0, 1 \ldots \frac{M}{4} - 1$, and the total SER can be expressed as

$$\Pr(e|\gamma) = \frac{4}{M}\sum_{k=0}^{\frac{M}{4}-1} Pe\left(\frac{2k\pi}{M},\gamma\right). \tag{3.29}$$

Finally, combining (3.28) and (3.29) with $\theta = \pi/M$, and using some algebraic

simplifications, it can be shown that the general closed-form expression for the conditional SER of MPSK over LN using the L_2 norm detector, $\Pr(e|\gamma)$, can be expressed as

$$\Pr(e|\gamma) = \frac{8}{M}\sum_{k=0}^{\frac{M}{4}-1} g(k,\gamma) + \frac{2\tan(\theta)^2 e^{-2\sqrt{\gamma}}}{M(1-\tan(\theta)^2)}, \tag{3.30}$$

where

$$\begin{aligned} g(k,\gamma) =& \frac{1}{2\cos\left(2(2k+1)\theta\right)}\left(\cos\left((2k+1)\theta\right)^2 e^{\frac{-2p\sqrt{\gamma}}{\cos((2k+1)\theta)}} - \sin\left((2k+1)\theta\right)^2 e^{\frac{-2p\sqrt{\gamma}}{\sin((2k+1)\theta)}}\right) \\ & - \frac{\sin(2\theta)}{8\left(\cos(2\theta)+\sin(4k\theta)\right)} e^{-2\sqrt{2}\cos\left(2k\theta-\frac{\pi}{4}\right)\sqrt{\gamma}}, \end{aligned} \tag{3.31}$$

and θ defined above as $\theta = \frac{\pi}{M}$. For $M \geq 8$, more simplification can be made using some of the properties of $g(k,\gamma)$. Hence (3.30) can be written compactly as

$$\begin{aligned} \Pr(e|\gamma) = \; & \frac{16}{M}\sum_{k=0}^{\frac{M}{8}-1} g(k,\gamma) \\ & -\frac{1}{M}\tan\left(\frac{\pi}{M}\right)\left(e^{-2\sqrt{2\gamma}} - \frac{2}{1-\tan(\frac{\pi}{M})}e^{-2\sqrt{\gamma}}\right). \end{aligned} \tag{3.32}$$

The above expression is valid for $M \geq 8$. However, the special case of $M = 4$ (i.e. $\theta \to \frac{\pi}{4}$) appears as a limit case of (3.30) where the SER can be expressed as

$$\Pr(e|\gamma) = \left(\frac{3}{4} + \sqrt{\gamma}\right) e^{-2\sqrt{\gamma}}. \tag{3.33}$$

For $M = 2$, the conditional SER can be evaluated from the original expression (3.20) as

$$\Pr(e|\gamma) = \frac{1}{2}e^{-2\sqrt{\gamma}} = Q_1(\sqrt{2\gamma}), \tag{3.34}$$

which is the same result found in (2.18) (rcall that $Q_1(x) = \frac{1}{2}e^{-\sqrt{2}x}$). Note, as mentioned at the end of subsection 3.2.1.2, that the results in (3.33) and (3.34) are the same using L_2 or L_1 norm. They will be treated as special cases in the following

section since they can not be included in the generic formula.

Let us focus now on the case of $M \geq 8$. Using some of the properties of $g(k,\gamma)$ (3.30) can be further simplified and written compactly as

$$\Pr(e|\gamma) = \frac{16}{M}\sum_{k=0}^{\frac{M}{8}-1} g(k,\gamma) - \frac{1}{M}\tan\left(\frac{\pi}{M}\right)\left(e^{-2\sqrt{2\gamma}} - \frac{2}{1-\tan(\frac{\pi}{M})}e^{-2\sqrt{\gamma}}\right). \quad (3.35)$$

In fact $g(k,\gamma)$ has the following property

$$g(\frac{M}{4}-k-1,\gamma) = g(k,\gamma) + \sin(2\delta)\left(\frac{e^{-2\sqrt{2}\cos\left(2k\delta-\frac{\pi}{4}\right)\sqrt{\gamma}}}{8\left(\cos(2\delta)+\sin(4k\delta)\right)} - \frac{e^{-2\sqrt{2}\cos\left(2(k+1)\delta-\frac{\pi}{4}\right)\sqrt{\gamma}}}{8\left(\cos(2\delta)+\sin(4(k+1)\delta)\right)}\right).$$

Thus the sum of $g(k,\gamma)$ can be simplified as follows

$$\begin{aligned}
\sum_{k=0}^{\frac{M}{4}-1} g(k,\gamma) &= \sum_{k=0}^{\frac{M}{8}-1} g(k,\gamma) + \sum_{k=\frac{M}{8}}^{\frac{M}{4}-1} g(k,\gamma) \\
&= \sum_{k=0}^{\frac{M}{8}-1} g(k,\gamma) + \sum_{l=0}^{\frac{M}{8}-1} g(\frac{M}{4}-l-1,\gamma) \\
&= 2\sum_{k=0}^{\frac{M}{8}-1} g(k,\gamma) + \sin(2\delta) \\
&\quad \times \sum_{k=0}^{\frac{M}{8}-1}\left(\frac{e^{-2\sqrt{2}\cos\left(2k\delta-\frac{\pi}{4}\right)\sqrt{\gamma}}}{8\left(\cos(2\delta)+\sin(4k\delta)\right)} - \frac{e^{-2\sqrt{2}\cos\left(2(k+1)\delta-\frac{\pi}{4}\right)\sqrt{\gamma}}}{8\left(\cos(2\delta)+\sin(4(k+1)\delta)\right)}\right) \\
&= 2\sum_{k=0}^{\frac{M}{8}-1} g(k,\gamma) + \sin(2\delta) \\
&\quad \times \left(\sum_{k=0}^{\frac{M}{8}-1}\frac{e^{-2\sqrt{2}\cos\left(2k\delta-\frac{\pi}{4}\right)\sqrt{\gamma}}}{8\left(\cos(2\delta)+\sin(4k\delta)\right)} - \sum_{k=1}^{\frac{M}{8}}\frac{e^{-2\sqrt{2}\cos\left(2k\delta-\frac{\pi}{4}\right)\sqrt{\gamma}}}{8\left(\cos(2\delta)+\sin(4k\delta)\right)}\right) \\
&= 2\sum_{k=0}^{\frac{M}{8}-1} g(k,\gamma) + \frac{\tan(2\delta)}{8}e^{-2\sqrt{\gamma}} - \frac{\sin(2\delta)}{8(\cos(2\delta)+1)}e^{-2\sqrt{2\gamma}}. \quad (3.36)
\end{aligned}$$

3.2.3 Comparison between the SER using L_1 Norm and L_2 Norm Detectors

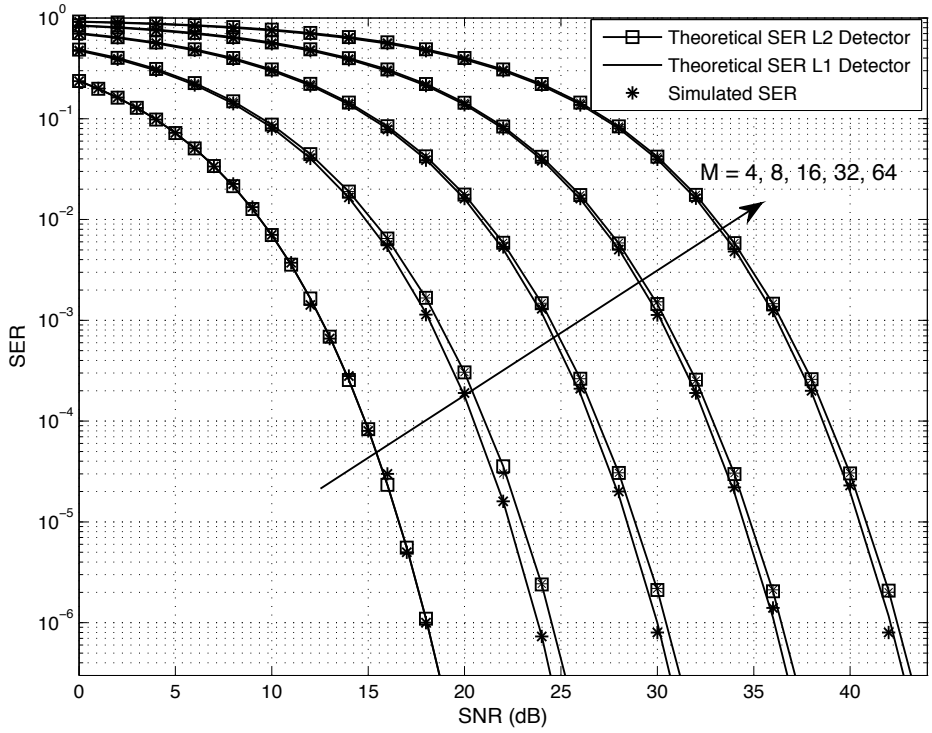

Figure 3.5: Difference between the L_1 norm and L_2 norm detectors in AWLN channel.

In Fig. 3.5 we draw the conditional SER for different size of constellation versus the instantaneous SNR for the ML detector and the MD detector. From the curves it is clear that the system performance degrades by increasing the constellation size M. Moreover, as mentioned before, the results in the QPSK case are the same using the L_1 norm or the L_2 norm detectors. For $M \geq 8$, the difference between the SER of both detectors is small with an advantage to the L_1 norm (solid lines), ML detector, as expected. In addition, it should be noted that by increasing M, the SNR gap for a fixed SER between the two detectors becomes smaller (from 0.6 dB for 8-PSK to 0.2 dB for 64-PSK at SER= 10^{-5}). To explain this fact, Fig. 3.6 represents the

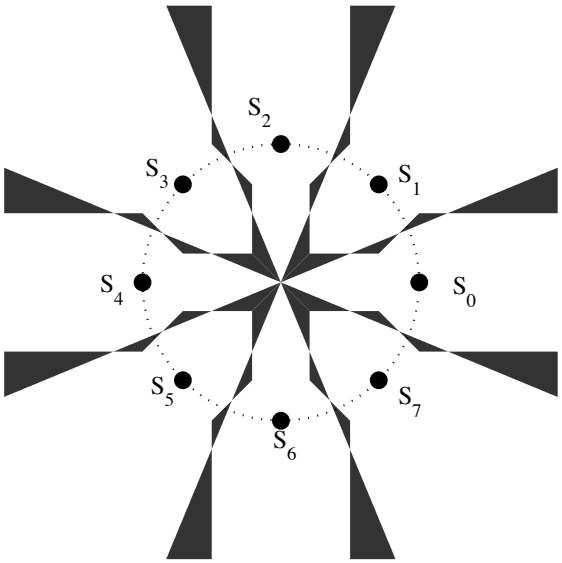

Figure 3.6: Intersection between decision regions created by the ML and MD detectors for 8-PSK.

intersection zones between the decision regions created by ML and MD detectors for 8-PSK (these zones are colored in black). From Fig. 3.6, we note that the area of different decisions between the two detectors is very low compared to the remaining surface, which explains why the performance gap is small. As a consequence of these results, the use of L_2 norm in detection of signals subject to AWLN, by wrong assumptions of the noise distribution or simplification of detector, does not affect harmfully the performance of the system especially for higher size of the constellation. In the next section, we include the multiplicative fading noise in our model to quantify the impact of fading on the performance of MPSK in presence of additive Laplace noise.

3.3 Average SER of MPSK

3.3.1 General Formula

All the analysis presented above are conditioned on the fading coefficient, and are as such function of the instantaneous SNR. In the presence of slow fading, the ASER can be obtained by averaging the SER issued from both detectors, (3.16) and (3.30), over the PDF of the SNR γ, $p_\gamma(\gamma)$, yielding

$$\Pr(e) = \int_0^\infty \Pr(e|\gamma) p_\gamma(\gamma)\, d\gamma. \tag{3.37}$$

Two types of integrals appears in the evaluations of the ASER, while the first integral, called $\mathcal{L}(x)$, considers an integral of the product of the PDF of γ, $p_\gamma(\gamma)$, and an exponential, the second integral, named $\mathcal{L}_1(x)$, consist of an integral of the product of the PDF of γ, an exponential function, and square root of γ. More specifically, they are defined as

$$\mathcal{L}(x) = \int_0^\infty p_\gamma(\gamma) e^{-x\sqrt{\gamma}}\, d\gamma, \quad \forall\ x \geq 0 \tag{3.38}$$

$$\mathcal{L}_1(x) = \int_0^\infty \sqrt{\gamma} p_\gamma(\gamma) e^{-x\sqrt{\gamma}}\, d\gamma = -\mathcal{L}'(x),\ \forall\ x \geq 0. \tag{3.39}$$

By derivation of $\mathcal{L}$ with respect to x, we can get easily $\mathcal{L}_1$ which is the opposite of the derivative of $\mathcal{L}$, namely $\mathcal{L}'$. Therefore, the ASER of the MPSK system, computed by L_1 norm or L_2 norm techniques, is expressed in terms of the functions $\mathcal{L}$ and $\mathcal{L}'$ in the next analysis.

3.3.1.1 General Expression using ML detector

The ASER of MPSK constellation using the ML detector can be deduced from the general conditional expression (3.16) and the averaging formula (3.37), the final

ASER expression, for $M \geq 8$, can be presented as

$$\begin{aligned}\mathrm{Pr}_{ML}(e) = \frac{1}{M}\sum_{k=1}^{\frac{M}{8}-1} F(k) - \mathcal{L}\left(2\sin(2\theta)\right) \\ +4\left[\mathcal{L}\left(2p\cos\left(\theta-\frac{\pi}{4}\right)\right) - \sqrt{2}p^2\mathcal{L}'\left(2p\cos\left(\theta-\frac{\pi}{4}\right)\right)\right. \\ \left.-p\cos\left(\theta+\frac{\pi}{4}\right)\mathcal{L}'\left(\sqrt{2}\right) + \mathcal{L}\left(\sin(2\theta)\right) - \sqrt{2}p\cos\left(\theta+\frac{\pi}{4}\right)\mathcal{L}'\left(\sin(2\theta)\right)\right]\end{aligned} \tag{3.40}$$

where the generic function $F(k)$ is expressed as

$$\begin{aligned}F(k) = 4\mathcal{L}\left(2p\cos\left((2k-1)\theta-\frac{\pi}{4}\right)\right) + 4\mathcal{L}\left(2p\cos\left((2k+1)\theta-\frac{\pi}{4}\right)\right) \\ +\mathcal{L}\left(2\cos\left(2k\theta+\frac{\pi}{4}\right)\right) - 4\sqrt{2}p\sin\left((2k-1)\theta\right)\mathcal{L}'\left(2p\cos\left((2k-1)\theta-\frac{\pi}{4}\right)\right) \\ -4p\cos\left((2k+1)\theta+\frac{\pi}{4}\right)\mathcal{L}'\left(2\cos\left(2k\theta+\frac{\pi}{4}\right)\right) - \mathcal{L}\left(2\cos\left(2(k-1)\theta+\frac{\pi}{4}\right)\right) \\ -4\sqrt{2}p\sin\left((2k+1)\theta\right)\mathcal{L}'\left(2p\cos\left((2k+1)\theta-\frac{\pi}{4}\right)\right).\end{aligned} \tag{3.41}$$

3.3.1.2 General Expression using MD Detector

Using the same method to compute the average probability of error, the ASER of MPSK constellation using MD detector can be expressed, for $M \geq 8$, as

$$\mathrm{Pr}_{MD}(e) = \frac{8}{M}\sum_{k=0}^{\frac{M}{4}-1} G(k) + \frac{2\tan(\theta)^2}{M(1-\tan(\theta)^2)}\mathcal{L}(2), \tag{3.42}$$

where

$$\begin{aligned}G(k) = -\frac{\sin(2\theta)}{8\left(\cos(2\theta)+\sin(4k\theta)\right)}\mathcal{L}\left(2\sqrt{2}\cos\left(2k\theta-\frac{\pi}{4}\right)\right) \\ +\frac{1}{2\cos 2(2k+1)\theta}\left[\cos\left((2k+1)\theta\right)^2\mathcal{L}\left(\frac{2\sin(\theta)}{\cos\left((2k+1)\theta\right)}\right)\right. \\ \left.-\sin\left((2k+1)\theta\right)^2\mathcal{L}\left(\frac{2\sin(\theta)}{\sin\left((2k+1)\theta\right)}\right)\right].\end{aligned} \tag{3.43}$$

As mentioned before, this expression is actually valid for $M \geq 4$, since the $M = 4$ case appears as a limit case. In particular, from (3.33), the ASER of QPSK with ML and MD detector can be evaluated as

$$\mathrm{Pr}_{QPSK}(e) = \frac{3}{4}\mathcal{L}(2) - \mathcal{L}'(2). \tag{3.44}$$

Finally, for $M = 2$, from (3.34) the ASER is equal to $\mathrm{Pr}_{BPSK}(e) = \mathcal{L}(2)/2$.
The major remark from the previous analysis is that the ASER, using ML and MD detectors, is fully defined by knowing $\mathcal{L}(\cdot)$ and $\mathcal{L}'(\cdot)$ for the desired type of fading. Consequently, we are focusing on the next subsections on the evaluation of $\mathcal{L}(\cdot)$ and $\mathcal{L}'(\cdot)$ for the case of EGK distribution based on the alternative formula of its PDF given in Sec. 2.1.3.

3.3.2 EGK Fading

Substitute the alternative expression of $p_\gamma(\gamma)$ (2.13) and the expression of the exponential in terms of the FHF [55, Eq. (2.9.4)] in $\mathcal{L}(x)$, and use the identity (2.21) that computes the integral of the product of two FHFs, the integral function $\mathcal{L}(x)$ can be expressed in terms of the FHF as

$$\begin{aligned}\mathcal{L}(x) =& \frac{1}{\Gamma(m_s)\Gamma(m)\gamma}\int_0^\infty e^{-x\sqrt{\gamma}}\mathrm{H}_{0,2}^{2,0}\left[\frac{\beta_s\beta}{\overline{\gamma}}\gamma\,\middle|\,\begin{matrix}\text{——}\\(m_s,\frac{1}{\xi_s}),(m,\frac{1}{\xi})\end{matrix}\right]d\gamma \\ =& \frac{2}{\Gamma(m_s)\Gamma(m)}\mathrm{H}_{1,2}^{2,1}\left[\frac{\beta_s\beta}{\overline{\gamma}x^2}\,\middle|\,\begin{matrix}(1,2)\\(m_s,\frac{1}{\xi_s}),(m,\frac{1}{\xi})\end{matrix}\right].\end{aligned} \tag{3.45}$$

The identity [55, Eq. (2.2.1)] gives the derivative of the FHF, that is used to computed $\mathcal{L}'(\cdot)$ and which is equal to

$$\mathcal{L}'(x) = \frac{-2}{x\Gamma(m_s)\Gamma(m)}\mathrm{H}_{1,2}^{2,1}\left[\frac{\beta_s\beta}{\overline{\gamma}x^2}\,\middle|\,\begin{matrix}(0,2)\\(m_s,\frac{1}{\xi_s}),(m,\frac{1}{\xi})\end{matrix}\right]. \tag{3.46}$$

The results given in (3.45) and (3.46) are valid for the general EGK fading scenario. In the next subsections, we simplify these results for some useful special cases such as the Generalized-K, Generalized Nakagami-m, Nakagami-m, and Rayleigh fading distributions.

3.3.3 Generalized-$\mathcal{K}$ Fading

As mentioned in the previous chapter, the GK fading is obtained by setting $\xi = 1$ and $\xi_s = 1$ in the parameters of the EGK distribution (2.7), and in this case m and m_s become the parameters of the GK distribution. By replacing ξ and ξ_s by their value in (3.45), $\mathcal{L}(\cdot)$ can be re-written as

$$\mathcal{L}(x) = \frac{2}{\Gamma(m_s)\Gamma(m)} \mathrm{H}_{1,2}^{2,1}\left[\frac{mm_s}{\overline{\gamma}x^2}\middle|\begin{matrix}(1,2)\\(m_s,1),(m,1)\end{matrix}\right]. \tag{3.47}$$

Using relation between the FHF and the MGF for rational parameters given in [60, Eq. (8.3.22)], $\mathcal{L}(\cdot)$ can be expressed in terms of the standard MGF as

$$\mathcal{L}(x) = \frac{1}{\Gamma(m_s)\Gamma(m)\sqrt{\pi}} \mathrm{G}_{2,2}^{2,2}\left[\frac{4mm_s}{\overline{\gamma}x^2}\middle|\begin{matrix}1,1/2\\m,m_s\end{matrix}\right]. \tag{3.48}$$

Using the derivative properties of the MGF [60, Eq. (8.2.34)], $\mathcal{L}'(\cdot)$ is evaluated as

$$\mathcal{L}'(x) = \frac{-2}{x\Gamma(m_s)\Gamma(m)\sqrt{\pi}} \mathrm{G}_{2,2}^{2,2}\left[\frac{4mm_s}{\overline{\gamma}x^2}\middle|\begin{matrix}0,1/2\\m,m_s\end{matrix}\right] \tag{3.49}$$

These final expressions in terms of the MGF are less complex than the expressions in terms of the FHF, since the MGF is already a built-in function in MATHEMATICA®.

3.3.4 Generalized Nakagami-m Fading

This type of fading is obtained by setting the quadruplet (m, ξ, m_s, ξ_s) to $(m, \xi, \infty, 1)$ in (2.7). Using the limit property given in (2.27) and the inverse Mellin transform of the extended incomplete Gamma function $\Gamma(\cdot,\cdot,\cdot,\cdot)$ [57, Eq. (6.29)], one can show that

$$\begin{aligned}\mathcal{L}(x) &= \frac{2}{\Gamma(m)}\mathrm{H}_{1,1}^{1,1}\left[\frac{\beta}{\overline{\gamma}x^2}\middle|\begin{matrix}(1,2)\\(m,\frac{1}{\xi})\end{matrix}\right] \\ &= \frac{2\xi}{\Gamma(m)}\left(\frac{\beta}{x^2\overline{\gamma}}\right)^{m\xi}\Gamma\left(2m\xi, 0; \left(\frac{\beta}{x^2\overline{\gamma}}\right)^{\xi}; -2\xi\right).\end{aligned} \tag{3.50}$$

A similar expression of $\mathcal{L}'(\cdot)$ is obtained using the derivative expression of the FHF and the Mellin transform of the extended incomplete Gamma function, its closed form is evaluated as

$$\mathcal{L}'(x) = \frac{-2\xi}{x\Gamma(m)}\left(\frac{\beta}{x^2\overline{\gamma}}\right)^{m\xi}\Gamma\left(1+2m\xi, 0; \left(\frac{\beta}{x^2\overline{\gamma}}\right)^{\xi}; -2\xi\right). \tag{3.51}$$

3.3.5 Nakgami-m Fading

From the previous case, the Nakagami-m fading may be obtained by replacing ξ by 1. By using the special case of the extended incomplete Gamma function [57, Eq. (6.44)], $\mathcal{L}(\cdot)$ can be expressed as

$$\begin{aligned}\mathcal{L}(x) =& \frac{2}{\Gamma(m)}\left(\frac{m}{x^2\overline{\gamma}}\right)^{m}\Gamma(2m, 0; \frac{m}{x^2\overline{\gamma}}; -2) \\ =& \frac{2\Gamma(2m)}{4^m\Gamma(m)}U\left(m, \frac{1}{2}, \frac{\overline{\gamma}x^2}{4m}\right),\end{aligned} \tag{3.52}$$

where $U(\cdot,\cdot,\cdot)$ is the Tricomi confluent hypergeometric function [58, Chapter 13]. Using the derivative of the $U(\cdot,\cdot,\cdot)$ function [58, Eq. (13.4.21)], we get $\mathcal{L}'(\cdot)$ as

$$\mathcal{L}'(x) = -\frac{\Gamma(2m)\overline{\gamma}x}{4^m\Gamma(m)}U\left(m+1,\frac{3}{2},\frac{\overline{\gamma}x^2}{4m}\right). \tag{3.53}$$

Table 3.2: $\mathcal{L}(\cdot)$ for Different Channels

Fading Distribution	$\mathcal{L}(x)$
No Fading	$e^{-x\sqrt{\gamma}}$
Rayleigh	$1-\sqrt{\overline{\gamma}x^2\pi}e^{\frac{\overline{\gamma}x^2}{4}}Q\left(\sqrt{\frac{\overline{\gamma}x^2}{2}}\right)$
Nakagami-m	$\frac{2\Gamma(2m)}{4^m\Gamma(m)}U\left(m,\frac{1}{2},\frac{\overline{\gamma}x^2}{4m}\right)$
Generalized Nakagami-m	$\frac{2}{\Gamma(m)}\mathrm{H}_{1,1}^{1,1}\left[\frac{\beta}{\overline{\gamma}x^2}\middle\vert\begin{matrix}(1,2)\\(m,\frac{1}{\xi})\end{matrix}\right]$ $=\frac{2\xi}{\Gamma(m)}\left(\frac{\beta}{x^2\overline{\gamma}}\right)^{m\xi}\Gamma\left(2m\xi,0;\left(\frac{\beta}{x^2\overline{\gamma}}\right)^{\xi};-2\xi\right)$
Generalized-K	$\frac{1}{\Gamma(m_s)\Gamma(m)\sqrt{\pi}}\mathrm{G}_{2,2}^{2,2}\left[\frac{4mm_s}{\overline{\gamma}x^2}\middle\vert\begin{matrix}1,1/2\\m,m_s\end{matrix}\right]$
EGK	$\frac{2}{\Gamma(m_s)\Gamma(m)}\mathrm{H}_{1,2}^{2,1}\left[\frac{\beta_s\beta}{\overline{\gamma}x^2}\middle\vert\begin{matrix}(1,2)\\(m_s,\frac{1}{\xi_s}),(m,\frac{1}{\xi})\end{matrix}\right]$

3.3.6 Rayleigh Fading

The Rayleigh fading is one of the basic fading models, and is a special case of the Nakagami-m fading be setting $m=1$. Using the special cases of the Hypergeometric function, and an integration by parts, the principal function $\mathcal{L}(\cdot)$ may be simplified in this case to

$$\begin{aligned}\mathcal{L}(x) =& \frac{1}{2}U\left(2,\frac{1}{2},\frac{\overline{\gamma}x^2}{4}\right) = \frac{1}{4}\sqrt{\overline{\gamma}x^2}e^{\frac{\overline{\gamma}x^2}{4}}\Gamma\left(-\frac{1}{2},\frac{\overline{\gamma}x^2}{4}\right)\\ =& 1-\sqrt{\overline{\gamma}x^2\pi}e^{\frac{\overline{\gamma}x^2}{4}}Q\left(\sqrt{\frac{\overline{\gamma}x^2}{2}}\right).\end{aligned} \tag{3.54}$$

Table 3.3: $\mathcal{L}'(\cdot)$ for Different Channels

Fading Distribution	$\mathcal{L}'(x)$
No Fading	$-\sqrt{\overline{\gamma}}e^{-x\sqrt{\overline{\gamma}}}$
Rayleigh	$\frac{1}{2}\overline{\gamma}x - \frac{1}{2}(2+\overline{\gamma}x^2)\sqrt{\frac{\overline{\gamma}\pi}{2}}e^{\frac{\overline{\gamma}x^2}{4}}Q\left(\sqrt{\frac{\overline{\gamma}x^2}{2}}\right)$
Nakagami-m	$-\frac{\Gamma(2m)\overline{\gamma}x}{4^m\Gamma(m)}U\left(m+1,\frac{3}{2},\frac{\overline{\gamma}x^2}{4m}\right)$
Generalized Nakagami-m	$\frac{-2}{x\Gamma(m)}\mathrm{H}_{1,1}^{1,1}\left[\frac{\beta}{\overline{\gamma}x^2}\middle\vert\begin{matrix}(0,2)\\(m,\frac{1}{\xi})\end{matrix}\right]$ $= \frac{-2\xi}{x\Gamma(m)}\left(\frac{\beta}{x^2\overline{\gamma}}\right)^{m\xi}\Gamma\left(1+2m\xi,0;\left(\frac{\beta}{x^2\overline{\gamma}}\right)^{\xi};-2\xi\right)$
Generalized-K	$\frac{-2}{x\Gamma(m_s)\Gamma(m)\sqrt{\pi}}\mathrm{G}_{2,2}^{2,2}\left[\frac{4mm_s}{\overline{\gamma}x^2}\middle\vert\begin{matrix}0,1/2\\m,m_s\end{matrix}\right]$
EGK	$\frac{-2}{x\Gamma(m_s)\Gamma(m)}\mathrm{H}_{1,2}^{2,1}\left[\frac{\beta_s\beta}{\overline{\gamma}x^2}\middle\vert\begin{matrix}(0,2)\\(m_s,\frac{1}{\xi_s}),(m,\frac{1}{\xi})\end{matrix}\right]$

Moreover, the derivative of $\mathcal{L}(\cdot)$ can be obtained easily by taking the derivative of the Q function yielding

$$\mathcal{L}'(x) = \frac{1}{2}\overline{\gamma}x - \frac{1}{2}(2+\overline{\gamma}x^2)\sqrt{\frac{\overline{\gamma}\pi}{2}}e^{\frac{\overline{\gamma}x^2}{4}}Q\left(\sqrt{\frac{\overline{\gamma}x^2}{2}}\right). \tag{3.55}$$

Finally to summarize all these cases and special cases, we note that from the generic expression of $\mathcal{L}(\cdot)$ and $\mathcal{L}'(\cdot)$ in (3.45) and (3.46), one can get the ASER of MPSK over any type of fading covered by the EGK distribution, perturbed by AWLN, and get a simplified expression by doing the necessary manipulations. As a conclusion, Tables 3.2 and 3.2 summarizes all these cases and define the generic integral $\mathcal{L}(\cdot)$ and its derivative.

3.4 Asymptotic Results for High SNR

It seems interesting to explore an asymptotic study of the SER for high SNR. Because the SER is expressible in terms of the FHF, the known results of the asymptotic expansion of the FHF, near zero (i.e. for high SNR $\overline{\gamma}$), could be used to write down the asymptotic expression of the SER for high SNR in presence of EGK fading. As the SER is totally defined by knowing $\mathcal{L}(x)$, an asymptotic expression of $\mathcal{L}(x)$ is studied for the different fading channels seen above. In fact, from (3.45) and [55, Eq. (1.8.4)], we have

$$\mathcal{L}(x) = \begin{cases} \frac{2\xi\Gamma\left(m_s - m\frac{\xi}{\xi_s}\right)\Gamma(2m\xi)}{\Gamma(m)\Gamma(m_s)} \left(\frac{\beta_s\beta}{\overline{\gamma}x^2}\right)^{m\xi} & \text{if } \mathrm{m_s}\xi_\mathrm{s} - \mathrm{m}\xi \geq 0 \\ \frac{2\xi_s\Gamma\left(m - m_s\frac{\xi_s}{\xi}\right)\Gamma(2m_s\xi_s)}{\Gamma(m)\Gamma(m_s)} \left(\frac{\beta_s\beta}{\overline{\gamma}x^2}\right)^{m_s\xi_s} & \text{otherwise.} \end{cases} \tag{3.56}$$

This asymptotic expression is more simplified than the general expression (3.45). Its derivative can also be easily found as its dependence on x is very simple. Finally, such expression of $\mathcal{L}(x)$ in the selected special cases of fading are summarized in Table 3.4.

Table 3.4: Asymptotic Expansion of $\mathcal{L}(x)$ and $\mathcal{L}'(x)$ for Different Channels

Fading Type	$\mathcal{L}(x)$	$\mathcal{L}'(x)$	Condition
Rayleigh	$\frac{2}{\overline{\gamma}x^2}$	$-\frac{4}{\overline{\gamma}x^3}$	
Nakagami-m	$\frac{2\Gamma(2m)}{\Gamma(m)}\left(\frac{m}{\overline{\gamma}x^2}\right)^m$	$-\frac{4m\Gamma(2m)}{x\Gamma(m)}\left(\frac{m}{\overline{\gamma}x^2}\right)^m$	
GNM	$\frac{2\xi\Gamma(2m\xi)}{\Gamma(m)}\left(\frac{\beta}{\overline{\gamma}x^2}\right)^{m\xi}$	$-\frac{4m\xi^2\Gamma(2m\xi)}{x\Gamma(m)}\left(\frac{\beta}{\overline{\gamma}x^2}\right)^{m\xi}$	
Generalized-K	$\frac{2\Gamma(m-m_s)\Gamma(2m_s)}{\Gamma(m)\Gamma(m_s)}\left(\frac{m_s m}{\overline{\gamma}x^2}\right)^{m_s}$	$-\frac{4m_s\Gamma(m-m_s)\Gamma(2m_s)}{x\Gamma(m)\Gamma(m_s)}\left(\frac{m_s m}{\overline{\gamma}x^2}\right)^{m_s}$	$m \geq m_s$
	$\frac{2\Gamma(m_s-m)\Gamma(2m)}{\Gamma(m)\Gamma(m_s)}\left(\frac{m_s m}{\overline{\gamma}x^2}\right)^{m}$	$-\frac{4m\Gamma(m_s-m)\Gamma(2m)}{x\Gamma(m)\Gamma(m_s)}\left(\frac{m_s m}{\overline{\gamma}x^2}\right)^{m}$	$m_s \geq m$
EGK	$\frac{2\xi_s\Gamma\left(m - m_s\frac{\xi_s}{\xi}\right)\Gamma(2m_s\xi_s)}{\Gamma(m)\Gamma(m_s)}\left(\frac{\beta_s\beta}{\overline{\gamma}x^2}\right)^{m_s\xi_s}$	$-\frac{4m_s\xi_s^2\Gamma\left(m - m_s\frac{\xi_s}{\xi}\right)\Gamma(2m_s\xi_s)}{x\Gamma(m)\Gamma(m_s)}\left(\frac{\beta_s\beta}{\overline{\gamma}x^2}\right)^{m_s\xi_s}$	$m\xi \geq m_s\xi_s$
	$\frac{2\xi\Gamma\left(m_s - m\frac{\xi}{\xi_s}\right)\Gamma(2m\xi)}{\Gamma(m)\Gamma(m_s)}\left(\frac{\beta_s\beta}{\overline{\gamma}x^2}\right)^{m\xi}$	$-\frac{4m\xi^2\Gamma\left(m_s - m\frac{\xi}{\xi_s}\right)\Gamma(2m\xi)}{x\Gamma(m)\Gamma(m_s)}\left(\frac{\beta_s\beta}{\overline{\gamma}x^2}\right)^{m\xi}$	$m_s\xi_s \geq m\xi$

3.5 Simulation of MPSK Constellation

In this section, we perform some numerical results to investigate the system performance by drawing the SER and the ASER versus the received average SNR and for different size of the MPSK constellation. Moreover, some types of fading are tested to see the impact of the channel on the system performance.

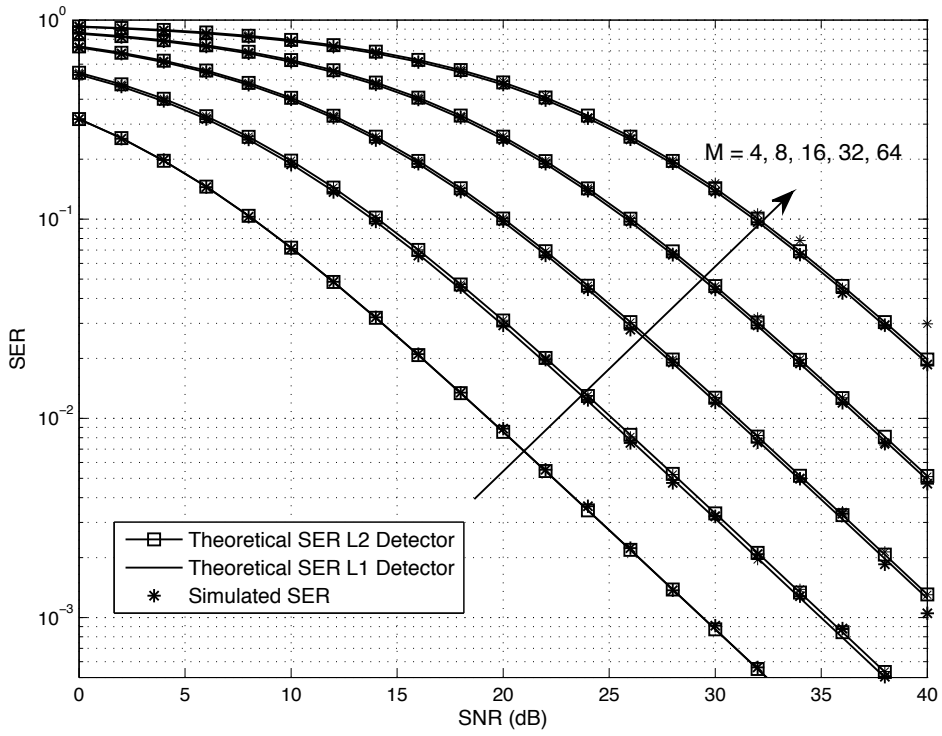

Figure 3.7: Difference between the L_1 norm and the L_2 norm detectors in a Rayleigh fading environment.

In Fig. 3.7, we compare the system performance of both the ML and MD detectors. This illustration is an extension of the results presented in Fig. 3.5 since the ASER of the system over Rayleigh fading is drawn with the conditional SER. In both cases we draw the SER for 4, 8, 16, 32, and 64 PSK. From a mathematical point of view, and from the simulation results, both detectors give the same results in QPSK case. However for $M \geq 8$ there is a small difference between the two detectors with a

little advantage to the ML detector (as described in subsection 3.2.3). Furthermore, it is clear that by increasing M the gap is going down. In the ideal case (without fading), the gap is clear and it is less than 1 dB for all cases. However in Rayleigh fading case, the curves are very close and the gap become very small (< 0.3 dB), and by increasing M the curves get close to each other. For example for 64-PSK the ML and MD detectors have approximately the same performance.

On the other hand it is clear that the system performance improves by decreasing the constellation size M. Also the SER is better in the environment without fading than in the Rayleigh fading case. One more remark is that the numerical results match perfectly the simulation results.

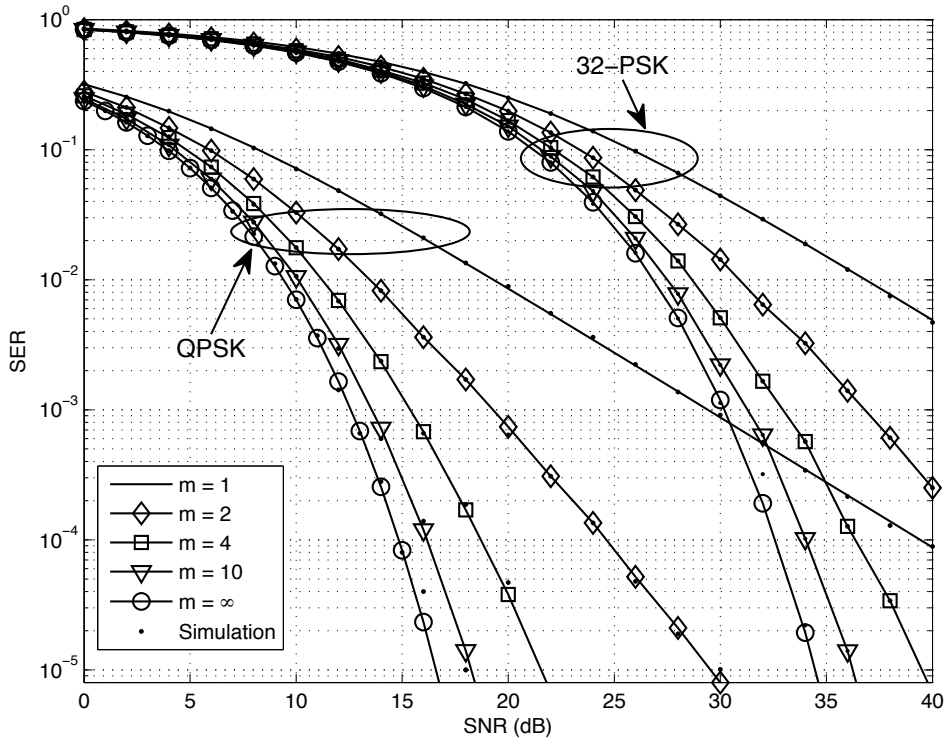

Figure 3.8: Comparison between different type of Nakagami fading severity for two constellations (QPSK and 32-PSK). The lines represent the analytical results while the dots denote the simulation results.

Fig. 3.8 shows the system performance in the presence of a Nakagami-m fading for different values of m, considering the QPSK and 32-PSK constellations. The first

remark that one can conclude is that the simulation results match perfectly with the analytical results. As in the previous figure, the performance in the QPSK case are better than the performance in the 32-PSK case, which is explained by the fact that the distance between the symbols in the QPSK case is bigger than the distance in the 32-PSK case. Looking at the effect of the fading, one can conclude that the SER has better values by increasing m, the fading figure, and the best curves appears for $m \to \infty$ in both cases. In fact for small values of the fading figure (i.e. $m = 1$) the fading dominates the error which becomes higher. Also by increasing m, the fading effect on the signal decreases and the system becomes without fading for large values of m ($m \to \infty$), which is the best scenario.

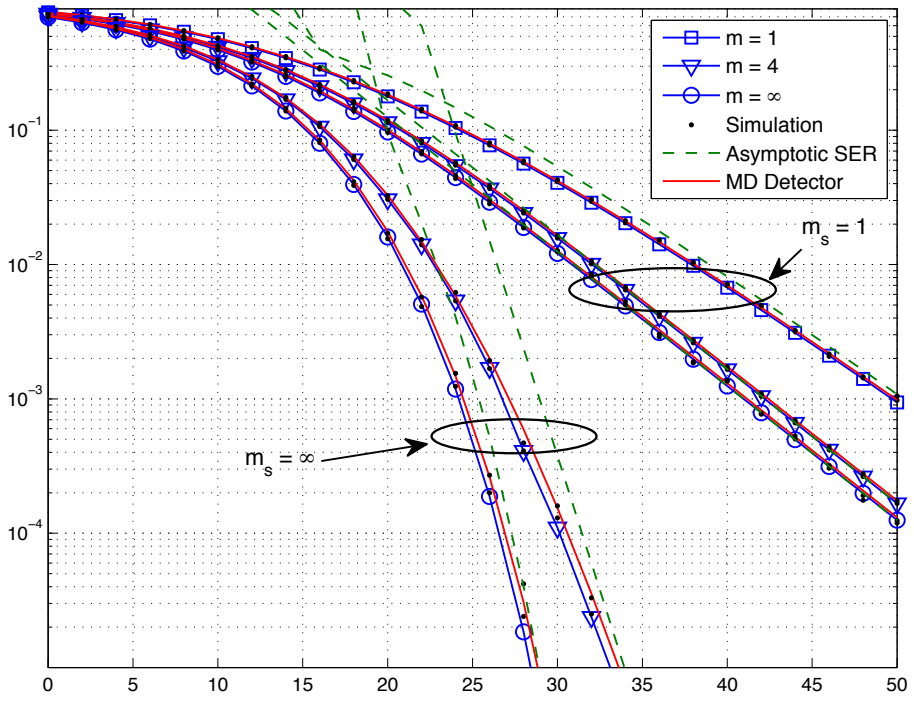

Figure 3.9: Comparison between ML and MD detectors in Generalized-K fading for 16-PSK. The lines represent the analytical results, while the dots denote the simulation results, and the dashed lines represent the asymptotic results for high SNR.

In the last illustration, Fig. 3.9 draws the SER issued from both detectors MD and ML for a generalized-K distribution (i.e. $\xi = 1$ and $\xi_s = 1$) for different values of the figures m and m_s. In fact such results allow us to compare both detectors in the presence of variety of fading severity. Also the asymptotic results for high SNR are drawn, but only using the ML detector, to confirm its utility. It is important to note that the results for $m_s = 1$ and $m = \infty$ (i.e. Rayleigh fading) are the same as $m_s = \infty$ and $m = 1$, so only one case is drawn. Also the case $m_s = \infty$ and $m = \infty$ represents the case without fading. Thereby, it is clear from the figure, that the system performance gets better by increasing the fading and shadowing figures (i.e. reduce the severity of the fading and shadowing). Moreover, it is seen that both detector keep a closer performance even for different values m and m_s. However, we note that for high severity (i.e. $m = 1$ and $m_s = 1$) the difference is negligible relative to the gap in less severity cases ($m_s = \infty$). On the other hand, the asymptotic results for high SNR (dashed lines) show a good approximation for the SER in the treated cases. Finally the simulated results match perfectly the theoretical results which validate again our mathematical model and analytical calculations.

3.6 Conclusion

In this chapter, we described the decision regions of an M-ary PSK constellation transmitted over a Laplace noise channel, assuming two detectors (ML and MD). According to these decision regions, the average symbol error rate is evaluated over an EGK distribution and a closed form is given using the FHF. A simplified expressions of the ASER are derived for special cases of fading. Finally some selected numerical results confirm the analytical results for different sizes of the constellation and many types of fading. It is worth mentioning that the probability

of error of MPSK over a generalized Gaussian noise has been studied also but since it is hard to get a closed form expressions and the mathematical derivations were very complicated. Thereby, that part has been omitted and only the Laplace noise case was presented in this chapter. In fact while dealing with the generalized Gaussian noise, it appears that the distribution of the sum of two generalized Gaussian random variable should be investigated which was not done before. This observation opens a new window of research, such the study of the distribution of the sum of two independent generalized Gaussian noise, the obtained results on this subject are presented in Appendix B. In future work, the obtained results regarding the sum of two GG random variables will be used to compute the SER of MPSK system perturbed by GGN.

On the other hand, as seen in this chapter, the analysis of the performance of digital communication systems over Laplace noise leads to some interesting results. Thus, another type of Laplace perturbation (additive interference) is studied in the following chapter in the context of full duplex communication networks.

Chapter 4

Error Rates and Throughput of Full-duplex Networks Through Laplacian Interference

This chapter presents a statistical study for the intra-cell interference problem in 3-node topology (3NT) full-duplex (FD) cellular networks. Assuming Rayleigh fading on the mutual channel between the interfering users equipment (UE) and that the interfering UE is transmitting Gaussian signals[1], we show that the intra-cell interference has circularly symmetric Laplacian distribution with dependent real and imaginary components. The interference distribution is exploited to characterize the error rates for BPSK, PAM, QAM, and MPSK modulations over EGK fading channel Sec.2.1.2. Moreover, a unified closed-from expression for the average SER is derived. To this end, the throughput of the 3NT FD scheme is characterized and compared to its half-duplex (HD) counterpart. It is ought to be mentioned that outage probability and achievable rate analysis for the 3NT network were conducted in [67, 68, 69, 70]. Different from [67, 68, 69, 70], in this chapter we present for the first closed form expressions for the intra-cell interference, then

[1]The Gaussian signaling abstraction for the interfering symbols is shown to have negligible effect on the error rate performance [65, 66]. The Gaussian signaling assumption is also validated in this chapter.

derive exact error rates for different modulation schemes, and show the explicit effect of intra-cell interference of the throughput of each modulation scheme.

Notations: In what follows subscripts r and i denote the real and imaginary parts, respectively, and $\rho(x) = 1 - \frac{1}{x}$.

4.1 Full Duplex Cellular Network

In-band full-duplex communication is introduced as a promising technology that would provide several benefits to cellular networks. Compared to its HD counterpart, FD communication has the potential to improve spectrum utilization, increase link capacity, enhance physical layer security, and reduce relaying latency [71]. The aforementioned benefits brought by FD communication are all derived from its ability to simultaneously transmit and receive within the same frequency band. The ability of simultaneous transmission and reception for FD transceivers emerges from recent advances in radio frequency circuit design that enables sufficient self-interference (SI) cancellation, and hence, eliminates the necessity for transmission/reception orthogonalization employed by HD transceivers [72, 71, 73, 74]. To reap the aforementioned benefits of FD communication, FD enabled transceivers are required at both sides of the communication link, which is hard to realize in the context of cellular networks. Cellular networks operators can only enforce FD upgrade in their networks from the base stations' (BS) side and do not have direct access to upgrade the UE side. Furthermore, implementing SI cancellation at the UE can be expensive in terms of complexity, power consumption, and/or terminal price. Hence, backward compatibility between FD BSs and HD UEs is required especially at the early FD rollout phase. In this context, the 3NT is proposed to serve HD users via FD BSs and yet benefit from FD communication [75, 76]. In the 3NT, the BS groups the

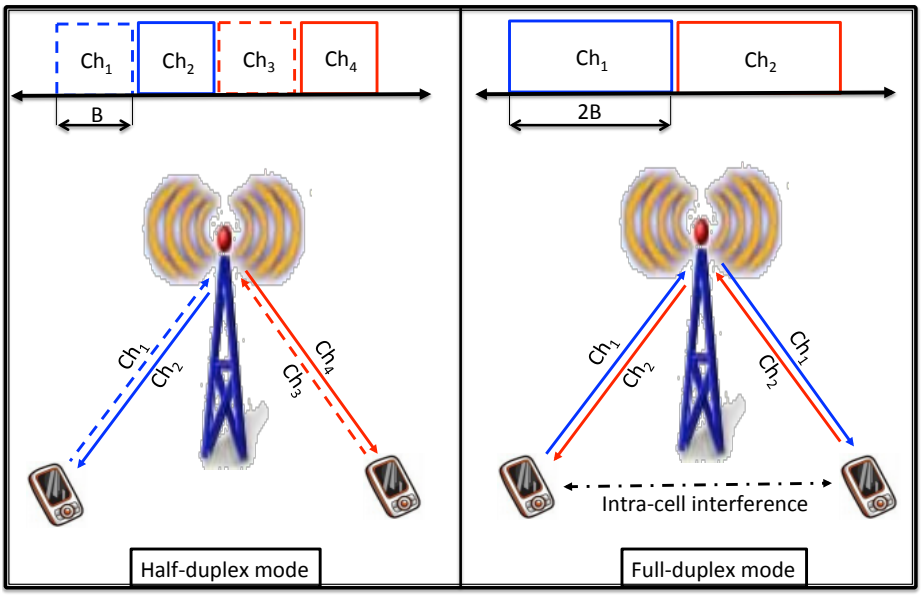

Figure 4.1: Channel assignment in the 3NT FD and HD schemes.

UEs into pairs and simultaneously reuse the uplink channel of one UE in the downlink direction of the other UE in each pair, as shown in Fig. 4.1. Compared to the HD case, the 3NT requires half the number of channels to serve the same number of users, and hence, the bandwidth (BW) occupied by each channel can be doubled.

Doubling the channel BW directly implies doubling the transmission rate, but not necessarily doubling the throughput. This is because the BW improvement offered by the 3NT comes at the expense of creating SI at the BS side and intra-cell interference at the UE side, which impose decoding errors. The BS exactly knows the interfering codeword and can accurately estimate the SI channel, and hence, SI can be sufficiently suppressed using SI cancellation techniques [72, 71, 73, 74]. However, the UE does not have information about the signal being transmitted by the interfering UE, and hence, interference cancellation is not always viable.

In the next section the system model of the 3NT system is described before handling the distribution of the intra-cell interference and the system performance.

4.2 System Model of 3NT FD Cellular Network

This chapter explicitly focuses on the intra-cell interference problem imposed by 3NT shown in Fig. 4.1. Therefore, we consider a single cell scenario with an FD BS and two HD UEs. Without loss in generality, we assume that the spectrum can be either divided into four non-overlapping channels that are assigned in HD mode or two non-overlapping channel that are assigned using the 3NT FD mode, as shown in Fig. 4.1. In the HD case, each user is assigned an interference free BW B Hz in each of the uplink and downlink directions. On the other hand, the 3NT FD mode doubles the BW to $2B$ in each of the uplink and downlink directions at the expense of SI in the uplink and intra-cell interference in the downlink. Without loss of generality, we focus on the downlink performance of one of the UE. The complex base-band received signal at the test UE can be expressed as

$$r = \sqrt{P_d \mathcal{A}_d} h s + \sqrt{P_u \mathcal{A}_u} g x + n, \tag{4.1}$$

where P_d is the downlink transmit power, $\mathcal{A}_d$ is a constant that captures downlink large-scale power attenuation, s is the intended symbol drawn from a unit power constellation, h is the intended channel with unit-mean EGK distributed power gain, P_u is the power transmitted by the interfering UE, $\mathcal{A}_u$ is a constant that captures large-scale interference power attenuation, x is the intra-cell interfering Gaussian symbol, g is the unit variance circularly symmetric complex Gaussian mutual channel gain between the UEs, and n is the additive white Gaussian noise. The random variables h, s, g, x, and n are assumed to be independent.

It is worth mentioning that the circularly symmetric Gaussian distribution of g models the sever Rayleigh fading, which occurs in non-line of sight (NLOS) environments with rich scattering object. The Rayleigh fading assumption on the interference channel can be justified by multi-user diversity in which the BS would

pair UE with poor mutual channel condition (i.e., NLOS UEs) on the same channel. It is worth noting that the analysis in [67, 68, 69, 70] is based on the Rayligh fading assumption on both the interfering and the useful links.

On the other hand and unlike g, which is assumed Rayleigh by virtue of the multi-user diversity, h is modeled using the more general EGK fading distribution which models diverse types of fading channels that can appear between the user and the BS.

Furthermore, Gaussian signals provide accurate approximation for the interference generated from a single node transmitting on a faded channel [65]. This assumption is also validated in Section 4.7. In addition, the intended signal power is P_d and the interfering signal power is P_u because we study the downlink transmission in which the intra-mode interference comes from an uplink UE, as shown in Fig. 4.1.

We assume that the intra-cell interference dominates the noise, and hence, the noise term is ignored in the analysis. The accuracy of this approximation is validated in the results section with realistic noise power. Ignoring the white noise, the received signal r can be re-written as

$$r \approx \sqrt{P_d \mathcal{A}_d} h s + \sqrt{P_u \mathcal{A}_u} g x. \tag{4.2}$$

The received signal r is a complex valued random variables with real and imaginary components, which are represented as $r = \Re(r) + j\Im(r)$, where $\Re(\cdot)$ and $\Im(\cdot)$ denote the real and imaginary parts r respectively, and $j = \sqrt{-1}$ is the imaginary unit. To study (4.2), we first focus on the interference term, which can be considered as an additive complex perturbation for the useful symbol s.

In the next section, we study the normalized intra-cell interference, denoted as $Z = gx$. The normalized intra-cell interference Z is characterized by closed form expressions for its PDF and CDF.

4.3 Distribution of the Intra-cell Interference

Since g and x are both zero-mean unit-variance complex Gaussian random variables, their real part and imaginary part are independent Gaussian random variables with zero-mean and variance $\frac{1}{2}$. The intra-cell Interference Z is represented as

$$Z \;=\; gx \;=\; \Big(\Re(g)\Re(x) - \Im(g)\Im(x)\Big) + j\Big(\Re(g)\Im(x) + \Im(g)\Re(x)\Big). \tag{4.3}$$

The distribution of Z can be obtaining using the relations between the characteristic function (CHF), the PDF, and the CDF (Fourier transform). To benefit from these relations, the CHF, denoted by $\varphi_Z(t_1, t_2)$, should be derived firstly.

4.3.1 CHF of Intra Cell Interference

Actually, from the definition of the CHF, we get

$$\varphi_Z(t_1, t_2) = \mathbb{E}\left[e^{j(t_1\Re(Z) + t_2\Im(Z))}\right]. \tag{4.4}$$

Replacing the real and imaginary parts of Z as follows in (4.4)

$$\begin{aligned} \Re(Z) &= g_r x_r - g_i x_i \\ \Im(Z) &= g_r x_i + g_i x_r, \end{aligned} \tag{4.5}$$

to obtain the following new expression of the CHF

$$\varphi_Z(t_1, t_2) = \mathbb{E}\Big[\exp\Big(jx_r(t_1 g_r + t_2 g_i)\Big) \times \exp\Big(jx_i(t_2 g_r - t_1 g_i)\Big)\Big]. \tag{4.6}$$

By conditioning with respect to g_r and g_i (which are independent Gaussian random variables), the CHF of Z can be written as the product of the CHF of x_r and x_i, since x_r and x_i are independent among themselves and independent to g_r and g_i.

Now the CHF of Z can be expressed as the mean over g_r and g_i of the conditional CHF

$$\varphi_Z(t_1, t_2) = \mathbb{E}_{g_i, g_r}\Big[\varphi_{x_r}(t_1 g_r + t_2 g_i) \times \varphi_{x_i}(t_2 g_r - t_1 g_i)\Big]. \tag{4.7}$$

Note that if Y follows a Gaussian distribution with zero mean and variance σ^2, its CHF is expressed as $\varphi_Y(y) = e^{-\frac{1}{2}\sigma^2 y^2}$. Using this fact in (4.7), will give us the expression of $\varphi_Z(\cdot, \cdot)$ as

$$\begin{aligned}\varphi_Z(t_1, t_2) &= \int_{\mathbb{R}}\int_{\mathbb{R}} f_{g_r}(g_r) f_{g_i}(g_i) e^{-\frac{1}{4}(t_1 g_r + t_2 g_i)^2} e^{-\frac{1}{4}(t_2 g_r - t_1 g_i)^2} dg_r dg_i \\ &= \left(\frac{1}{\sqrt{\pi}} \int_{\mathbb{R}} e^{-\frac{1}{4}u^2(4 + t_1^2 + t_2^2)} du\right)^2. \end{aligned} \tag{4.8}$$

Finally, the last integral can be solved using the Gaussian PDF as

$$\frac{1}{\sqrt{\pi}} \int_{\mathbb{R}} e^{-\frac{1}{4}vu^2} du = \frac{2}{\sqrt{v}}, \quad \forall v > 0. \tag{4.9}$$

Thus, the CHF of the intra-cell interference from a dominant UE transmitting Gaussian signals over a Rayleigh faded channel has the following characteristic function

$$\varphi_Z(t_1, t_2) = \frac{4}{4 + t_1^2 + t_2^2} = \frac{1}{1 + \frac{|\mathbf{t}|^2}{4}}, \tag{4.10}$$

where the vector $\mathbf{t} = (t_1, t_2)$.

We can conclude at this point that the expression of the CHF of Z in (4.10) is a special case of the bivariate Laplace distribution [77]. Furthermore, the CHF of Z is independent of the angle between the real and imaginary components. Consequently, (4.10) shows that Z follows a circularly symmetric complex Laplace distribution.

4.3.2 CDF of Intra Cell Interference

The CDF is defined as the primitive of the inverse Laplace transform of the CHF (also primitive of the PDF that vanishes at $(-\infty,-\infty)$). The relation between the CHF and the CDF of a vector of two random variable can be given as follows

$$F_Z(z_r, z_i) = F_{Z_r}(z_r) + F_{Z_i}(z_i) + c + \frac{1}{4\pi^2} \iint_{z_r,z_i} \iint_{t_1,t_2} e^{j(z_r t_1 + z_i t_2)} \varphi_Z(t_1, t_2) dt_1 dt_2 dz_r dz_i,$$

where $F_{Z_r}(\cdot)$ and $F_{Z_i}(\cdot)$ are the CDFs of Z_r and Z_i respectively, and c is a real constant to be determined. In the following analysis we are focusing on the last part (four integrals), namely $\overline{F}_Z(z_r, z_i)$, which is the CCDF.

Looking at the CHF (4.10), one notice that it is an even function on both variables, so the Laplace transform becomes a cosine transform

$$\begin{aligned} \overline{F}_Z(z_r, z_i) &= \frac{1}{\pi^2} \iint_{z_r,z_i} \int_0^\infty \int_0^\infty \cos(z_r t_1) \cos(z_i t_2) \varphi_Z(t_1, t_2) dt_1 dt_2 dz_r dz_i \\ &= \frac{4}{\pi^2} \int_0^\infty \int_0^\infty \frac{\sin(z_r t_1) \sin(z_i t_2)}{t_1 t_2 (4 + t_1^2 + t_2^2)} dt_1 dt_2. \end{aligned} \tag{4.11}$$

Using the representation of the sine function in terms of the MGF and its Mellin-Barnes representation [55, Eq. (1.1.2)], yields

$$\begin{aligned} \sin(x) &= \sqrt{\pi}\ \mathrm{G}_{0,2}^{1,0}\left[\frac{x^2}{4}\,\middle|\,\begin{matrix} - \\ \frac{1}{2}, 0 \end{matrix}\right] \\ &= \sqrt{\pi} \frac{1}{2\pi j} \int_{\mathcal{C}} \frac{\Gamma(\frac{1}{2} + s)}{\Gamma(1 - s)} \left(\frac{x}{2}\right)^{-2s} ds. \end{aligned} \tag{4.12}$$

Substituting the expression of the sine function (4.12) in (4.11), we get another

expression of the CCDF as

$$\overline{F}_Z(z_r,z_i)=\frac{4}{\pi}\frac{1}{(2\pi j)^2}\int_{\mathcal{C}_1}\int_{\mathcal{C}_2}\frac{\Gamma(\frac{1}{2}+s)\Gamma(\frac{1}{2}+t)}{\Gamma(1-s)\Gamma(1-t)}\left(\frac{z_r}{2}\right)^{-2s}\left(\frac{z_i}{2}\right)^{-2t}\times\int_0^\infty\int_0^\infty\frac{t_1^{-2s-1}t_2^{-2t-1}}{4+t_1^2+t_2^2}dt_1dt_2dsdt. \tag{4.13}$$

The last double integral over t_1 and t_2 has a closed from solution which is equal to

$$\int_0^\infty\int_0^\infty\frac{t_1^{-2s-1}t_2^{-2t-1}}{4+t_1^2+t_2^2}dt_1dt_2=2^{-4-2s-2t}\Gamma(1+s+t)\frac{\Gamma(1-s)\Gamma(1-t)\Gamma(s)\Gamma(t)}{\Gamma(1+s)\Gamma(1+t)}. \tag{4.14}$$

This result is valid for $s\in\mathcal{C}_1$ and $t\in\mathcal{C}_2$. Hence (4.13) can be re-written as a double Mellin-Barnes type contour integral [62]

$$\begin{aligned}\overline{F}_Z(z_r,z_i)&=\frac{1}{4\pi}\frac{1}{(2\pi j)^2}\int_{\mathcal{C}_1}\int_{\mathcal{C}_2}\Gamma(1+s+t)\Gamma(s)\Gamma(t)\frac{\Gamma(\frac{1}{2}+s)\Gamma(\frac{1}{2}+t)}{\Gamma(1+s)\Gamma(1+t)}z_r^{-2s}z_i^{-2t}dsdt\\&=\frac{1}{4\pi}\mathrm{G}^{0,1,0,2,0,2}_{1,0,2,1,2,1}\left[\frac{1}{z_r^2},\frac{1}{z_i^2}\middle|\begin{matrix}0\\\hline\end{matrix}\middle|\begin{matrix}\frac{1}{2},1\\0\end{matrix}\middle|\begin{matrix}\frac{1}{2},1\\0\end{matrix}\right].\end{aligned} \tag{4.15}$$

Since Z_r and Z_i have marginal Laplace distribution, their CDFs have the same form that is given by

$$\begin{cases}F_{Z_r}(z_r) &= 1-\frac{1}{2}e^{-2z_r}\\ F_{Z_i}(z_i) &= 1-\frac{1}{2}e^{-2z_i}.\end{cases} \tag{4.16}$$

Finally it is easy to proof that $c=-1$ by setting the limit of $F_{Z_r,Z_i}(\cdot,\cdot)$ at (∞,∞) to 1. Thereby, the CDF of the intra-cell interference from a dominant UE transmitting Gaussian signals over a Rayleigh faded channel, Z, has the following expression

$$F_Z(z_r,z_i)=1-\frac{1}{2}\left(e^{-2z_r}+e^{-2z_i}\right)+\frac{1}{4\pi}\mathrm{G}^{0,1,0,2,0,2}_{1,0,2,1,2,1}\left[\frac{1}{z_r^2},\frac{1}{z_i^2}\middle|\begin{matrix}0\\\hline\end{matrix}\middle|\begin{matrix}\frac{1}{2},1\\0\end{matrix}\middle|\begin{matrix}\frac{1}{2},1\\0\end{matrix}\right], \tag{4.17}$$

Consequently, the PDF can be derived by derivation in the next subsection.

4.3.3 PDF of Intra Cell Interference

The PDF is the derivative of the CDF with respect to z_r and z_i,

$$f_Z(z_r, z_i) = \frac{\partial^2 F_Z(z_r, z_i)}{\partial z_r \partial z_i}.$$

While both marginal CDF components vanish after the second derivation, only the CCDF component is remaining. Therefore, from (4.15) and with the help of a change of variable, the PDF of Z can be written as

$$\begin{aligned} f_Z(z_r, z_i) &= \frac{1}{\pi}\frac{1}{(2\pi j)^2}\int_{\mathcal{C}_1}\int_{\mathcal{C}_2}\Gamma(1+s+t)\Gamma(\frac{1}{2}+s)\Gamma(\frac{1}{2}+t)z_r^{-2s-1}z_i^{-2t-1}dsdt \\ &\overset{v=1/2+s,u-v=t+1/2}{=} \frac{1}{\pi}\frac{1}{(2\pi j)^2}\int_{\mathcal{C}_1}\Gamma(u)z_i^{-2u}\int_{\mathcal{C}_2}\Gamma(u-v)\Gamma(v)\left(\frac{z_r}{z_i}\right)^{-2v}dvdu. \quad (4.18) \end{aligned}$$

Using the identity [55, Eq. (2.9.5)] to solve the second integral, we can write

$$\begin{aligned} \frac{1}{2\pi j}\int_{\mathcal{C}_2}\Gamma(u-v)\Gamma(v)\left(\frac{z_r}{z_i}\right)^{-2v}dv &= \mathrm{G}_{1,1}^{1,1}\left[\frac{z_r^2}{z_i^2}\middle|\begin{matrix}1-u\\0\end{matrix}\right] \\ &= \Gamma(u)\left(1+\frac{z_r^2}{z_i^2}\right)^{-u}. \end{aligned}$$

Finally, the PDF is simplified to the desired expression in terms of the MGF using the identity [55, Eq. (2.9.31)]

$$\begin{aligned} f_Z(z_r, z_i) &= \frac{1}{\pi}\frac{1}{2\pi j}\int_{\mathcal{C}_1}\Gamma(s)\Gamma(s)\left(z_r^2+z_i^2\right)^{-s}ds \\ &= \frac{1}{\pi}\mathrm{G}_{0,2}^{2,0}\left[z_r^2+z_i^2\middle|\begin{matrix}\text{——}\\0,0\end{matrix}\right] \quad (4.19) \end{aligned}$$

By the end, using the identity [55, Eq. (2.9.39)], the intra-cell interference from a dominant UE transmitting Gaussian signals over a Rayleigh faded channel has the following PDF

$$f_Z(z_r, z_i) = \frac{2}{\pi}K_0\left(2\sqrt{z_r^2+z_i^2}\right), \quad (4.20)$$

where $K_0(\cdot)$ is the 0-th order modified Bessel function of the second kind [58, Eq. (9.6.21)].

The PDF expression in (4.20) clearly shows that Z does not have independent real and imaginary components because the joint PDF in (4.20) cannot be expressed as the product of two marginal Laplace PDFs (3.4). Moreover, the problem of decoding in the presence of additive Laplacian perturbation (i.e., noise or interference) has been widely addressed in Chapter 3 and the literature [42, 44]. However, as assumed in Chapter 3, a common assumption in this literature is that the Laplacian perturbation have independent real and imaginary components. Hence, the work presented in this chapter contributes to the present thesis by modeling the case with dependent real and imaginary components. Furthermore, the previous analysis rigorously derives the Laplacian distribution of the interference from the system model rather than assuming a Laplacian perturbation. By the end, exploiting the interference characterization in this section, the error rate performance is analyzed in the next sections.

4.4 Conditional Error Rates

This section characterizes the downlink decoding errors that may occur due to the Laplacian intra-cell interference. In particular, we evaluate the probability of BPSK, PAM, QAM, and MPSK. At first, the conditional (i.e., conditioning on the intended channel gain) SER as a function of the signal-to-interference ratio (SIR), denoted as $\gamma = \frac{P_d \mathcal{A}_d |h|^2}{P_u \mathcal{A}_u}$, is investigated. The conditional error rate analysis can also be considered as the error rate over unfaded downlink channel[2]. A unified expression of the conditional SER is given in the end this section.

For the sake of organized presentation, and since all the constellations studied in the

[2]An important application for the unfaded channels appears in massive MIMO systems due to the channel hardening effect [78].

previous chapters are treated here, we classify the studied modulation schemes into two sets, namely, (i) one dimensional constellations $(1D)$ (i.e. BPSK and M-PAM) and (ii) two dimensional constellations $(2D)$ (i.e. M-QAM and MPSK).

4.4.1 Error Rates for 1D Constellations

4.4.1.1 BER of BPSK

Since the BPSK transmits real symbols $s = \pm E_s$, the conditional PDF of the received signal r is obtained from (4.20) as $f_r(r) = e^{-2|r \mp E_s|}$. Moreover, the optimal decision, ML detector, is obtained by minimizing the distance $d(r, \pm E_s)$. Given that the BPSK symbols are equiprobable, the probability of error can be computed as

$$Pr(e|\gamma) = \int_0^\infty f_r(r|S = -E_s)\, dr.$$

Assuming unit energy constellation, and set $E_s = 1$, the conditional downlink bit error rate in 3NT with Laplacian intra-cell interference and maximum likelihood detector for the BPSK modulation is given by

$$P_{BPSK}(e|\gamma) = \frac{1}{2} e^{-2\sqrt{\gamma}}. \tag{4.21}$$

4.4.1.2 SER of PAM

The SER of PAM directly follows from the BER of a BPSK modulation as

$$P_{PAM}(e) = 2\left(1 - \frac{1}{M}\right) P_{BPSK}(e).$$

Hence, the conditional downlink bit error rate in 3NT with Laplacian intra-cell interference and maximum likelihood detector for the PAM modulation can be

deduced from (4.21) as

$$P_{PAM}(e|\gamma) = \left(1 - \frac{1}{M}\right) e^{-2\sqrt{\frac{3\gamma}{M^2-1}}}, \tag{4.22}$$

where the exponent argument $\sqrt{\frac{3\gamma}{M^2-1}}$ is obtained by calculating the average energy per symbol for PAM.

4.4.2 Error Rates for 2D Constellations

In this section we consider 2D constellations formed by in-phase and quadrature phase components. Particularly, we focus on the M-QAM and the MPSK constellations. While the exact closed-from expressions of the SER for the M-QAM and the MPSK schemes are derived, we also present simplified approximations in order to present a unified error rate expression for all of the considered modulation schemes.

4.4.2.1 SER for Rectangular QAM

A rectangular M-QAM is formed by one in-phase M_I-PAM and orthogonal quadrature phase M_Q-PAM, as mentioned in Sec. 2.4, which means that QAM constellation contains $M = M_I M_Q$ symbols. These symbols can be classified as follows: 4 corner symbols, $2(M_I - 2)$ edge symbols with decision distance d_I, $2(M_Q - 2)$ edge symbols with decision distance d_Q, and $(M_I - 2)(M_Q - 2)$ inner symbols. To compute the conditional error probability, we need to get the probability of error of each symbol and then the SER is obtained by averaging these probabilities over the probability of occurrence of each symbol. Let us begin with the corner symbols. Actually the probability of error of the corner symbol can be

given as

$$P_e^{cor} = 1 - \int_{-\frac{d_I}{2}}^{\infty} \int_{-\frac{d_Q}{2}}^{\infty} f_Z(x,y)dxdy = 1 - F_Z(\frac{d_I}{2}, \frac{d_Q}{2})$$
$$= \frac{1}{2}\left(e^{-d_I} + e^{-d_Q}\right) - \overline{F}_Z(\frac{d_I}{2}, \frac{d_Q}{2}), \tag{4.23}$$

where $\overline{F}_Z(\cdot,\cdot)$ is defined in (4.15).

The calculation of the probability of error of the edge points is similar for the in-phase points and the quadrature-phase points, hence we are focusing on the in-phase points. Furthermore, the probability of error detection of an in-phase edge symbol is obtained as

$$P_e^{edg,I} = 1 - \int_{-\frac{d_I}{2}}^{\infty} \int_{-\frac{d_Q}{2}}^{\frac{d_Q}{2}} f_Z(x,y)dxdy$$
$$= 2 - \frac{1}{2}e^{-d_I} - 2F_Z(\frac{d_I}{2}, \frac{d_Q}{2})$$
$$= \frac{1}{2}\left(e^{-d_I} + 2e^{-d_Q}\right) - 2\overline{F}_Z(\frac{d_I}{2}, \frac{d_Q}{2}). \tag{4.24}$$

Per consequence, the probability of error detection of a quadrature phase edge symbol is given by

$$P_e^{edg,Q} = \frac{1}{2}\left(e^{-d_Q} + 2e^{-d_I}\right) - 2\overline{F}_Z(\frac{d_Q}{2}, \frac{d_I}{2})$$
$$= \frac{1}{2}\left(e^{-d_Q} + 2e^{-d_I}\right) - 2\overline{F}_Z(\frac{d_I}{2}, \frac{d_Q}{2}). \tag{4.25}$$

Finally, the probability of error detection of an inner symbol is obtained as

$$P_e^{inn} = 1 - \int_{-\frac{d_I}{2}}^{\frac{d_I}{2}} \int_{-\frac{d_Q}{2}}^{\frac{d_Q}{2}} f_Z(x,y)dxdy$$
$$= e^{-d_I} + e^{-d_Q} - 4\overline{F}_Z(\frac{d_I}{2}, \frac{d_Q}{2}). \tag{4.26}$$

Hence, assuming equiprobable symbols, the SER of rectangular QAM is derived as

$$P_{QAM}(e|\gamma) = \frac{1}{M_I M_Q}\Big(4P_e^{cor} + 2(M_Q-2)P_e^{edg,Q} + 2(M_I-2)P_e^{edg,I} + (M_Q-2)(M_I-2)P_e^{inn}\Big). \tag{4.27}$$

Let us defined the in-phase-to-quadrature phase decision distance ratio τ as $\tau = \frac{d_Q}{d_I}$ and $d = \sqrt{(M_I^2-1) + \tau^2\left(M_Q^2-1\right)}$. Then the probability of error of rectangular can be obtained by replacing the decision distances by their values $d_I = \frac{2\sqrt{3\gamma}}{d}$, $d_Q = \tau d_I$, and operating some algebraic manipulation to (4.27). Thereby, the conditional downlink bit error rate in 3NT with Laplacian intra-cell interference and maximum likelihood detector for the rectangular QAM modulation is given by

$$P_{QAM}(e|\gamma) = \rho(M_I)e^{-2\frac{\sqrt{3\gamma}}{d}} + \rho(M_Q)e^{-2\tau\frac{\sqrt{3\gamma}}{d}} - \frac{1}{\pi}\rho(M_I)\rho(M_Q)\mathrm{G}_{1,0,2,1,2,1}^{0,1,0,2,0,2}\left[\frac{d^2}{3\gamma}, \frac{d^2}{3\tau^2\gamma}\,\middle|\, \begin{matrix}0\\-\end{matrix}\middle|\, \begin{matrix}\frac{1}{2},1\\0\end{matrix}\middle|\, \begin{matrix}\frac{1}{2},1\\0\end{matrix}\right], \tag{4.28}$$

recall that $\rho(x) = 1 - \frac{1}{x}$.

A special case of that result is the square QAM, where $M_I = M_Q = \sqrt{M}$ and $\tau = 1$. Using the double Mellin-Barnes contour integral of the BMGF [62] and the expression of the SER in (4.28), the SER of square QAM can be deduced to

$$P_{QAM}(e|\gamma) = 2\rho(\sqrt{M})e^{-\sqrt{\frac{6\gamma}{M-1}}} - \frac{1}{\pi}\rho(\sqrt{M})^2\mathrm{G}_{2,1,1,0,1,2}^{0,2,0,1,2,0}\left[\frac{2(M-1)}{3\gamma}, 1\,\middle|\, \begin{matrix}\frac{1}{2},1\\0\end{matrix}\middle|\, \begin{matrix}1\\\frac{1}{2},0\end{matrix}\middle|\, \begin{matrix}0\\-\end{matrix}\right]. \tag{4.29}$$

The error rate for rectangular QAM modulation given in (4.28) is expressed in terms of the BMGF, which imposes high computational complexity. Therefore, a simpler approximation of the SER is proposed. In fact, the approximation is obtained by considering a QAM modulation formed by two orthogonal (approximated as

independent in presence of Laplace interference) PAMs. Thereby, a correct detection of the M-QAM appears only for a correct detection in the M_I-PAM and M_Q-PAM. Consequently, the probability of error of M-QAM may be approximated as

$$\begin{aligned} P^A_{QAM}(e) &= 1 - (1 - P_{PAM_I}(e))\left(1 - P_{PAM_Q}(e)\right) \\ &= P_{PAM_I}(e) + P_{PAM_Q}(e) - P_{PAM_I}(e)P_{PAM_Q}(e). \end{aligned} \tag{4.30}$$

Then by replacing (4.22) in (4.30), the conditional downlink bit error rate in 3NT with Laplacian intra-cell interference and maximum likelihood detector for the rectangular QAM modulation can be approximated by

$$P^A_{QAM}(e|\gamma) = \rho(M_I)e^{-2\frac{\sqrt{3\gamma}}{d}} + \rho(M_Q)e^{-2\tau\frac{\sqrt{3\gamma}}{d}} - \rho(M_I)\rho(M_Q)e^{-2(1+\tau)\frac{\sqrt{3\gamma}}{d}}. \tag{4.31}$$

In the case of square QAM modulation, the SER approximation reduces to

$$P^A_{SQAM}(e|\gamma) = 2\rho\left(\sqrt{M}\right)e^{-\sqrt{\frac{6\gamma}{M-1}}} - \rho\left(\sqrt{M}\right)^2 e^{-2\sqrt{\frac{6\gamma}{M-1}}}. \tag{4.32}$$

4.4.2.2 SER of MPSK

This section considers the case where the transmitted signal s is modulated via an MPSK scheme with M being a power of 2. The MPSK symbols are distributed uniformly over the unit circle and all symbols are equiprobable. Unlike the previous modulation schemes, the decision regions for the MPSK symbols is not known a priori for that type of perturbation and has to be characterized for each complex perturbation. Using the same notation as Chapter 3, let I and Q be the received normalized in-phase and quadrature phase components of transmitted MPSK symbol. Then, according to the PDF of Z in (4.20), the likelihood function can be written as

$$\ell_k = \frac{2\gamma}{\pi}K_0\left(2\sqrt{\gamma}\sqrt{(I-\cos\varphi_k)^2 + (Q-\sin\varphi_k)^2}\right), \tag{4.33}$$

where

$$\begin{cases} I &= s_r^{(k)} + \frac{z_r}{\sqrt{\gamma}} &= \cos\varphi_k + \frac{z_r}{\sqrt{\gamma}} \\ Q &= s_i^{(k)} + \frac{z_i}{\sqrt{\gamma}} &= \sin\varphi_k + \frac{z_i}{\sqrt{\gamma}}. \end{cases} \tag{4.34}$$

From [58, Eqs. (9.6.27) & (9.6.1)], we know that $\frac{\mathrm{d}K_0(x)}{\mathrm{d}x} = -K_1(x)$ and that $K_1(x)$ is positive for $x > 0$, $K_1(\cdot)$ is 1-st order modified Bessel function of the second kind. Hence, $K_0(\cdot)$ is a monotonically decreasing function. Consequently, the likelihood function, ℓ_k, is maximized by minimizing the Bessel function argument, i.e., minimizing the distance $(I - \cos\varphi_k)^2 + (Q - \sin\varphi_k)^2$. Using some algebraic simplification, ℓ_k can be expressed as follows

$$\begin{aligned} \ell_k &= I\cos\varphi_k + Q\sin\varphi_k \\ &= R\left(\cos\psi\cos\varphi_k + \sin\psi\sin\varphi_k\right), \end{aligned}$$

where $R = \sqrt{I^2 + Q^2}$ and $\psi = \arctan\left(\frac{Q}{I}\right)$.

Thus, the likelihood function for the k-th symbol s_k in and MPSK constellation under the complex Laplacian perturbation given in (4.20) can be expressed as

$$\ell_k = R\cos(\psi - \varphi_k), \tag{4.35}$$

Consequently, the decision criterion for MPSK symbols can be defined by selecting the symbol which minimizes $|\psi - \varphi_k|$, where $\varphi_k = \frac{2k\pi}{M}$.

An illustrative example for the MPSK decision regions, with $M = 8$, that maximizes the likelihood function ℓ_k is shown in Fig.4.2 (same decision regions as those analyzed in Sec. 3.1.3). Following similar methodology to 3.2.2, the decision regions are obtained by defining the two coordinates rotations (X_1, Y_1), with rotation angle $\phi - \theta$, and (X_2, Y_2), with rotation angle $\phi + \theta$, where ϕ is the symbol phase and $\theta = \frac{\pi}{M}$. The circular symmetry of the interference PDF in (4.20) implies that all symbols have similar error probability, and we can focus our study to the region

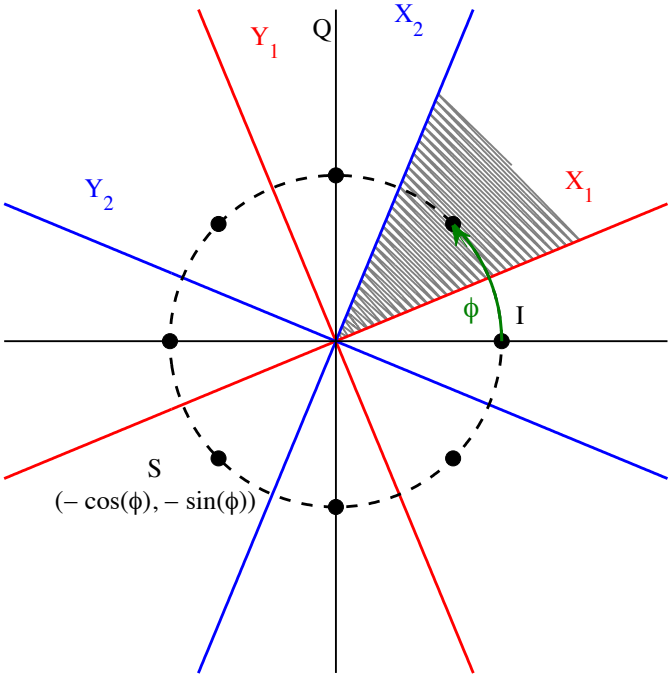

Figure 4.2: Decision regions using maximum likelihood detector for 8-PSK.

between 0 and $\frac{\pi}{2}$. Hence, the total error probability can be deduced by considering a generic single symbol and the error probability can be explicitly expressed in terms of Y_1 and Y_2 as

$$Pe(\gamma, \phi) = \Pr[Y_1 \geq 0] + \Pr[Y_2 \leq 0] - \Pr[Y_1 \geq 0, Y_2 \leq 0]. \tag{4.36}$$

where Y_1 and Y_2 are obtained from the aforementioned rotation as

$$\begin{bmatrix} Y_1 \\ Y_2 \end{bmatrix} = \begin{bmatrix} -\sin(\phi - \theta) & \cos(\phi - \theta) \\ -\sin(\phi + \theta) & \cos(\phi + \theta) \end{bmatrix} \begin{bmatrix} I \\ Q \end{bmatrix}. \tag{4.37}$$

Let us begin by computing $\Pr[Y_1 \geq 0]$. In fact the probability that $Y_1 > 0$ is equivalent to $\Pr[\tan(\varphi - \theta)I - Q \leq 0]$, because $\varphi \in [0, \frac{\pi}{2} - \frac{\pi}{M}]$. Now let's call

$X = \tan(\varphi - \theta)I - Q$, then the PDF of X can be written as

$$f_X(x) = \int_{\mathbb{R}} f_{I,Q}(u, \tan(\varphi - \theta)u - x)du. \tag{4.38}$$

Which gives to the following expression of the first term of (4.36) as

$$\begin{aligned} \Pr[Y_1 \geq 0] &= \Pr[X \leq 0] \\ &= \int_0^\infty \int_{\mathbb{R}} f_{I,Q}(u, \tan(\varphi - \theta)u + x)dudx \\ &= \frac{2\gamma}{\pi} \int_0^\infty \int_{\mathbb{R}} K_0\left(2\sqrt{\gamma\ A(u,x)}\right) dudx, \end{aligned} \tag{4.39}$$

where $A(u, x) = (u + \cos\varphi)^2 + (\tan(\varphi - \theta)u + x + \sin\varphi)^2$.

Using a change of variable and the fact that the marginal of (4.20) is Laplacian, we get

$$\int_{\mathbb{R}} \frac{2}{\pi} K_0\left(2\sqrt{u^2 + v^2}\right) du = e^{-2|v|},$$

and (4.39) can be further simplified to

$$\Pr[Y_1 \geq 0] = \frac{1}{2} e^{-2\sin\theta\sqrt{\gamma}}. \tag{4.40}$$

The same analysis can be used to compute the second term of (4.36), and a similar results can be easily obtained

$$\Pr[Y_2 \leq 0] = \frac{1}{2} e^{-2\sin\theta\sqrt{\gamma}}. \tag{4.41}$$

Finally, to compute the last term in (4.36), $\Pr[Y_1 \geq 0, Y_2 \leq 0]$, we define $W_1 = Q - \tan(\varphi - \theta)I$ and $W_2 = \tan(\varphi + \theta)I - Q$, then we have

$$\Pr[Y_1 \geq 0, Y_2 \leq 0] = \Pr[W_1 \geq 0, W_2 \leq 0].$$

The PDF of the couple (W_1, W_2) can be written using the PDF of (I, Q), as

$$f_{W_1,W_2}(w_1, w_2) = \frac{2\gamma}{\pi} \frac{\cos\varphi^2 - \sin\theta^2}{\sin 2\theta} K_0\left(2\sqrt{\gamma}\frac{\cos\varphi^2 - \sin\theta^2}{\sin 2\theta}\sqrt{A_1(w_1, w_2)}\right), \quad (4.42)$$

where $A_1(w_1, w_2) = (w_1 + w_2 + \cos\varphi)^2 + (\tan(\varphi + \theta)w_1 + \tan(\varphi - \theta)w_2 + \sin\varphi)^2$. The desired probability can be written as

$$\begin{aligned}\Pr[Y_1 \geq 0, Y_2 \leq 0] &= \Pr[W_1 \geq 0, W_2 \leq 0] \\ &= \int_0^\infty \int_0^\infty f_{W_1,W_2}(w_1, w_2) dw_1 dw_2. \end{aligned} \quad (4.43)$$

By developing the squares in $A_1(w_1, w_2)$ and using a change of variable, (4.43) can be expressed as

$$\Pr[Y_1 \geq 0, Y_2 \leq 0] = \frac{1}{2\pi \sin 2\theta} \int_B^\infty \int_B^\infty K_0\left(\frac{1}{\sin 2\theta}\sqrt{u^2 + v^2 + 2uv\cos 2\theta}\right) dudv, \quad (4.44)$$

where $B = \sqrt{\gamma}\frac{\cos\varphi^2 - \sin\theta^2}{\cos\theta}$.

An integral representation of the Bessel function, available in [79, Eq. (2.13)], $K_0(x) = \frac{1}{2}\int_0^\infty \frac{1}{t} e^{-t - \frac{x^2}{4t}}$, can be used in (4.44). Hence we obtain a double incomplete integral of an exponential with square argument, such term can be solved using the two dimensional Gaussian Q function $Q(\cdot, \cdot, \cdot)$ [49, Eq. (4.3)]. Consequently, (4.44) can be reduced to one integral as follows

$$\Pr[Y_1 \geq 0, Y_2 \leq 0] = \int_0^\infty e^{-t} Q\left(\frac{B}{\sqrt{2t}}, \frac{B}{\sqrt{2t}}, -\cos 2\theta\right) dt. \quad (4.45)$$

On the other hand, from [49, Eq. (4.7)], the two dimensional Q function can be

reduced to only one integral if its first two arguments are equal

$$Q(x,x,\alpha)=\frac{1}{\pi}\int_0^{\frac{\pi}{4}}\frac{\sqrt{1-\alpha^2}}{1-\alpha\sin 2\Phi}e^{-\frac{x^2}{2}\frac{1-\alpha\sin 2\Phi}{(1-\alpha^2)\sin^2\Phi}}d\Phi,$$

which is the case in (4.45). Using a suitable change of variable, and the integral representation of $K_1(\cdot)$ [79, Eq. (2.13)], (4.45) can be re-written as

$$\Pr[Y_1\geq 0,Y_2\leq 0]=\frac{B}{2\pi}\int_1^{\infty}\frac{1}{\sqrt{u}\sqrt{u-\sin^2\theta}}K_1\left(\frac{B\sqrt{u}}{\sin\theta}\right)du. \tag{4.46}$$

An alternative expression of the Bessel function and the first term, that contains the square root, in terms of the MGF is available in [55, Eq. (2.9.19)] and [55, Eq. (2.9.6)], respectively

$$\begin{aligned}K_1(x)&=\frac{1}{x}\mathrm{G}_{0,2}^{2,0}\left[\frac{x^2}{4}\,\middle|\,\begin{matrix}-\\0,1\end{matrix}\right]\\ \frac{1}{\sqrt{1-x}}&=\sqrt{\pi}\mathrm{G}_{1,1}^{1,0}\left[x\,\middle|\,\begin{matrix}\frac{1}{2}\\0\end{matrix}\right].\end{aligned} \tag{4.47}$$

These alternative expressions transform the integral in (4.46) as an incomplete integral of the product of two MGF functions, which can be transformed also to an integral of 3 MGFs

$$\begin{aligned}\Pr[Y_1\geq 0,Y_2\leq 0]=\frac{\sin\theta}{2\sqrt{\pi}}\int_0^{\infty}u^{-3/2}&\mathrm{G}_{1,1}^{0,1}\left[x\,\middle|\,\begin{matrix}1\\0\end{matrix}\right]\\ &\times\mathrm{G}_{1,1}^{0,1}\left[\frac{x}{\sin^2\theta}\,\middle|\,\begin{matrix}1\\1/2\end{matrix}\right]\mathrm{G}_{0,2}^{2,0}\left[x\frac{B^2}{4\sin\theta}\,\middle|\,\begin{matrix}-\\0,1\end{matrix}\right]dx.\end{aligned} \tag{4.48}$$

Such integral can be easily solved using [62, Eq. (2.3)] in terms of BMGF. The probability of error detection of one symbol with phase φ using maximum likelihood

detector is given as follows

$$P_e(\gamma,\varphi) = e^{-2\delta\sqrt{\gamma}} - \frac{\delta}{2\sqrt{\pi}} \mathrm{G}^{0,1,1,0,0,2}_{1,1,1,1,2,0}\left[\delta^2, \frac{4\delta^2(1-\delta^2)}{\gamma\left(\cos^2\varphi - \delta^2\right)} \middle| \begin{matrix} \frac{1}{2} \\ -\frac{1}{2} \end{matrix} \middle| \begin{matrix} \frac{1}{2} \\ 0 \end{matrix} \middle| \begin{matrix} 1,0 \\ - \end{matrix}\right], \tag{4.49}$$

where $\delta = \sin\left(\frac{\pi}{M}\right)$ and φ takes the values $\frac{2k\pi}{M}$.

The total probability of error of MPSK modulation can be computed as the average of the probability of error detection over all the symbols. Since we are focusing our study to the region between 0 and $\frac{\pi}{4}$, the total SER of MPSK can be written as

$$P_{MPSK}(e|\gamma) = \frac{4}{M}\sum_{k=0}^{\frac{M}{4}-1} P_e(\gamma,\varphi_k) = \frac{4}{M}\sum_{k=0}^{\frac{M}{4}-1} P_e(\gamma,\frac{2k\pi}{M}). \tag{4.50}$$

Finally by replacing (4.49) in (4.50), the conditional downlink bit error rate in 3NT with Laplacian intra-cell interference and maximum likelihood detector for the MPSK modulation is given by

$$\begin{aligned} P_{MPSK}(e|\gamma) =& e^{-2\delta\sqrt{\gamma}} - \frac{2\delta}{M\sqrt{\pi}} \\ &\times \sum_{k=0}^{\frac{M}{4}-1} \mathrm{G}^{0,1,1,0,0,2}_{1,1,1,1,2,0}\left[\delta^2, \frac{4\delta^2(1-\delta^2)}{\gamma\left(\cos\left(\frac{2k\pi}{M}\right)^2 - \delta^2\right)} \middle| \begin{matrix} \frac{1}{2} \\ -\frac{1}{2} \end{matrix} \middle| \begin{matrix} \frac{1}{2} \\ 0 \end{matrix} \middle| \begin{matrix} 1,0 \\ - \end{matrix}\right]. \end{aligned} \tag{4.51}$$

Similar to the MQAM scheme, the SER of MPSK is expressed in terms of the BMGF which impose high computational complexity. Therefore, a simplifying approximation for the SER in MPSK modulation needed to be investigated. Actually, the exact expressions for $\Pr[Y_1 \geq 0]$ and $\Pr[Y_2 \leq 0]$ are already in the exponential form, and hence, no approximation is required for these terms. On the other hand, the BMGF appears in $\Pr[Y_1 \geq 0, Y_2 \leq 0]$, which can be approximated assuming independent interference components as in (3.27). Thereby, the conditional downlink bit error rate in 3NT with Laplacian intra-cell interference for

the MPSK modulation can be approximated by

$$P^{A}_{MPSK}(e|\gamma) = e^{-2\delta\sqrt{\gamma}} + \frac{2\tan\theta}{M(1+\tan\theta)}e^{-2\sqrt{\gamma}} + \frac{1}{M}\sum_{k=1}^{\frac{M}{4}-1}\frac{\sin 2\theta}{\cos 2\theta + \sin\frac{4k\pi}{M}}e^{-2\sqrt{2\gamma}\sin\left(\frac{2k\pi}{M}+\frac{\pi}{4}\right)}. \quad (4.52)$$

4.4.3 Unified Expression of the SER

The error rates derived in (4.21), (4.22), (4.31), (4.32), and (4.52), can be expressed using the following unified expression

$$SER = \sum_{k=1}^{n} a_k e^{-b_k\sqrt{\gamma}}, \quad (4.53)$$

where $n,\ a_k$, and b_k are related to the used modulation. Their possible values are summarized in Table 4.1.

4.5 Average SER over EGK Fading Channel

Using the conditional error rates obtained in the previous section, the average SER is derived by averaging over the EGK fading distribution on the downlink channel. In the present model, assuming that $\mathbb{E}[|h|^2] = 1$, the average SIR is given by $\bar{\gamma} = \mathbb{E}[\gamma] = \frac{P_d\mathcal{A}_d}{P_u\mathcal{A}_y}$. The PDF of γ was defined in Sec. 2.1.2. The alternative expressions of that PDF described in Sec. 2.1.3 will be used in the following subsections to characterize the average SER.

Table 4.1: SER Modulation-Specific Parameters $n,\ a_k$, and b_k

Modulation Scheme	**Modulation Specific Parameters**			
	n	k	a_k	b_k
BPSK	1	1	$\frac{1}{2}$	1
PAM	1	1	$\rho(M)$	$2\sqrt{\frac{3}{M^2-1}}$
Approximated Square-QAM	2	1	$2\rho(\sqrt{M})$	$\sqrt{\frac{6}{M-1}}$
		2	$-\rho(\sqrt{M})^2$	$2\sqrt{\frac{6}{M-1}}$
Approximated Rectangular-QAM	3	1	$\rho(M_I)$	$2\frac{\sqrt{3}}{d}$
		2	$\rho(M_Q)$	$2\tau\frac{\sqrt{3}}{d}$
		3	$\rho(M_I)\rho(M_Q)$	$2(1+\tau)\frac{\sqrt{3}}{d}$
Approximated MPSK	$\frac{M}{4}+1$	$1 \le k \le n-2$	$\frac{\sin 2\theta}{M(\cos 2\theta + \sin\frac{4k\pi}{M})}$	$2\sqrt{2}\sin\left(\frac{2k\pi}{M}+\frac{\pi}{4}\right)$
		$n-1$	$\frac{2\tan\theta}{M(1+\tan\theta)}$	2
		n	1	2δ

4.5.1 Unified Average SER

From (4.53), the average SER can be determined by solving the integral $\mathcal{L}(b_k) = \int_0^\infty p_\gamma(\gamma) e^{-b_k\sqrt{\gamma}}$, where b_k terms are defined in Table 4.1. Such integral has been studied in the previous chapter (3.38), it was solved using the FHF in (3.45). Hence, the average unified SER for BPSK, PAM, approximated QAM, and approximated MPSK in 3NT with EKG fading on the downlink, Laplacian intra-cell interference, and maximum likelihood detector is given by

$$\overline{SER} = \sum_{k=1}^{n} \frac{2a_k}{\Gamma(m)\Gamma(m_s)} \mathrm{H}_{1,2}^{2,1}\left[\frac{\beta\beta_s}{\overline{\gamma} b_k^2}\middle| \begin{matrix}(1,2)\\ (m,\frac{1}{\xi})(m_s,\frac{1}{\xi_s})\end{matrix}\right], \tag{4.54}$$

where a_k and b_k are defined in Table 4.1.

4.5.2 Exact Average SER for Rectangular QAM

The exact average SER of the QAM constellation is obtained by averaging (4.28) over the SIR distribution (2.13). From (4.28), the average SER can be determined by solving an integral in the form $\int_0^\infty p_\gamma(\gamma) P_{QAM}(e|\gamma) d\gamma$. The first two terms are similar to (4.54) and expressed in terms of the FHF. While the last term is solved using the Mellin representation of the BMGF [62]. Thereby, the average SER of rectangular QAM in 3NT with EGK fading on the downlink, Laplacian intra-cell interference, and maximum likelihood detector is described as

$$\begin{aligned}\overline{SER}_{QAM} &= \frac{2\rho(M_I)}{\Gamma(m)\Gamma(m_s)} \mathrm{H}_{1,2}^{2,1}\left[\frac{\beta\beta_s d^2}{12\overline{\gamma}}\middle| \begin{matrix}(1,2)\\ (m,\frac{1}{\xi})(m_s,\frac{1}{\xi_s})\end{matrix}\right] \\ &+ \frac{2\rho(M_Q)}{\Gamma(m)\Gamma(m_s)} \mathrm{H}_{1,2}^{2,1}\left[\frac{\beta\beta_s d^2}{12\tau^2\overline{\gamma}}\middle| \begin{matrix}(1,2)\\ (m,\frac{1}{\xi})(m_s,\frac{1}{\xi_s})\end{matrix}\right] \\ &- \frac{\rho(M_I)\rho(M_Q)}{\pi\Gamma(m)\Gamma(m_s)} \mathrm{H}_{2,1,1,2,1,2}^{0,2,2,0,2,1}\left[\tau^2, \frac{\beta\beta_s d^2}{3\overline{\gamma}}\middle| \begin{matrix}(\frac{1}{2},1),(1,1)\\ (0,1)\end{matrix}\middle| \begin{matrix}(1,1)\\ (\frac{1}{2},1),(0,1)\end{matrix}\middle| \begin{matrix}(0,1)\\ (m,\frac{1}{\xi}),(m_s,\frac{1}{\xi_s})\end{matrix}\right].\end{aligned} \tag{4.55}$$

4.5.3 Exact Average SER for MPSK

Using a similar proof to (4.55), the average SER of MPSK modulation can be obtained by averaging (4.51) over the PDF of γ. The first two terms will give a results similar to (4.54), while the last term can be expressed in terms of the BFHF using the Mellin representation of the BMGF. Thus, the average SER of MPSK in 3NT with EGK fading on the downlink, Laplacian intra-cell interference, and maximum likelihood detector is given by

$$\overline{SER}_{MPSK} = \frac{2}{\Gamma(m)\Gamma(m_s)} \mathrm{H}_{1,2}^{2,1}\left[\frac{\beta\beta_s}{4\delta^2\overline{\gamma}}\middle|\begin{matrix}(1,2)\\(m,\frac{1}{\xi})(m_s,\frac{1}{\xi_s})\end{matrix}\right] - \frac{2\delta}{M\sqrt{\pi}}\frac{1}{\Gamma(m)\Gamma(m_s)} \times \sum_{k=0}^{\frac{M}{4}-1} \mathrm{H}_{1,1,1,1,2,2}^{0,1,1,0,2,2}\left[\delta^2, \frac{4\beta\beta_s\delta^2(1-\delta^2)}{\overline{\gamma}\left(\cos\left(\frac{2k\pi}{M}\right)^2-\delta^2\right)}\middle|\begin{matrix}(\frac{1}{2},1)\\(-\frac{1}{2},1)\end{matrix}\middle|\begin{matrix}(\frac{1}{2},1)\\(0,1)\end{matrix}\middle|\begin{matrix}(1,1),(0,1)\\(m,\frac{1}{\xi})(m_s,\frac{1}{\xi_s})\end{matrix}\right]. \quad (4.56)$$

4.5.4 Special Cases of Fading and Simplification of $\overline{SER}$

In what follows we investigate several special cases for the EKG distribution where average SER reduces to more simplified expression. Note that we only consider the special cases for the unified average SER given in (4.54), which is given in terms of a_k and b_k defined in Table 4.1. On the other hand, the exact average SER of the rectangular QAM and MPSK cannot be further simplified because they are expressed in terms of the BFHF. Hence, only the approximations of the QAM and MPSK SER (that are included in the unified formula in (4.54)) are investigated in the following special cases. Note also that we are using the results described in Table 3.2 that contains the special cases of $\mathcal{L}(\cdot)$ for different type of fading.

4.5.4.1 Generalized-$\mathcal{K}$ Fading

The GK fading is obtained by setting $\xi = \xi_s = 1$. From Table 3.2, the average SER can be simplified to

$$\overline{SER} = \sum_{k=1}^{n} \frac{a_k}{\sqrt{\pi}\Gamma(m)\Gamma(m_s)} \mathrm{G}_{2,2}^{2,2}\left[\frac{4mm_s}{\overline{\gamma}b_k^2}\middle|\begin{matrix}1, \frac{1}{2}\\ m, m_s\end{matrix}\right]. \tag{4.57}$$

This expression is in terms of the MGF which is less complex in terms of computation than the FHF.

4.5.4.2 $\mathcal{K}$ Fading Distribution

The $\mathcal{K}$ distribution is a special case of the generalized-$\mathcal{K}$ fading distribution, that is obtained by setting $\xi_s = \xi = 1$ and $m_s = 1$. Hence the average SER can be simplified to

$$\overline{SER} = \sum_{k=1}^{n} \frac{a_k}{\sqrt{\pi}\Gamma(m)} \mathrm{G}_{2,2}^{2,2}\left[\frac{4m}{\overline{\gamma}b_k^2}\middle|\begin{matrix}1, \frac{1}{2}\\ 1, m\end{matrix}\right]. \tag{4.58}$$

4.5.4.3 Generalized Nakagami-m GNM

From Table 3.2 the ASER expression of GNM fading can be reduced to

$$\overline{SER} = \sum_{k=1}^{n} \frac{2a_k\xi}{\Gamma(m)} \left(\frac{\beta}{b_k^2\overline{\gamma}}\right)^{m\xi} \Gamma\left(2m\xi, 0, \left(\frac{\beta}{b_k^2\overline{\gamma}}\right)^{\xi}, -2\xi\right). \tag{4.59}$$

4.5.4.4 Nakagami-m

The Nakagami-m fading distribution is a special case of the GNM when $\xi = 1$. Using the special case of $\mathcal{L}(\cdot)$ in Table 3.2, the average SER further simplifies to

$$\overline{SER} = \sum_{k=1}^{n} \frac{2a_k\Gamma(2m)}{4^m\Gamma(m)} U\left(m, \frac{1}{2}, \frac{b_k^2\overline{\gamma}}{4m}\right). \tag{4.60}$$

4.5.4.5 Rayleigh Fading

Rayleigh fading is the last and simplest special case, which is a special case of the Nakagami-m fading for $m = 1$. In this case, the SER is obtained in its simplest form as

$$\overline{SER} = \sum_{k=1}^{n} a_k \left(1 - b_k \sqrt{\pi \overline{\gamma}} e^{\frac{b_k^2 \overline{\gamma}}{4}} Q\left(b_k \sqrt{\frac{\overline{\gamma}}{2}} \right) \right). \tag{4.61}$$

Although the average SER over any special case of fading of the EGK can be deduced from (4.54) by setting the quadruplet (m, m_s, ξ, ξ_s) to the desired values, the previous studied special cases are highlighted because they are the most commonly used distribution to characterize the flat fading channels. Moreover, the results obtained in this section and Table 3.2 are given in their simplest forms, which require several manipulations after substituting (m, m_s, ξ, ξ_s) by their desired values.

4.6 Throughput Analysis

The error rate analysis shown in Section 4.4 shows only the negative effect of the FD communication in 3NT. This is because the error rate for a given modulation scheme is a function of the SIR only which is degraded by the intra-cell interference. In order to see the overall effect of the 3NT FD communication, we look at the throughput which is a function of both the degraded SIR as well as the improved BW. The throughput is defined as

$$\mathcal{T} = \frac{\log_2(M) \left(1 - \overline{SER}\right)}{t_s} \tag{4.62}$$

where $\log_2(M)$ is the number of bits per symbol, t_s is the symbol duration, and $\overline{SER}$ is the average SER. For the HD case, we assume error free transmission and

channel BW of B. Consequently, the HD throughput is given by

$$\mathcal{T}_{HD} = B \log_2(M). \tag{4.63}$$

For the FD case, the 3NT increases the channel BW to $2B$ on the expense of intra-cell interference that imposes detection errors. Consequently, the FD throughput is given by

$$\mathcal{T}_{FD} = 2B \log_2(M) \left(1 - \overline{SER}\right). \tag{4.64}$$

For each modulation scheme, we define the throughput gain imposed by the 3NT FD communication as

$$\mathcal{G} = \frac{\mathcal{T}_{FD}}{\mathcal{T}_{HD}} = 2 \left(1 - \overline{SER}\right). \tag{4.65}$$

where $\overline{SER}$ is given in (4.54), (4.55), and (4.56).

4.7 Numerical Results

This section shows some selected numerical results supported by Monte Carlo Matlab® simulations to validate the developed mathematical paradigm and obtain insights into the 3NT FD operation. Particularly, we validate the Gaussian signaling assumption for the interfering symbol in (4.1), the dominance of the intra-cell interference when compared to the noise in (4.2), and the MQAM and MPSK error rates approximations in (4.31) and (4.52), respectively.
All results are plotted against the average SIR $\bar{\gamma} = \frac{P_d \mathcal{A}_d}{P_u \mathcal{A}_u}$, which is varied from 0 dB to 40 and/or 50 dB to capture the 3NT operation in different types of BSs. That is, we can infer the cell size (i.e., BS type) from the average SIR value. For instance, the transmit power of small BSs (e.g., femto and pico BSs) is comparable to the UE power, which is typically in the range of 200 mW to 1 W. Therefore, in small BS

scenario the average SIR term depends on the relative large-scale attenuation factors $\mathcal{A}_d$ and $\mathcal{A}_u$, which may lead to small values of $\bar{\gamma}$. Macro BSs transmit power is typically several tens of watts, and hence, in a Macro BSs scenario the downlink power P_d dominates the average SIR term leading to high values of $\bar{\gamma}$.

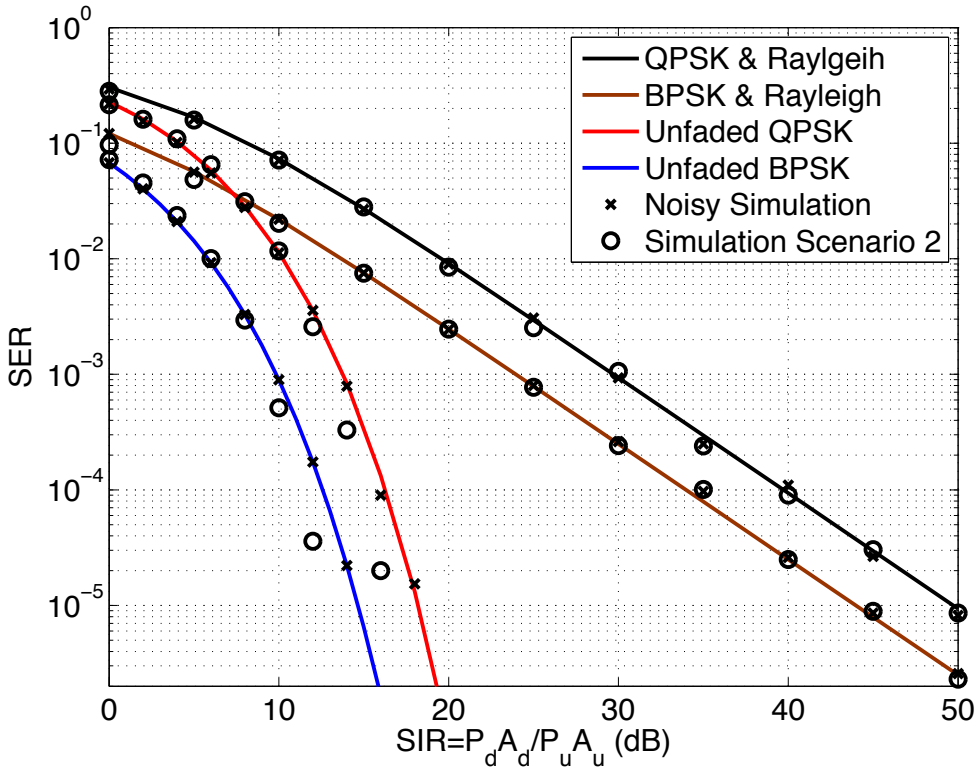

Figure 4.3: SER of BPSK and QPSK schemes with and without Rayleigh fading.

Fig. 4.3 shows the SER of BPSK and 4-QAM (or equivalently QPSK). In Fig. 4.3 the analysis is validated via two simulation scenarios, namely the *"Noisy Simulation"* and *"Simulation Scenario 2"*. In the *Noisy Simulation*, the received signal is perturbed by a Gaussian noise in addition to the Laplacian interference, which perfectly matches the analysis and validates the derived SER expressions. The interfering UE in *Simulation Scenario 2* randomly and uniformly alternates between BPSK and M-QAM for $M \in \{4, 16, 64\}$. Hence, *Simulation Scenario 2* validates the Gaussian signaling assumption of the interfering UEs. The figure shows

that the accuracy of the Gaussian signaling assumption is better for faded downlink scenarios. This is because fading on the downlink increases the level of uncertainties in the detection process at the test UE, which puts less significance on the interfering symbol distribution from the interfering UE and vice versa. Nevertheless, the Gaussian signaling approximation always shows good accuracy in the low SIR regime, which is a critical region of operation to avoid throughput degradation.

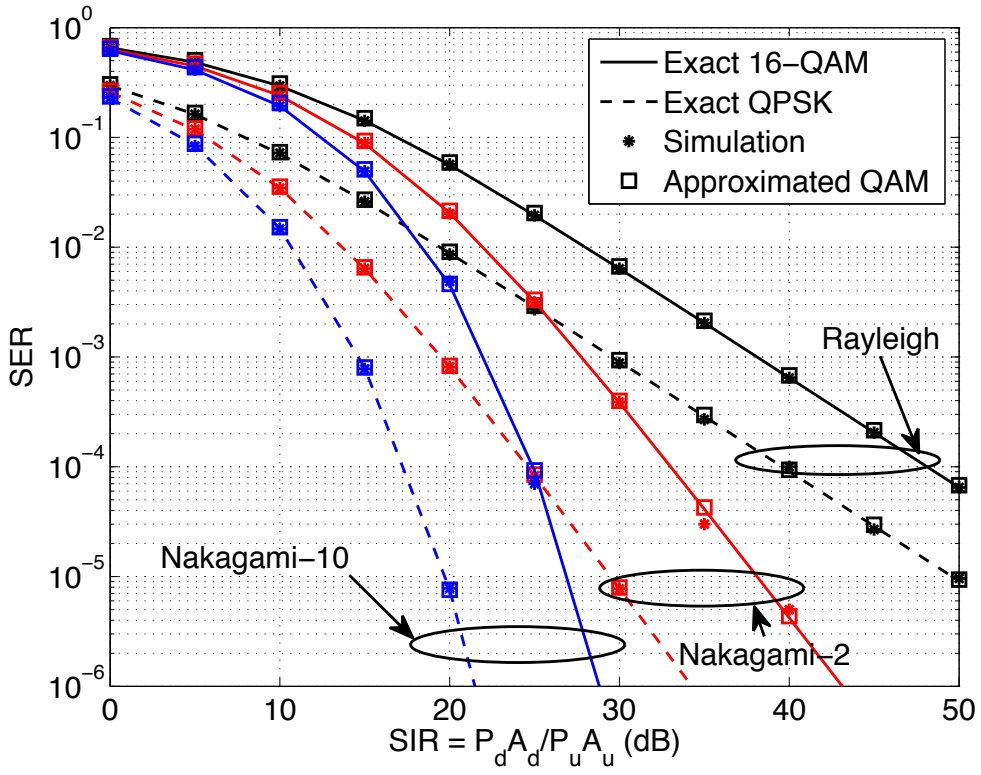

Figure 4.4: SER of QPSK and 16-QAM schemes over Nakagami-m fading for $m = 1,\ 2$, and 10 and negligible noise. The stars denote the simulation results and the squares denote the approximation SER.

Fig. 4.3 and Fig. 4.4 show the cost of intra-cell interference in terms of error probability for different modulation schemes and fading models on the downlink. Generally, the figures show that intra-cell interference can severely degrade the downlink performance at low SIR, which may happen in small-cell scenario due to the small transmit power as well as the small BS footprint (i.e., users pairs can be

close to each other). On the other hand, the effect of intra-cell interference diminishes in macro cells (i.e., at high $\bar{\gamma}$ value) specially for good downlink channel condition. The figure also shows that the gap between the constellations decreases by increasing the fading severity (from 5dB to 2dB for SER=10^{-5}), which is due to the dominance of the fading conditions on the error probability.

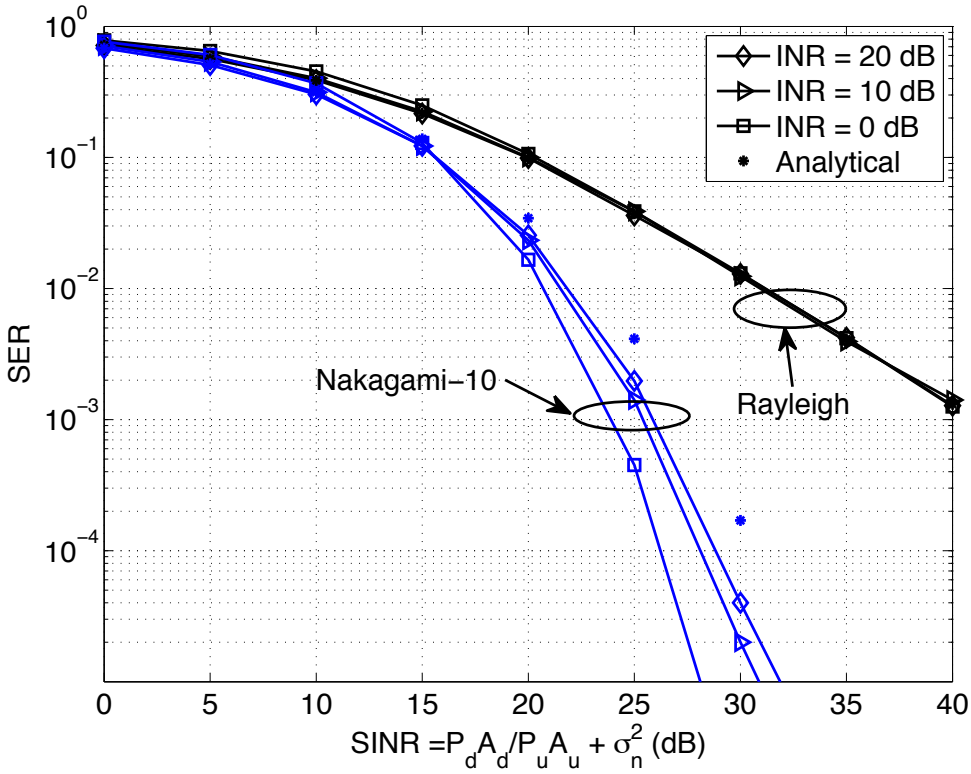

Figure 4.5: SER of 16PSK scheme through Rayleigh fading and Nakagami-4 channels with different values of INR. The stars denote the analytical results without noise.

Fig. 4.5 is plotted to investigate the Laplacian interference dominance assumption in (4.2) and to show the model accuracy when varying the interference-to-noise-power-ratio (INR). The figure draws the SER of 16PSK scheme in two types of fading channel, namely, Nakagami-4 channel and Rayleigh channel. The SER is plotted versus the signal to interference plus noise ratio (SINR) (where σ_n^2 represents the noise power) for fixed noise-plus-interference power but different

values for the INR. Particularly, three values of INR are investigated, (i) dominant interference INR = 20 dB, (ii) less dominant interference INR = 10 dB, and (iii) equal ratio between interference and thermal noise INR= 0dB. At first, the figure shows a close match between the theoretical results and simulations in all fading scenarios and INR values at low SINR regime. However, at high SINR regime, the model accuracy depends on the fading scheme. In the Rayleigh fading scenario, the noise effect is negligible and the theoretical results exactly matches all INR cases in the high SINR regime. However, in Nakagami-4 scenario (i.e., less fading severity) the theoretical results represent an upper-bound for the SER at high SINR regime due to the heavy tailed distribution of the Laplacian perturbation. Note that the gap between the theoretical results and simulations diminishes at sever fading (i.e., Rayleigh) and/or low SINR regime because the effect of the noise/interference tail distributions on the SER performance is not significant. That is, the error may occur at low values of interference plus noise, and hence, the tail distribution does not have a prominent effect. On the other hand, at high SINR regime and/or less sever fading, the error occurs at high interference plus noise power. Hence, the tail distribution effect becomes prominent and the gap is more noticeable.

Fig. 4.6 shows the complete picture of the intra-cell interference effect imposed by the 3NT FD by looking at the throughput gain with respect to the interference free HD scenario. Interestingly, the figure shows that the throughput gain is always greater than unity for BPSK regardless of the SIR severity. This is because the FD doubles the transmission rate while the worst case error probability for BPSK is one half. However, for higher modulation schemes, which are typical for downlink transmission, the intra-cell interference can significantly degrade the effective throughout. For instate, and 80% throughout degradation occurs for 64-QAM modulation at 0 dB SIR. On the other hand, at high SIR regime, 3NT doubles the effective throughput. The throughput gain, which relays on the developed error rate

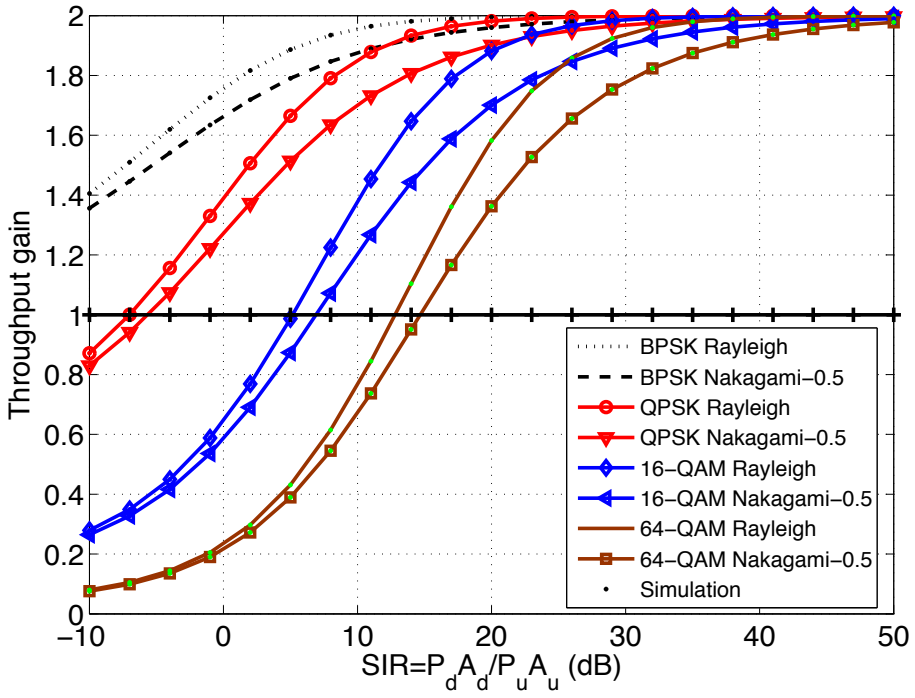

Figure 4.6: Throughput gain of BPSK and QPSK over Rayleigh and Nakagami-0.5.

model, can be used to maximize the transmission rate via adaptive modulation based on the experienced SIR and fading severity.

4.8 Conclusion

This chapter developed a mathematical paradigm to study downlink error rate and throughput for half-duplex users when served by FD BSs via 3-node topology (3NT). Assuming that the interfering user transmits Gaussian signals and the interference channel experience Rayleigh fading, the base-band intra-cell interference is shown to be Laplacian with dependent real and imaginary parts. A closed form expressions were derived later for the average symbol error rate for BPSK, PAM, and QAM modulation schemes for unfaded and EKG faded downlink channel. To this end, we derive the effective throughput gain imposed by 3NT FD when

compared to an idealized interference and noise free HD scenario. The results show the severe degradation that may happen when employing 3NT FD in small cells, specially for schemes with big constellation sizes. On the other hand, 3NT provide nontrivial gains when employed in macro cells which high downlink transmission power. The developed paradigm can be used to adaptively change the modulation scheme according the SIR and downlink channel condition to maximize the downlink throughput.

By the end of this part of the thesis, we may notice that we studied the performance of several communication system that are perturbed by generalized Gaussian noise, independent Laplace noise, and dependent Laplace interference. However, another type of perturbation namely α stable noise is of interest. In the following chapter, the statistics of the symmetric α stable distribution are investigated. Moreover, the performance of some digital communication systems operating in environments perturbed by α-stable noise is presented.

Chapter 5

Performance Analysis over a Channel with Additive Symmetric α Stable Noise

The α-stable distribution was defined the first time by Lévy [31]. Actually, the stable distribution is defined only by its CHF[12]. This distribution is parameterized by the stable parameter α ($0 < \alpha \leq 2$), the skewness parameter β ($-1 \leq \beta \leq 1$), the scale parameter γ ($\gamma > 0$), also known as the dispersion, and the location μ ($\mu \in \mathbb{R}$) that gives the distribution mean for $1 < \alpha \leq 2$ and the median for $0 < \alpha \leq 1$. The dispersion γ denotes the spread around the location parameter μ, it behaves like the variance [48]. The symmetric α-stable distribution, noted also as $S\alpha S$, is obtained by setting $\beta = 0$. We are focusing on this chapter on the symmetric distribution rather than the general distribution because it is the mainly used distribution in the literature.

It should be mentioned that the PDF and CDF of the α-stable distribution were not expressed in closed-form previously. Thus the purpose of this chapter is to find a closed form expressions of the PDF and CDF of the $S\alpha S$ distribution by solving the inverse Fourier integral using the $S\alpha S$ characteristic function. In addition, and as

an application, a closed form of the probability of error of SISO digital communication system in presence of $S\alpha S$ perturbation is investigated using different modulation schemes (BPSK, PAM, and QAM).

5.1 Statistics of the $S\alpha S$ Distribution

If a random variable X follows an $S\alpha S$ distribution, then its CHF can be expressed as [12]

$$\varphi_X(t) = e^{j\mu t - |ct|^\alpha}, \tag{5.1}$$

where μ is the location parameter and c is the dispersion parameter. Note that γ in [12] is replaced by c to avoid any confusion in what follows with the SNR γ.

5.1.1 PDF of $S\alpha S$ Random Variable

The PDF of the $S\alpha S$ distribution can be obtained by the inverse Fourier transform of the CHF. Actually the PDF of X, denoted by $f_X(x, \alpha)$ has an integral expression as follows

$$f_X(x, \alpha) = \frac{1}{2\pi} \int_{-\infty}^{+\infty} \varphi_X(t) e^{-jxt} \, \mathrm{d}t. \tag{5.2}$$

The major result in this chapter is obtained by solving this integral. In fact, we may replace the CHF by its expression in (5.2) to get

$$f_X(x, \alpha) = \frac{1}{2\pi} \int_{-\infty}^{+\infty} e^{jt(\mu - x) t - |ct|^\alpha} \, \mathrm{d}t. \tag{5.3}$$

Since the function $t \to |t|$ is an even function, the integral in (5.3) can be written as a cosine transform of $e^{-|ct|^\alpha}$

$$f_X(x, \alpha) = \frac{1}{\pi} \int_0^{\infty} \cos\left(t(x - \mu)\right) e^{-c^\alpha t^\alpha} \, \mathrm{d}t. \tag{5.4}$$

Now we recall an alternative expressions of the cosine function [55, Eq. (2.9.8)] and exponential function [55, Eq. (2.9.4)] in terms of the FHF

$$\cos(x) = \sqrt{\pi}\ \mathrm{H}_{0,2}^{1,0}\left[\frac{x^2}{4}\,\middle|\,\begin{matrix}\overline{\qquad}\\(0,1),(\frac{1}{2},1)\end{matrix}\right] \tag{5.5}$$

$$e^{-x^\alpha} = \frac{1}{\alpha}\mathrm{H}_{0,1}^{1,0}\left[x\,\middle|\,\begin{matrix}\overline{\qquad}\\(0,\frac{1}{\alpha})\end{matrix}\right]. \tag{5.6}$$

Then (5.4) is transformed to an integral of a product of two FHFs

$$f_X(x,\alpha) = \frac{1}{\alpha\sqrt{\pi}}\int_0^\infty \mathrm{H}_{0,1}^{1,0}\left[ct\,\middle|\,\begin{matrix}\overline{\qquad}\\(0,\frac{1}{\alpha})\end{matrix}\right]\mathrm{H}_{0,2}^{1,0}\left[\frac{(x-\mu)^2}{4}t^2\,\middle|\,\begin{matrix}\overline{\qquad}\\(0,1),(\frac{1}{2},1)\end{matrix}\right]\,\mathrm{d}t, \tag{5.7}$$

which can be solved using the identity (2.21) to get a closed form of the PDF of the $S\alpha S$ distribution as follows

$$f_X(x,\alpha) = \frac{1}{\alpha c\sqrt{\pi}}\mathrm{H}_{1,2}^{1,1}\left[\frac{(x-\mu)^2}{4c^2}\,\middle|\,\begin{matrix}(1-\frac{1}{\alpha},\frac{2}{\alpha})\\(0,1),(\frac{1}{2},1)\end{matrix}\right]. \tag{5.8}$$

Since μ is the median of the $S\alpha S$ distribution and the mean is not defined for $\alpha < 1$, we will assume that μ behaves like the mean in the analysis below. In the same analogy, the variance is not defined for all values of α so the Gaussian variance (i.e. $\sigma^2 = 2c^2$) will be considered as the variance of the random variable X.

5.1.2 CDF of $S\alpha S$ Random Variable

The CDF appears as the primitive of the PDF that vanishes at $-\infty$. From (5.4), the cosine function is replaced by its primitive (i.e. sine function) and using the representation of the sine function in terms of the FHF available in (4.12) and [55, Eq. (2.9.7)]

$$\sin(x) = \sqrt{\pi}\ \mathrm{H}_{0,2}^{1,0}\left[\frac{x^2}{4}\,\middle|\,\begin{matrix}\overline{\qquad}\\(\frac{1}{2},1),(0,1)\end{matrix}\right], \tag{5.9}$$

we get an integral of a product of two H functions which can be solved in closed-form (2.21) to express the CDF of $S\alpha S$ distribution as

$$F_X(x,\alpha) = \frac{1}{2} + \frac{sign(x-\mu)}{\alpha\sqrt{\pi}} \mathrm{H}_{1,2}^{1,1}\left[\frac{(x-\mu)^2}{4c^2}\middle| \begin{matrix}(1,\frac{2}{\alpha})\\ (\frac{1}{2},1),(0,1)\end{matrix}\right], \tag{5.10}$$

where $sign(x)$ is the signum of x, and the $\frac{1}{2}$ term is to ensure that the CDF vanishes at $-\infty$.

Another function, that looks interesting to define, is the CCDF. Actually the CCDF is used essentially to compute the probability of error of different communication systems. To simplify things, we denote by $\psi_\alpha(x)$ the CCDF of a standard $S\alpha S$ distribution, i.e. $\mu = 0$ and $\sigma = 1$ ($c^2 = \frac{1}{2}$). In other words, $\psi_\alpha(x) = 1 - F_X(x,\alpha)$ can be expressed as

$$\psi_\alpha(x) = \frac{1}{2} - \frac{1}{\alpha\sqrt{\pi}} \mathrm{H}_{1,2}^{1,1}\left[\frac{x^2}{2}\middle| \begin{matrix}(1,\frac{2}{\alpha})\\ (\frac{1}{2},1),(0,1)\end{matrix}\right],\ \forall\ x \geq 0, \tag{5.11}$$

and $\psi_\alpha(x) = 1 - \psi_\alpha(-x)$ for $x < 0$.

5.1.3 $S\alpha S$ Distribution for Rational α

For rational values of α, the PDF of zero median $S\alpha S$ distribution can be expressed in terms of the MGF [55, Eq. (2.9.1)]. In fact, by application of the identity [60, Eq. (8.3.22)], that relates the FHF and the MGF for rational parameters, to (5.8), a new epxression of the PDF can be given as

$$f_X(x,\frac{p}{q}) = \frac{(2q)^{\frac{q}{p}}}{c\,(2\pi)^q}\sqrt{\frac{q}{p}}\mathrm{G}_{2q,2p}^{p,2q}\left[\frac{x^{2p}(2q)^{2q}}{(2pc)^{2p}}\middle| \begin{matrix}\Delta\left(2q,1-\frac{q}{p}\right)\\ \Delta(p,0),\Delta(p,\frac{1}{2})\end{matrix}\right], \tag{5.12}$$

where p and q are positive integers defined as $\alpha = \frac{p}{q}$, and $\Delta(k,b)$ is the sequence defined by $\Delta(k,b) = \frac{b}{k}, \frac{b+1}{k}, \cdots, \frac{b+k-1}{k}$.

Using the same identity [60, Eq. (8.3.22)], the CCDF can be written also in terms of

the MGF for rational values of α as

$$\psi_{\frac{p}{q}}(x) = \frac{1}{2} + \frac{1}{(2\pi)^q}\sqrt{\frac{q}{p}}\mathrm{G}_{2q,2p}^{p,2q}\left[\frac{x^{2p}(2q)^{2q}}{(2pc)^{2p}}\,\middle|\,\begin{matrix}\Delta\,(2q,1)\\ \Delta(p,\frac{1}{2}),\Delta(p,0)\end{matrix}\right]. \tag{5.13}$$

5.2 Conditional Error Rates

In this section we investigate the probability of error of a SISO communication system with different modulation schemes conditioned over the defined SNR. In fact, let's assume that the mathematical model of the system is similar to the system in (2.14), $\mathcal{R} = \mathcal{H}\,\mathcal{S} + \mathcal{N}$. The perturbation $\mathcal{N} \in \mathbb{R}$ is modeled by an $S\alpha S$ distribution (rather than generalized Gaussian in Chapter 2). It can represent either additive noise or additive interference with negligible thermal noise according to the application in use. We assume that the discrete time model at the output of the optimal filter is the same as described in (2.14). In addition, the noise defined variance is σ^2 and the instantaneous SNR is defined in (2.9) by $\gamma = \frac{\mathcal{H}^2 E_S}{\sigma^2}$, while the average SNR per symbol at the receiver is equal to $\overline{\gamma} = \mathbb{E}[\gamma] = \frac{\mathbb{E}[\mathcal{H}^2]E_S}{\sigma^2}$. In what follows, the conditional error probability of several digital communication systems over $S\alpha S$ perturbation is investigated.

5.2.1 BER of BPSK over $S\alpha S$ Perturbation

Let $S_\pm = \pm\sqrt{E_S}$ be the binary transmitted signal. Hence, the received signal $\mathcal{R}$ is considered as an $S\alpha S$ random variable with location parameter $\mu = \pm\mathcal{H}\sqrt{E_S}$. Since the transmitted symbols have the same a-priori probability of occurrence, the ML detector decides $\pm\sqrt{E_S}$ if $f_\mathcal{R}(r|\pm\sqrt{E_S}) \geq f_\mathcal{R}(r|\mp\sqrt{E_S})$. Using a similar analysis as that provided in Section 2.2, the decision can be made using the monotonicity of the PDF. To do so, let us compute the derivative of the PDF of a standard $S\alpha S$ to confirm its decreasing behavior in the positive range. Actually using the derivative

formula of the FHF [55, Eq. (2.2.7)], we obtain the following expression

$$\frac{df_X}{dx}(x,\alpha) = -\frac{2}{\alpha c x\sqrt{\pi}}\mathrm{H}_{1,2}^{1,1}\left[\frac{x^2}{4c^2}\,\middle|\,\begin{matrix}(1-\frac{1}{\alpha},\frac{2}{\alpha})\\(1,1),(\frac{1}{2},1)\end{matrix}\right]. \tag{5.14}$$

The FHF in (5.14) is similar to the FHF in (5.8) and so it is a positive function (it was also checked numerically that its a positive function). Thus it is clear from (5.14) that the $f_{\mathcal{R}}$ is a decreasing function. Then the ML detector can be given as (2.16)

$$\text{Decide } \mathrm{S}_{\pm} \text{ if } \left|\mathcal{R} - \sqrt{\frac{\mathrm{N}_0}{\mathrm{E}_{\mathcal{S}}}\gamma}\,\mathrm{S}_{\pm}\right| \leq \left|\mathcal{R} - \sqrt{\frac{\mathrm{N}_0}{\mathrm{E}_{\mathcal{S}}}\gamma}\,\mathrm{S}_{\mp}\right|. \tag{5.15}$$

Finally the the BER of BPSK system can be obtained as

$$P_{BPSK}\left(e|\gamma\right) = \psi_{\alpha}(\sqrt{\gamma}). \tag{5.16}$$

5.2.2 SER of PAM Constellation

In this application, we consider an M-PAM constellation with distance between symbols d, the symbol error rate of PAM can be deduced from the BER of a BPSK modulation. Similar to the analysis done in Section 2.3, the SER of PAM contains two terms, the first term related to the outermost symbols (2 symbols), while the second term considers the remaining $M-2$ symbols. In more details, the first term is equal to the error between an outermost symbol and its closest neighbor with distance between them d, which results on $P_{out} = P_{BPSK}(e|\frac{d}{\sigma}) = \psi_{\alpha}(\frac{d}{\sigma})$. The second term is equal to the error between one of the $M-2$ remaining symbols and its neighbors (2 symbols), so $P_{in} = 2P_{BPSK}(e|\frac{d}{\sigma}) = 2\psi_{\alpha}(\frac{d}{\sigma})$. By combining all the terms we get the SER of the M-PAM constellation as

$$P_{PAM}\left(e|d\right) = \frac{2}{M}\left(\psi_{\alpha}\left(\frac{d}{\sigma}\right) + (M-2)\psi_{\alpha}\left(\frac{d}{\sigma}\right)\right) = 2\left(1-\frac{1}{M}\right)\psi_{\alpha}\left(\frac{d}{\sigma}\right), \tag{5.17}$$

where the average energy per symbol is computed as $E_S = \frac{d^2}{12}(M^2 - 1)$. Finally the conditional SER in terms of the SNR, γ, is obtained as

$$P_{PAM}\left(e|\gamma\right) = 2\left(1 - \frac{1}{M}\right)\psi_\alpha\left(\sqrt{\frac{3\gamma}{M^2-1}}\right). \tag{5.18}$$

5.2.3 SER of QAM Modulation

The QAM constellation is constructed by two orthogonal PAM modulations, such that the in-phase M_I-PAM and the quadrature phase M_Q-PAM. Since both component of noise (or interference) are assumed to be independent, a correct reception of the QAM symbol holds only when there is a correct reception of the independent PAM signals. An expression of the SER of QAM modulation in presence of $S\alpha S$ noise is given by

$$\begin{aligned} P_{QAM}(e) = & 2\left(1-\frac{1}{M_I}\right)\psi_\alpha\left(\frac{d_I}{\sigma}\right) + 2\left(1-\frac{1}{M_Q}\right)\psi_\alpha\left(\frac{d_Q}{\sigma}\right) \\ & - 4\left(1-\frac{1}{M_I}\right)\left(1-\frac{1}{M_Q}\right)\psi_\alpha\left(\frac{d_I}{\sigma}\right)\psi_\alpha\left(\frac{d_Q}{\sigma}\right), \end{aligned} \tag{5.19}$$

where d_I and d_Q are the in-phase and quadrature phase decision distance, respectively. Note that the average energy per symbol is expressed as

$$E_S = \frac{1}{12}d_Q^2(M_Q^2 - 1) + \frac{1}{12}d_I^2(M_I^2 - 1). \tag{5.20}$$

The product of two ψ_α functions is negligible regarding one ψ_α, so the expression of the SER of QAM modulation can be approximated as the sum of the first two terms. It is worth mentioning that all the previous BER and SER are expressed in terms of $\psi_\alpha(t\sqrt{\gamma})$, where t depends on the desired modulation.

5.3 Average Error Rates Over EGK Fading

5.3.1 Exact Expressions

The previous analysis is done conditioned on the channel fading. As mentioned previously, let's assume that the fading follows an EGK distribution Sec. 2.1.2. Using the fact that the error rates of the BPSK, PAM, and QAM are expressed in terms of $\psi_\alpha(t\sqrt{\gamma})$, we need to average that function over the SNR distribution to get $\Psi_\alpha(t)$

$$\Psi_\alpha(t) = \int_0^\infty \psi_\alpha(t\sqrt{\gamma}) p_\gamma(\gamma) \mathrm{d}\gamma. \tag{5.21}$$

In fact the $\psi_\alpha(\cdot)$ function is already expressed in terms of the FHF and an expression of the $p_\gamma(\gamma)$ in terms of FHF is available in (2.13). An integral of the product of two FHF occurs, which can be solved using the identity (2.21) to get

$$\Psi_\alpha(t) = \frac{1}{2} - \frac{1}{\alpha\sqrt{\pi}\Gamma(m)\Gamma(m_s)} \mathrm{H}_{2,3}^{3,1}\left[\frac{2\beta\beta_s}{\overline{\gamma}t^2}\middle|\begin{matrix}(\frac{1}{2},1)(1,1)\\(0,\frac{2}{\alpha})(m,\frac{1}{\xi})(m_s,\frac{1}{\xi_s})\end{matrix}\right]. \tag{5.22}$$

Thus the average error rates of BPSK and PAM and approximately the QAM are expressed as

$$\begin{aligned}
\mathrm{Pr}_{BPSK}(e) &= \Psi_\alpha(1)\\
\mathrm{Pr}_{PAM}(e) &= 2\left(1-\frac{1}{M}\right)\Psi_\alpha\left(\sqrt{\frac{3}{M^2-1}}\right)\\
\mathrm{Pr}_{QAM}(e) &\approx 2\left(1-\frac{1}{M_I}\right)\Psi_\alpha\left(A_I\right) + 2\left(1-\frac{1}{M_Q}\right)\Psi_\alpha\left(A_Q\right),
\end{aligned} \tag{5.23}$$

where $A_I = d_I/\sigma$ and $A_Q = d_Q/\sigma$.

The last expression of the SER of QAM constellation is an approximation of the exact value. In fact the last term, which is the product of two $\psi_\alpha(\cdot)$ functions , is neglected regarding the first two terms that contains the sum of two $\psi_\alpha(\cdot)$. In

addition, the average of the neglected term appears as an integral of the product of three FHF, such integral can be solved using the BFHF and the identity (2.48) which is considered as a future work together with the SER of MPSK subject to $S\alpha S$ perturbation.

5.3.2 Asymptotic Expansion

Since the expressions of the error probability are in terms of a complex function, such that the FHF, an approximation of the error rates at high SNR is important to study. In fact, the asymptotic approximation of the function $\Psi_\alpha(\cdot)$ for high SNR can be obtained from the properties of the FHF [55, Ch. 1] as

$$\Psi_\alpha(a) \overset{\gamma \gg 1}{\approx} \frac{1}{\alpha\sqrt{\pi}\Gamma(m)\Gamma(m_s)} \left(h_1 \left(\frac{2\beta\beta_s}{\overline{\gamma}a^2} \right)^{m_s\xi_s} + h_2 \left(\frac{2\beta\beta_s}{\overline{\gamma}a^2} \right)^{m\xi} \right), \tag{5.24}$$

where h_1 and h_2 are given by

$$h_1 = \frac{\Gamma\left(m - m_s\frac{\xi_s}{\xi}\right)\Gamma\left(-2m_s\frac{\xi_s}{\alpha}\right)\Gamma\left(\frac{1}{2} + m_s\xi_s\right)}{m_s\,\Gamma(-m_s\xi_s)}$$
$$h_2 = \frac{\Gamma\left(m_s - m\frac{\xi}{\xi_s}\right)\Gamma\left(-2m\frac{\xi}{\alpha}\right)\Gamma\left(\frac{1}{2} + m\xi\right)}{m\,\Gamma(-m\xi)}.$$

5.3.3 Special Cases of $S\alpha S$

The closed form of $\Psi_\alpha(\cdot)$ in (5.22) is a general formula. We now focus on some special cases of noise and fading. Three cases of noises will be studied in this section. In particular, we focus on the noise with $\alpha = \frac{1}{2}$, the Cauchy noise for which $\alpha = 1$, and the Gaussian noise for which $\alpha = 2$.

5.3.3.1 $S\alpha S$ with $\alpha = \frac{1}{2}$

The averaged CCDF over the EGK distribution, $\Psi_{\frac{1}{2}}(t)$, is obtained from (5.22) as

$$\Psi_{\frac{1}{2}}(t) = \frac{1}{2} - \frac{2}{\sqrt{\pi}\Gamma(m)\Gamma(m_s)} \mathrm{H}_{2,3}^{3,1}\left[\frac{2\beta\beta_s}{\overline{\gamma}t^2}\middle|\begin{matrix}(\frac{1}{2},1)(1,1)\\(0,4)(m,\frac{1}{\xi})(m_s,\frac{1}{\xi_s})\end{matrix}\right]. \tag{5.25}$$

In Table 5.1, a simplified expressions of the function $\Psi_{\frac{1}{2}}(\cdot)$ and its asymptotic expansion are given for the GNM, Nakagami-m and Rayleigh fading distribution. Actually these distributions can be obtained from the EGK by setting the parameters (m, m_S, ξ, ξ_s) to $(m, \infty, \xi, 1)$, $(m, \infty, 1, 1)$, and $(1, \infty, 1, 1)$ respectively.

Table 5.1: Average CCDF, $\Psi_{\frac{1}{2}}(a)$ and its asymptotic expansion

Fading	$\Psi_{\frac{1}{2}}(a)$	Asymptotic
GNM	$\frac{1}{2} - \frac{2}{\sqrt{\pi}\Gamma(m)}\mathrm{H}_{2,2}^{2,1}\left[\frac{2\beta}{\overline{\gamma}a^2}\middle\vert\begin{matrix}(\frac{1}{2},1)(1,1)\\(0,4)(m,\frac{1}{\xi})\end{matrix}\right]$	$\frac{2}{\sqrt{\pi}\Gamma(m+1)}\frac{\Gamma(-4m\xi)\Gamma(\frac{1}{2}+m\xi)}{\Gamma(-m\xi)}\left(\frac{2\beta}{\overline{\gamma}a^2}\right)^{m\xi}$
Nakagami-m	$\frac{1}{2} - \frac{1}{2\sqrt{2}\pi^2\Gamma(m)}\mathrm{G}_{2,5}^{5,1}\left[\frac{m}{128\overline{\gamma}a^2}\middle\vert\begin{matrix}\frac{1}{2},1\\0,\frac{1}{4},\frac{1}{2},\frac{3}{4},m\end{matrix}\right]$	$\frac{2\Gamma(m-\frac{1}{4})}{\sqrt{\pi}\Gamma(m)}\left(\frac{m}{128\overline{\gamma}a^2}\right)^{\frac{1}{4}} - \frac{4\Gamma(m-\frac{1}{2})}{\pi\Gamma(m)}\left(\frac{m}{128\overline{\gamma}a^2}\right)^{\frac{1}{2}}$ $+\frac{4\Gamma(m-\frac{3}{4})}{3\sqrt{\pi}\Gamma(m)}\left(\frac{m}{128\overline{\gamma}a^2}\right)^{\frac{3}{4}}$ $-\frac{\Gamma(\frac{1}{4}-m)\Gamma(\frac{1}{2}-m)\Gamma(\frac{3}{4}-m)\Gamma(\frac{1}{2}+m)}{2\sqrt{2}\pi^2\Gamma(m+1)}\left(\frac{m}{128\overline{\gamma}a^2}\right)^{m}$
Rayleigh	$\frac{1}{2} - \frac{1}{2\sqrt{2}\pi^2}\mathrm{G}_{1,4}^{4,1}\left[\frac{m}{128\overline{\gamma}a^2}\middle\vert\begin{matrix}\frac{1}{2}\\0,\frac{1}{4},\frac{1}{2},\frac{3}{4}\end{matrix}\right]$	$\frac{1}{\sqrt{\pi}}\left(\frac{8\Gamma(3/4)}{(128\overline{\gamma}a^2)^{\frac{1}{4}}} - \frac{1}{a\sqrt{2\overline{\gamma}}} + \frac{4\Gamma(1/4)}{3(128\overline{\gamma}a^2)^{\frac{3}{4}}}\right)$

5.3.3.2 Cauchy Distribution, $\alpha = 1$

The averaged CCDF over the EGK distribution, $\Psi_1(t)$, is obtained from (5.22) by replacing α by 1. The simplified results for the Cauchy distribution are summarized in Table 5.2. In Table 5.2, $\Gamma(\cdot,\cdot)$ is the upper incomplete Gamma function [57, Eq. (2.2)].

Table 5.2: Cauchy Distribution: Average CCDF, $\Psi_1(a)$ and its asymptotic expansion

Fading	$\Psi_1(a)$	Asymptotic
GNM	$\frac{1}{2}-\frac{1}{2\pi\Gamma(m)}\mathrm{H}_{2,3}^{3,1}\left[\frac{\beta}{2\overline{\gamma}a^2}\middle\vert\begin{matrix}(\frac{1}{2},1)(1,1)\\(0,1)(\frac{1}{2},1)(m,\frac{1}{\xi})\end{matrix}\right]$	$\frac{\Gamma(m-\frac{1}{2\xi})}{\pi\Gamma(m)}\sqrt{\frac{\beta}{2a^2\overline{\gamma}}}+\frac{\Gamma(\frac{1}{2}-m\xi)\Gamma(\frac{1}{2}+m\xi)}{2\pi\Gamma(m+1)}\left(\frac{\beta}{2\overline{\gamma}a^2}\right)^{m\xi}$
Nakagami-m	$\frac{1}{2}-\frac{1}{2\pi\Gamma(m)}\mathrm{G}_{2,3}^{3,1}\left[\frac{m}{2\overline{\gamma}a^2}\middle\vert\begin{matrix}\frac{1}{2},1\\0,\frac{1}{2},m\end{matrix}\right]$	$\frac{\Gamma(m-\frac{1}{2})}{\pi\Gamma(m)}\sqrt{\frac{m}{2a^2\overline{\gamma}}}+\frac{\Gamma(\frac{1}{2}-m)\Gamma(\frac{1}{2}+m)}{2\pi\Gamma(m+1)}\left(\frac{m}{2\overline{\gamma}a^2}\right)^{m}$
Rayleigh	$\frac{1}{2}-\frac{1}{2\sqrt{\pi}}e^{\frac{1}{2\overline{\gamma}a^2}}\Gamma\left(\frac{1}{2},\frac{1}{2\overline{\gamma}a^2}\right)$	$\frac{1}{\sqrt{\pi}}\frac{1}{a\sqrt{2\overline{\gamma}}}-\frac{1}{4a^2\overline{\gamma}}$

5.3.3.3 Gaussian Distribution, $\alpha = 2$

The Gaussian distribution is obtained from the $S\alpha S$ distribution by setting $\alpha = 2$. The simplified results for the Gaussian distribution and asymptotic approximation are summarized in Table 5.3. Note that this is a new way to get the average SER of the studied constellation in the presence of EGK fading and Gaussian noise. The results presented in Table 5.3 are in agreement with those investigated in (2.23), (2.58), and (2.62). Moreover, the newly obtained asymptotic approximations of these SER are expressed in terms of elementary functions and can be used also in Chapter 2.

Table 5.3: Gaussian Distribution: Average CCDF, $\Psi_2(a)$ and its asymptotic expansion

Fading	$\Psi_2(a)$	Asymptotic
GNM	$\frac{1}{2}-\frac{1}{2\sqrt{\pi}\Gamma(m)}\mathrm{H}_{2,2}^{2,1}\left[\frac{2\beta}{\overline{\gamma}a^2}\middle\vert\begin{matrix}(\frac{1}{2},1)(1,1)\\(m,\frac{1}{\xi})(0,1)\end{matrix}\right]$ $=\frac{1}{2\sqrt{\pi}\Gamma(m)}\mathrm{H}_{2,2}^{1,2}\left[\frac{2\beta}{\overline{\gamma}a^2}\middle\vert\begin{matrix}(\frac{1}{2},1)(1,1)\\(m,\frac{1}{\xi})(0,1)\end{matrix}\right]$	$\frac{\Gamma(\frac{1}{2}+m\xi)}{2\sqrt{\pi}\Gamma(1+m)}\left(\frac{2\beta}{\overline{\gamma}a^2}\right)^{m\xi}$
Nakagami-m	$\frac{1}{2\sqrt{\pi}\Gamma(m)}\mathrm{G}_{2,2}^{1,2}\left[\frac{2m}{\overline{\gamma}a^2}\middle\vert\begin{matrix}\frac{1}{2},1\\m,0\end{matrix}\right]$	$\frac{\Gamma(\frac{1}{2}+m)}{2\sqrt{\pi}\Gamma(1+m)}\left(\frac{2m}{\overline{\gamma}a^2}\right)^{m}$
Rayleigh	$\frac{1}{2}-\frac{1}{2}\sqrt{\frac{\overline{\gamma}a^2}{2+\overline{\gamma}a^2}}$	$\frac{1}{2a^2\overline{\gamma}}$

5.4 Simulations and Numerical Results

In this section, we show some selected numerical and simulated results to illustrate the analytical results derived earlier in this chapter. The simulations are done using the Monte Carlo method using Matlab®. The $S\alpha S$ random variables are generated using the process described in [12].

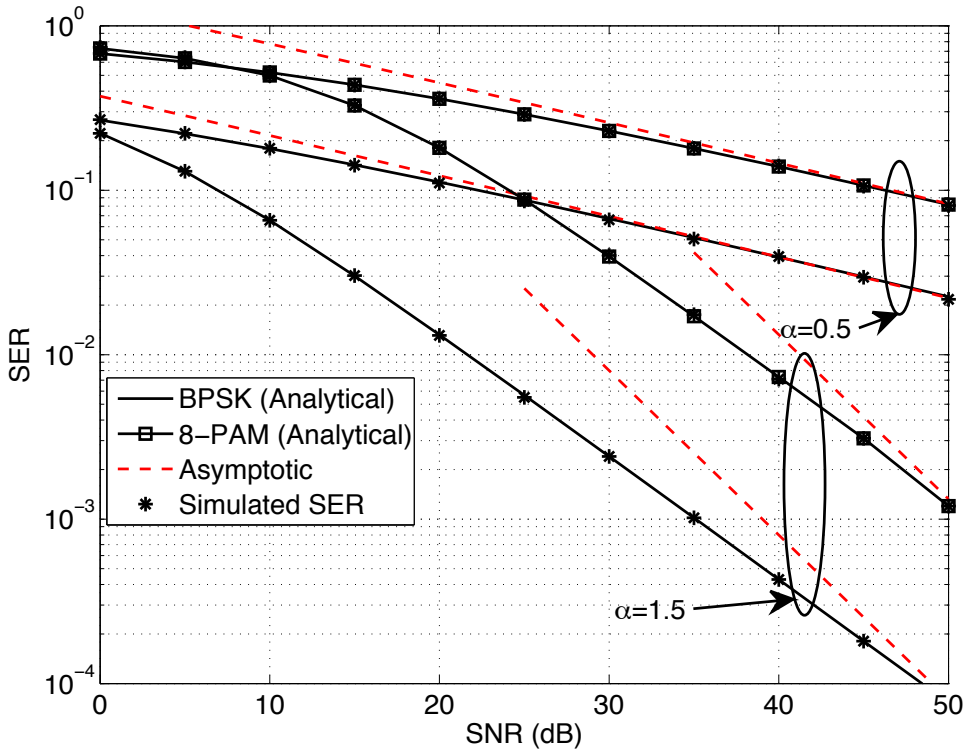

Figure 5.1: SER of BPSK and 8-PAM schemes with $\alpha = 0.5$ and 1.5 and Rayleigh fading. The dashed lines denote the asymptotic results, while the stars represent the simulated results

In Fig. 5.1, we draw the probability of error versus the received SNR (dB) for two modulation schemes (BPSK and 8-PAM) and using two values of α (0.5 and 1.5) over a Rayleigh fading. From the figure, and as expected, both modulation schemes have better performance when operating under the larger value of the stable parameter α. As a confirmation of our mathematical derivations, note that, (i) the

simulation results match perfectly the analytical results, (ii) the asymptotic results converge to the exact analytical results for high SNR.

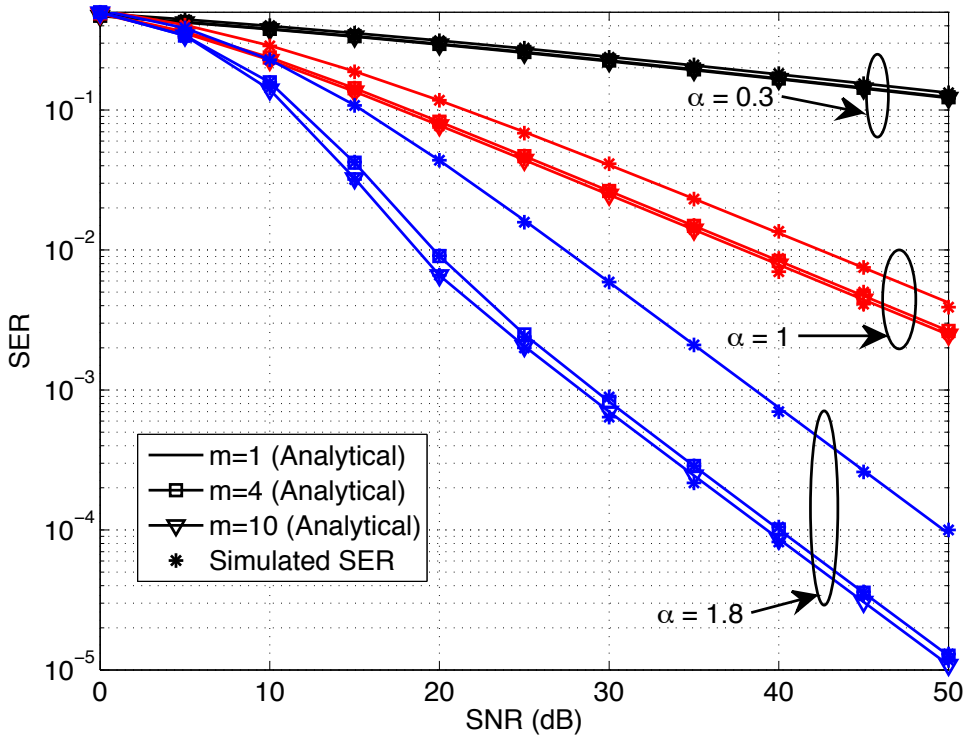

Figure 5.2: SER of 4-PAM over $S\alpha S$ noise, $\alpha = 0.3,\ 1,$ and 1.8 through Nakagami-m fading ($m = 1,\ 4,$ and 10). The stars represent the simulated results

The second illustration in Fig. 5.2 shows the performance of 4-PAM over the stable noise for 3 values of the stable parameter α, low value $\alpha = 0.3$, moderate value $\alpha = 1$ (Cauchy), and high value $\alpha = 1.8$ (near Gaussian) with a Nakagami-m channel with high fading severity $m = 1$, moderate severity $m = 4$, and low severity $m = 10$. A general overview from the figure shows that the system performance increases by increasing α and the best performance is obtained when the noise tends to be Gaussian ($\alpha \to 2$). Furthermore, the SER decreases by increasing the fading figure (reduce the fading severity) as expected. However, for low value of $\alpha = 0.3$, the gap between the SER corresponding to $m = 1$ and $m = 10$ is small, while for

$\alpha = 1.8$ the gap is more important. In fact for small values of α, the noise becomes more impulsive, so the error mainly happen from the potential high amplitudes of the noise and this effect dominates the errors due to the presence of the fading. On the other hand when the noise approaches a Gaussian behavior (i.e. α close to 2), it loses its impulsive nature and the system tends to be an AWGN channel subject to flat fading and this explains the well-known gap between the high and low severity fading scenarios.

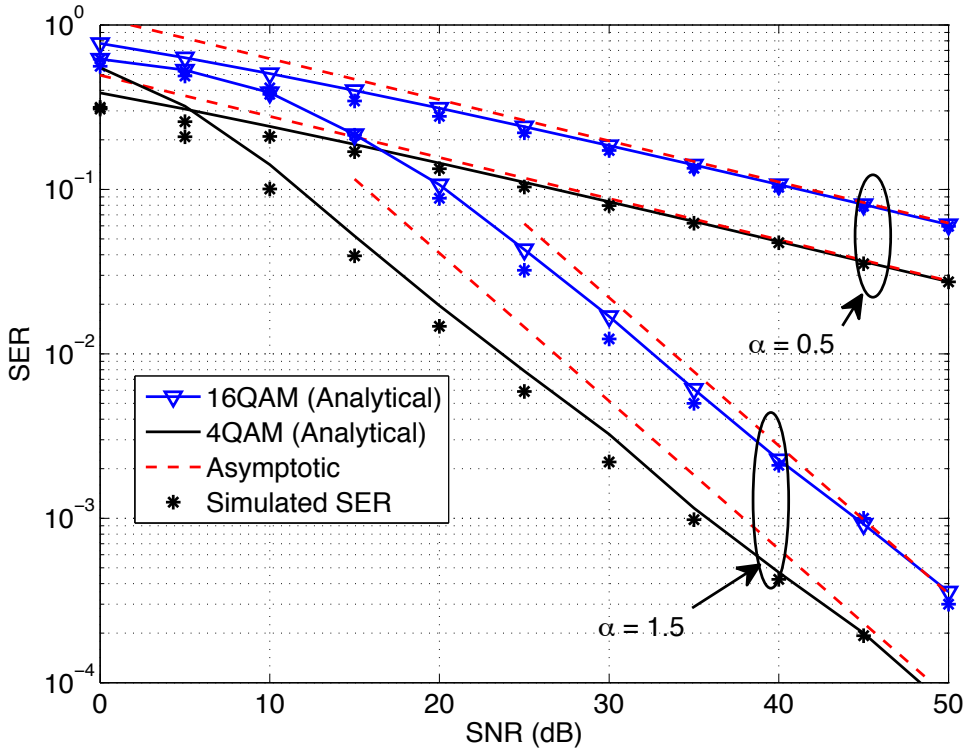

Figure 5.3: SER of 4QAM and 16QAM for $\alpha = 0.5$, and 1.5 over Nakagami-4 fading. The dashed lines denote the asymptotic results, while the stars represent the simulated results

Fig. 5.3 shows the performance of a QAM modulation under $S\alpha S$ noise and compare the approximated result with the exact values of the SER. As seen in Fig. 5.1, the system performance improves by increasing α. Moreover, the gap between the approximated analytical expression (5.23) and the exact results,

obtained by simulation, is small for low SNR. The gap decreases for moderate and high SNR and both curves match almost perfectly for high SNR and both schemes (4-QAM and 16-QAM) and both values of α. In addition, the asymptotic expansion shows a good approximation of the SER for high SNR which confirm their usefulness in such conditions.

5.5 Conclusion

In this chapter, we derived a closed-form expression of the PDF of a symmetric α stable distribution using the properties of the FHF and the inverse Fourier transform of its CHF. As a consequence, the CDF of the $S\alpha S$ distribution has been also derived and used to compute the conditional error probability of different modulation schemes in digital communication system (BPSK, PAM, and QAM). Next, the average probability of error of these systems has been investigated over an EGK flat fading distribution and some special cases were analyzed to get more simplified expressions. Finally, Monte-Carlo simulation results confirmed the exact, approximated mathematical results and the simpler asymptotic expressions for high SNR. Though the average SER of QAM constellation has been derived approximately, the exact ASER of QAM will be investigated in a future work together with the SER of MPSK subject to $S\alpha S$ perturbation.

Chapter 6

Conclusion

6.1 Summary

In this work, we considered the performance of many communication systems perturbed by non-Gaussian noise. Such performance are analyzed by getting the probability of error. Many families of non-Gaussian distribution have been studied in the literature, three of them were further investigated in this thesis, viz the GG noise, the Laplace noise/interference, and the α-stable noise. The work done in the GG part concentrated on computing and getting a closed form of the probability of error (BER and SER) and its average for many constellation, i.e. BPSK, PAM, QAM. For the Laplace noise, the study focused on the SER of an MPSK constellation while the Laplace interference part, in this thesis, presented an investigation on the PDF of the interference with application to full duplex cellular network performance. Finally, the PDF and CDF of the α stable were expressed in closed form and the error rates of BPSK, PAM, and QAM over channels perturbed by additive α stable noise have been derived and averaged over the EGK distribution.

In BPSK and PAM case, namely $1-D$ constellation, the probability of error (PE) was easily found using the generalized Gaussian Q function, $Q_\alpha(\cdot)$, which is averaged over a generalized multiplicative noise modeled by an EGK distribution,

such distribution can model the most common fading types. To derive a closed form of the PE, the $Q_\alpha(\cdot)$ function and the EGK distribution were alternatively expressed in terms of the FHF, which leads to express the ABER/ASER in terms of the FHF. On the other hand, for the $2-D$ constellations, QAM and MPSK, the study was more complicated. In QAM model, the PE was expressed by assuming that a correct decision results from a correct decision in the two phases PAM signals, in-phase and quadrature phase signals. Hence the resulting SER contains the product of two Q_α. By averaging it, the ASER ends up being an integral containing a product of three FHFs and as a result the final closed form is derived in terms the BFHF. Note that the simplified expressions were presented for special cases of noise (e.g. Gaussian, Laplace, and uniform) and fading (e.g. Rayleigh and Nakagami-m). The other studied constellation was the MPSK constellation. Due to its circular character, it is difficult to study such constellation in GG noise, so we reduced the study to a special case of non-Gaussian distribution, namely the Laplace distribution.
Two types of Laplace distribution were used. In the first family, the complex component of the noise are assumed to be independent and so the performance of two detectors were analyzed, ML and MD detectors. The ML detector, that is based on the L_1 norm, gives better results than the MD detector, based on minimum distance. However the latter presents simpler derivation of the ASER. The gap between these detectors was drawn using simulation results and it is shown that its very small especially in presence of fading and by increasing the constellation size. The selected numerical results confirm the analytical results and show the impact of the fading parameters on the average probability of error. On the other hand, the second Laplace family consists of a Laplace interference where the complex components are dependent and uncorrelated. In this context, it was proved that the intra cell interference in a full duplex BS via 3-node topology has a Laplacian distribution with dependent complex component. A mathematical paradigm was

developed to study downlink error rate and throughput for half-duplex users when served by FD BSs via 3NT . Assuming that the interfering user transmits Gaussian signals and the interference channel experience Rayleigh fading, the base-band intra-cell interference is shown to be Laplacian with dependent real and imaginary parts. As a result, a closed form expressions was derived for the average symbol error rate for BPSK, PAM, QAM, and MPSK modulation schemes for unfaded and EKG faded downlink channel. Furthermore, it was proved that the ML coincide with the MD when dealing with such type of interference. To this end, we derive the effective throughput gain imposed by 3NT FD when compared to an idealized interference and noise free HD scenario. The results show the severe degradation that may happen when employing 3NT FD in small cells, specially for schemes with big constellation sizes. On the other hand, 3NT provides nontrivial gains when employed in macro cells which high downlink transmission power. The developed paradigm can be used to adaptively change the modulation scheme according to the SIR and downlink channel condition to maximize the downlink throughput. Finally, a closed-form expression of the PDF of a symmetric α stable distribution was derived using the properties of the FHF and the inverse Fourier transform of its CHF. As a consequence, the CDF of the $S\alpha S$ distribution was also derived and used to compute the conditional error probability of different modulation schemes in communication system (BPSK, PAM, and QAM). An approximation of the SER of the QAM was described and an asymptotic expansion for high SNR of the SER of the deployed constellations was investigated also. Thereby, some selected numerical results have showed that these expressions present a good approximations of the error rates. Finally, the average probability of error was investigated over an EGK flat fading distribution and some special cases were analyzed to get more simplified expressions.

6.2 Possible Extensions

The present work has opened a new window on the system performance analysis area by assuming a non Gaussian perturbation and during the period of time allocated to that project, many other works dealing with non Gaussian noise (and especially the GGN) have been published where different schemes are used to analyze their performance (MIMO scheme, adaptive filtering, study of capacity...). While this thesis presents a drop on that field, it can be extended in many ways to explore the obtained results in the analysis performance of digital communication system. Actually the probability of error of MPSK perturbed by an α stable noise/interference can be studied using the CDF of $S\alpha S$, its PDF also can be used to get the decision regions of that scheme. Other possible extension is the error rate of MPSK over GGN which was omitted in this thesis because it relies on the distribution of the sum of two independent GG random variables. This has been actually recently done and presented in Appendix B. In addition, a similar study focusing on the distribution of the phase angle between two vectors perturbed by GGN would be of great interest. Initial investigations resulted in some integral expressions which could not be solved using the available tools in the literature, even using the BFHF because of the definition of the GGN. However, it is expected that some results can be obtained for the Laplacian special case. Other extensions can also be made in the signal processing field along the lines of our work on the design of a reduced rank adaptive filter operating in an impulsive noise environment, which was modeled by an α stable distribution [45].

REFERENCES

[1] N. Beaulieu, "A useful integral for wireless communication theory and its application to rectangular signaling constellation error rates," *IEEE Trans. Commun.*, vol. 54, no. 5, pp. 802–805, May 2006.

[2] G. Karagiannidis, "On the symbol error probability of general order rectangular QAM in Nakagami-m fading," *IEEE Commun. Lett.*, vol. 10, no. 11, pp. 745–747, November 2006.

[3] R. Mallik, "Average of product of two Gaussian Q-functions and its application to performance analysis in Nakagami fading," *IEEE Trans. Commun.*, vol. 56, no. 8, pp. 1289–1299, August 2008.

[4] H. Suraweera and J. Armstrong, "A simple and accurate approximation to the SEP of rectangular QAM in arbitrary nakagami-m fading channels," *IEEE Communications Letters*, vol. 11, no. 5, pp. 426–428, May 2007.

[5] J. G. Proakis and M. Salehi, *Communication Systems Engineering*, 2nd ed. Upper Saddle River, NJ, USA: Prentice-Hall, August 2001.

[6] S. Kassam and J. Thomas, *Signal detection in non-Gaussian noise*, ser. Springer texts in electrical engineering. Springer-Verlag, 1988.

[7] X. Yang, M. Li, and X. Zhao, "Optimum detectors of line spectrum signals in generalized Gaussian noise," in *Proceedings of the Third International Conference on Measuring Technology and Mechatronics Automation (ICMTMA'2011), Sanya, China*, Jan. 2011, pp. 819–822.

[8] R. Viswanathan and A. Ansari, "Distributed detection of a signal in generalized Gaussian noise," *IEEE Transcations on Acoustics, Speech and Signal Processing*, vol. 37, no. 5, pp. 775–778, May 1989.

[9] S. Zahabi and A. Tadaion, "Local spectrum sensing in non-Gaussian noise," in *Proc. of the IEEE 17th International Conference on Telecommunication (ICT'2010), Doha, Qatar*, April 2010, pp. 843–847.

[10] N. C. Beaulieu and D. J. Young, "Designing time-hopping ultrawide bandwidth receivers for multiuser interference environments," *Proceedings of the IEEE*, vol. 97, no. 2, pp. 255–284, Feb. 2009.

[11] M. Chiani and A. Giorgetti, "Coexistence between UWB and narrow-band wireless communication systems," *Proceedings of the IEEE*, vol. 97, no. 2, pp. 231–254, Feb. 2009.

[12] J. Xian and Y. Geng, "Multi-user detection based on particle filter in impulsive noise," *International Journal of Advancements in Computing Technology*, vol. 5, no. 4, p. 259, Feb. 2013.

[13] S. Ambike, J. Ilow, and D. Hatzinakos, "Detection for binary transmission in a mixture of Gaussian noise and impulsive noise modeled as an alpha-stable process," *IEEE Signal Processing Letters*, vol. 1, no. 3, pp. 55–57, March 1994.

[14] J. Park, G. Shevlyakov, and K. Kim, "Maximin distributed detection in the presence of impulsive alpha-stable noise," *IEEE Transactions on Wireless Communications*, vol. 10, no. 6, pp. 1687–1691, June 2011.

[15] X. Li, Y. Jiang, and M. Liu, "A near optimum detection in alpha-stable impulsive noise," in *IEEE International Conference on Acoustics, Speech and Signal Processing (ICASSP'2009)*, Taipei, Taiwan, April 2009, pp. 3305–3308.

[16] N. Beaulieu and B. Hu, "Soft-limiting receiver structures for time-hopping UWB in multiple-access interference," *IEEE Transactions on Vehicular Technology*, vol. 57, no. 2, pp. 810–818, March 2008.

[17] B. Hu and N. Beaulieu, "On characterizing multiple access interference in TH-UWB systems with impulsive noise models," in *Proc. of the IEE Radio and Wireless Symposium*, Orlando, FL, USA, Jan. 2008, pp. 879–882.

[18] ——, "Accurate evaluation of multiple-access performance in TH-PPM and TH-BPSK UWB systems," *IEEE Transactions on Communications*, vol. 52, no. 10, pp. 1758–1766, Oct. 2004.

[19] Y. Dhibi and T. Kaiser, "On the impulsiveness of multiuser interferences in TH-PPM-UWB systems," *IEEE Transactions on Signal Processing*, vol. 54, no. 7, pp. 2853–2857, July 2006.

[20] ——, "Impulsive noise in UWB systems and its suppression," *Mobile Networks and Applications, Kluwer Academic Publishers*, vol. 11, no. 4, pp. 441–449, 2006.

[21] J. Fiorina, "A simple IR-UWB receiver adapted to multi-user interferences," in *Proc. of the IEEE Global Telecommunications Conference (GLOBECOM'2006)*, San Francisco, CA, USA, Nov. 2006, pp. 1–4.

[22] S. Jiang and N. Beaulieu, "BER of antipodal signaling in Laplace noise," in *Proc. of the 25th Biennial Symposium on Communications (QBSC'2010)*, Kingston, ON, Canada, May 2010, pp. 110–113.

[23] G. Durisi and G. Romano, "On the validity of Gaussian approximation to characterize the multiuser capacity of UWB TH PPM," in *Proc. of the IEEE Conference on Ultra Wideband Systems and Technologies*, Baltimore, MD, USA, May 2002, pp. 157–161.

[24] Q. Ahmed, K.-H. Park, and M.-S. Alouini, "Ultrawide Bandwidth receiver based on a multivariate generalized Gaussian distribution," *IEEE Transactions on Wireless Communications*, vol. 14, no. 4, pp. 1800–1810, April 2015.

[25] A. Kamboj, R. Mallik, M. Agrawal, and R. Schober, "Diversity combining in FSO systems in presence of non-Gaussian noise," in *Proc. of the International Conference on Signal Processing and Communications (SPCOM), Bangalore, India*, July 2012, pp. 1–5.

[26] S. Banerjee and M. Agrawal, "Underwater acoustic noise with generalized gaussian statistics: Effects on error performance," in *Proc. IEEE OCEANS - Bergen, 2013 MTS/*, 2013, pp. 1–8.

[27] X. Zhong, A. Premkumar, and A. Madhukumar, "Particle filtering for acoustic source tracking in impulsive noise with alpha-stable process," *IEEE Sensors Journal*, vol. 13, no. 2, pp. 589–600, Feb 2013.

[28] M. Bergamasco and L. Piroddi, "Active noise control of impulsive noise using online estimation of an alpha-stable model," in *49th IEEE Conference on Decision and Control (CDC'2010)*, Atlanta, Georgia, USA, Dec 2010, pp. 36–41.

[29] P. Cardieri, "Modeling interference in wireless ad hoc networks," *IEEE Communications Surveys & Tutorials*, vol. 12, no. 4, pp. 551–572, Fourth Quarter 2010.

[30] W. Feller, *An Introduction to Probability Theory and Its Applications*. Wiley, January 1968, vol. 1.

[31] P. Lévy, *Calcul des Probabilités*, ser. PCMI collection. Gauthier-Villars, 1925.

[32] T. Gansler, S. Gay, M. Sondhi, and J. Benesty, "Double-talk robust fast converging algorithms for network echo cancellation," *IEEE Transactions on Speech and Audio Processing*, vol. 8, no. 6, pp. 656 –663, 2000.

[33] T. Gansler and J. Benesty, "The fast normalized crosscorrelation double-talk detector," *Signal Processing*, vol. 86, no. 6, pp. 1124 –1139, 2006.

[34] Y. Zou, S.-C. Chan, and T.-S. Ng, "Least mean m-estimate algorithms for robust adaptive filtering in impulse noise," *IEEE Transactions on Circuits and Systems II: Analog and Digital Signal Processing*, vol. 47, no. 12, pp. 1564–1569, Dec. 2000.

[35] J. Arenas-Garcia and A. Figueiras-Vidal, "Adaptive combination of normalised filters for robust system identification," *Electronics Letters*, vol. 41, no. 15, pp. 874–875, Jul. 2005.

[36] E. Papoulis and T. Stathaki, "Improved performance adaptive algorithm for system identification under impulsive noise," *Electronics Letters*, vol. 39, no. 11, pp. 878–880, May 2003.

[37] L. Vega, H. Rey, J. Benesty, and S. Tressens, "A robust adaptive filtering algorithm against impulsive noise," in *Proc. IEEE International Conference on Acoustics, Speech and Signal Processing (ICASSP'2007)*, vol. 3, Honolulu, HI, April 2007, pp. III–1437–III–1440.

[38] G. Samorodnitsky and M. S. Taqqu, *Stable non-Gaussian random processes : stochastic models with infinite variance*, ser. Stochastic modeling. New York: Chapman & Hall, 1994.

[39] Q. Zhao, H.-W. Li, and Y.-T. Shen, "On the sum of generalized Gaussian random signals," in *Proc. of the 7th International Conference on Signal Processing (ICSP'2004)*, vol. 1, Beijing, China, Aug. 2004, pp. 50–53 vol.1.

[40] N. C. Beaulieu, G. Bartoli, D. Marabissi, and R. Fantacci, "The structure and performance of an optimal continuous-time detector for Laplace noise," *IEEE Communications Letters*, vol. 17, no. 6, pp. 1065–1068, June 2013.

[41] H. Shao and N. C. Beaulieu, "An investigation of block coding for Laplacian noise," *IEEE Transactions on Wireless Communications*, vol. 11, no. 7, pp. 2362–2372, July 2012.

[42] S. Jiang and N. C. Beaulieu, "Precise BER computation for binary data detection in bandlimited white Laplace noise," *IEEE Trans. Commun.*, vol. 59, no. 6, pp. 1570–1579, Jun. 2011.

[43] C. W. Helstrom, "Detectability of signals in Laplace noise," *IEEE Trans. Aerosp. Electron. Syst.*, vol. 25, no. 2, pp. 190–196, Mar. 1989.

[44] M. W. Thompson and H.-S. Chang, "Coherent detection in Laplace noise," *IEEE Trans. Aerosp. Electron. Syst.*, vol. 30, no. 2, pp. 452–461, Apr. 1994.

[45] H. Soury, K. Abed-Meraim, and M.-S. Alouini, "Reduced rank adaptive filtering in impulsive noise environments," in *48th Asilomar Conference on Signals, Systems and Computers*, Monterey, CA, USA, Nov 2014, pp. 2037–2041.

[46] E. Kuruoglu, "Density parameter estimation of skewed α-stable distributions," *IEEE Transactions on Signal Processing*, vol. 49, no. 10, pp. 2192–2201, Oct 2001.

[47] P. Tsakalides and C. L. Nikias, "A practical guide to heavy tails," R. J. Adler, R. E. Feldman, and M. S. Taqqu, Eds. Cambridge, MA, USA: Birkhauser Boston Inc., 1998, ch. Deviation from Normality in Statistical Signal Processing: Parameter Estimation with Alpha-stable Distributions, pp. 379–404.

[48] A. Briassouli, P. Tsakalides, and A. Stouraitis, "Hidden messages in heavy-tails: DCT-domain watermark detection using alpha-stable models," *IEEE Transactions on Multimedia*, vol. 7, no. 4, pp. 700–715, Aug 2005.

[49] M. K. Simon and M.-S. Alouini, *Digital Communication Over Fading Channels*, 1st ed. New York: Wiley, 2005.

[50] M. K. Simon, S. M. Hinedi, and W. C. Lindsey, *Digital Communication Techniques: Signal Design And Detection*. Upper Saddle River, NJ: Prentice Hall, 1995.

[51] J. Lu, K. B. Letaief, J. C.-I. Chuang, and M. L. Liou, "M-PSK and M-QAM BER computation using signal-space concepts," *IEEE Transactions on Communications*, vol. 47, pp. 181–184, February 1999.

[52] D. Yoon, "New expression for the SER of M-ary PSK," *IEICE Transactions*, vol. 88-B, no. 4, pp. 1672–1676, Apr. 2005.

[53] R. Pawula, S. Rice, and J. Roberts, "Distribution of the phase angle between two vectors perturbed by gaussian noise," *IEEE Transactions on Communications*, vol. 30, no. 8, pp. 1828–1841, Aug. 1982.

[54] F. Yilmaz and M.-S. Alouini, "A new simple model for composite fading channels: Second order statistics and channel capacity," in *Proc. of the IEEE 7th International Symposium on Wireless Communication Systems (ISWCS'2010), York, UK*, Sept. 2010, pp. 676–680.

[55] A. Kilbas and M. Saigo, *H-Transforms : Theory and Applications (Analytical Method and Special Function)*, 1st ed. CRC Press, 2004.

[56] I. Marks, R.J., G. Wise, D. Haldeman, and J. Whited, "Detection in Laplace noise," *IEEE Transactions on Aerospace and Electronic Systems*, vol. AES-14, no. 6, pp. 866–872, Nov. 1978.

[57] M. A. Chaudhry and S. M. Zubair, *On a Class of Incomplete Gamma Function with Applications*. Boca Raton-London-Ney York-Washington, D.C.: Chapman & Hall/CRC, 2002.

[58] M. Abramowitz and I. A. Stegun, *Handbook of Mathematical Functions with Formulas, Graphs, and Mathematical Tables*, ser. National Bureau of Standards Applied Mathematics Series. New York: Dover Publications, 1964.

[59] M. Nardon and P. Pianca, "Simulation techniques for generalized Gaussian densities," Departement of Applied Mathematics, Universitá Ca' Foscari Venezia, Working Papers 145, Nov 2006.

[60] A. P. Prudnikov, Y. A. Brychkov, and O. I. Marichev, *Integral and Series: Volume 3, More Special Functions*. CRC Press Inc., 1990.

[61] F. Yilmaz and M.-S. Alouini, "Product of the powers of generalized Nakagami-m variates and performance of cascaded fading channels," in *Proc. of the IEEE Global Telecommunication Conference (GLOBECOM'2009), Honolulu, Hawai, USA*, Dec 2009, pp. 1–8.

[62] P. Mittal and K. Gupta, "An integral involving generalized function of two variables," in *Indian Acad. Sci.*, 1972, pp. 117–123.

[63] K. Peppas, "A new formula for the average bit error probability of dual-hop amplify-and-forward relaying systems over generalized shadowed fading channels," *IEEE Wireless Commun. Lett.*, vol. 1, no. 2, pp. 85–88, Apr 2012.

[64] I. Ansari, S. Al-Ahmadi, F. Yilmaz, M.-S. Alouini, and H. Yanikomeroglu, "A new formula for the BER of binary modulations with dual-branch selection

over generalized-K composite fading channels," *IEEE Trans. Commun.*, vol. 59, pp. 2654–2658, Oct 2011.

[65] S. Kotz, T. Kozubowski, and K. Podgórski, *The Laplace Distribution and Generalizations: A Revisit With Applications to Communications, Exonomics, Engineering, and Finance*, ser. Progress in Mathematics Series. Springer Verlag, N.Y., 2001.

[66] A. Giorgetti and M. Chiani, "Influence of fading on the Gaussian approximation for BPSK and QPSK with asynchronous cochannel interference," *IEEE Trans. on Wireless Commun.*, vol. 4, no. 2, pp. 384–389, March 2005.

[67] L. H. Afify, H. ElSawy, T. Y. Al-Naffouri, and M.-S. Alouini, "The influence of Gaussian signaling approximation on error performance in cellular networks," *IEEE Communications Letters*, vol. 19, no. 12, pp. 2202–2205, Dec 2015.

[68] C. Psomas and I. Krikidis, "Outage analysis of full-duplex architectures in cellular networks," in *Vehicular Technology Conf. (VTC Spring), 2015 IEEE 81st*, May 2015, pp. 1–5.

[69] M. Mohammadi, H. A. Suraweera, I. Krikidis, and C. Tellambura, "Full-duplex radio for uplink/downlink transmission with spatial randomness," in *Proc. IEEE Int. Conf. Commun. (ICC)*, London, UK, Jun. 2015, pp. 1908–1913.

[70] S. Goyal, P. Liu, S. Hua, and S. Panwar, "Analyzing a full-duplex cellular system," in *Proc. 47th Annu. Conf. on Information Sciences and Systems (CISS)*, Mar. 2013, pp. 1–6.

[71] A. AlAmmouri, H. ElSawy, and M.-S. Alouini, "Harvesting full-duplex rate gains in cellular networks with half-duplex user terminals," in *Proc. 2016 IEEE Int. Conf. on Commun. (ICC), Accepted.*, 2016.

[72] S. Hong *et al.*, "Applications of self-interference cancellation in 5g and beyond," *IEEE Commun. Mag.*, vol. 52, no. 2, pp. 114–121, Feb. 2014.

[73] A. Sabharwal, P. Schniter, D. Guo, D. Bliss, S. Rangarajan, and R. Wichman, "In-band full-duplex wireless: Challenges and opportunities," *IEEE J. Select. Areas Commun*, vol. 32, no. 9, pp. 1637–1652, Sep. 2014.

[74] M. Jain *et al.*, "Practical, real-time, full duplex wireless," in *Proc. of the 17th Annu. Int. Conf. on Mobile Computing and Networking (MobiCom)*, Las Vegas, NV, USA, Sep. 2011, pp. 301–312.

[75] J. Bai and A. Sabharwal, "Distributed full-duplex via wireless side-channels: Bounds and protocols," *IEEE Trans. on Wireless Commun.*, vol. 12, no. 8, pp. 4162–4173, August 2013.

[76] K. Sundaresan *et al.*, "Full-duplex without strings: Enabling full-duplex with half-duplex clients," in *Proc. of the 20th Annu. Int. Conf. on Mobile Computing and Networking (MobiCom)*, Maui, Hawaii, USA, Sep. 2014.

[77] K. M. Thilina, H. Tabassum, E. Hossain, and D. I. Kim, "Medium access control design for full duplex wireless systems: challenges and approaches," *IEEE Communications Magazine*, vol. 53, no. 5, pp. 112–120, May 2015.

[78] T. Eltoft, T. Kim, and T.-W. Lee, "On the multivariate Laplace distribution," *IEEE Sig. Proces. Lett.*, vol. 13, no. 5, pp. 300–303, May 2006.

[79] B. M. Hochwald, T. L. Marzetta, and V. Tarokh, "Multiple-antenna channel hardening and its implications for rate feedback and scheduling," *IEEE Transactions on Information Theory*, vol. 50, no. 9, pp. 1893–1909, 2004.

[80] L. Glasser, K. T. Kohl, C. Koutschan, V. H. Moll, and A. Straub, "The integrals in Gradshteyn and Ryzhik. Part 22: Bessel-K functions." *Scientia. Series A: Mathematical Sciences. New Series*, vol. 22, pp. 129–151, 2012.

[81] E. Stacy, "A generalization of the gamma distribution," *The Annals of Mathematical Statistics*, vol. 3, no. 33, pp. 1187–1192, Sep. 1962.

[82] V. Aalo, T. Piboongungon, and C.-D. Iskander, "Bit-error rate of binary digital modulation schemes in generalized gamma fading channels," *IEEE Communications Letters*, vol. 9, no. 2, pp. 139–141, Feb. 2005.

[83] H. Suzuki, "A statistical model for urban radio propogation," *IEEE Transactions on Communications*, vol. 25, no. 7, pp. 673–680, July 1977.

[84] M. H. Ismail and M. M. Matalgah, "Outage probability in multiple access systems with weibull-faded lognormal-shadowed communication links," in *Proc. of the IEEE 62nd Vehicular Technology Conference (VTC-2005-Fall), Dallas, TX*, vol. 4, Sept. 2005, pp. 2129–2133.

[85] A. T. Walden and J. W. J. Hosken, "The nature of the non-Gaussianity of primary reflection coefficients and its significance for deconvolution," *Geophysical Prospecting*, vol. 34, pp. 1038–1066, 1986.

[86] J. Miller and J. B. Thomas, "Detectors for discrete-time signals in non-Gaussian noise," *IEEE Transactions on Information Theory*, vol. 18, no. 2, pp. 241–250, Mar. 1972.

[87] T. K. Pogány and S. Nadarajah, "On the characteristic function of the generalized normal distribution," *Comptes Rendus Mathematique*, vol. 348, no. 348, pp. 203–206, 2010.

[88] A. D. D. Craik, "Prehistory of Faà di Bruno's formula." *The American Mathematical Monthly*, vol. 112, no. 2, pp. 119–130, Feb. 2005.

APPENDICES

Appendix A: Special Cases of the EGK Distribution

Table A.1: Some Special Cases of the EGK Distribution

Envelope Distribution	$\boldsymbol{m}$	$\boldsymbol{\xi}$	$\boldsymbol{m_s}$	$\boldsymbol{\xi_s}$
Rayleigh	1	1	∞	1
	∞	1	1	1
Maxwell	3/2	1	∞	1
	∞	1	3/2	1
Half-Normal	1/2	1	∞	1
	∞	1	1/2	1
Exponential	1	1/2	∞	1
	∞	1	1	1/2
Weibull	1	ξ	∞	1
	∞	1	1	ξ_s
Nakagami-m	m	1	∞	1
	∞	1	m_s	1
GNM[61]	m	ξ	∞	1
	∞	1	m_s	ξ_s
Gamma	m	1/2	∞	1
	∞	1	m_s	1/2
Generalized Gamma [80, 81]	m	$\xi/2$	∞	1
	∞	1	m_s	$\xi_s/2$

Envelope Distribution	m	ξ	m_s	ξ_s
Half-Normal-Exponential	$1/2$	1	1	1
	1	1	$1/2$	1
Half-Normal-Gamma	$1/2$	1	m_s	1
	m	1	$1/2$	1
GNM-Lognormal	∞	0	m_s	ξ_s
	m	ξ	∞	0
Suzuki[82]	∞	0	1	1
	1	1	∞	0
Rayleigh-Exponential	1	1	1	1
Maxwell-Lognormal	∞	0	$3/2$	1
	$3/2$	1	∞	0
Maxwell-Exponential	1	1	$3/2$	1
	$3/2$	1	1	1
Maxwell-Gamma	m	1	$3/2$	1
	$3/2$	1	m_s	1
Weibull-Lognormal[83]	∞	0	1	ξ_s
	1	ξ	∞	0
Weibull-Exponential	1	1	1	ξ_s
	1	ξ	1	1
Weibull-Weibull	1	ξ	1	ξ_s
Weibull-Gamma	m	1	1	ξ_s
	1	ξ	m_s	1
Nakagami-Lognormal	∞	0	m_s	1
	m	1	∞	0
K-Distribution	m	1	1	1
	1	1	m_s	1
Generalized-K	m	1	m_s	1
GNM-Exponential	1	1	m_s	ξ_s
	m	ξ	1	1
GNM-Weibull	m	ξ	1	ξ_s
	1	ξ	m_s	ξ_s
GNM-Gamma	m	1	m_s	ξ_s
	m	ξ	m_s	1

Appendix B: Sum of Generalized Gaussian Random Variables

As mentioned in [39], we need sometimes to study the sum of independent GGRV (SGG), or a linear system of GG white noise such as AR(1) process driven by a GG process. Furthermore, in seismic signal processing, the received seismic signal is modeled by a convolution of seismic signals, where seismic reflective coefficient can be modeled by GGD [84]. Thereby the distribution of the sum, that appears also as the convolution of the single distribution, is needed in this seismic model. Moreover, in communications, it is shown above that in some instances the noise and the multi user interference can be modeled as GG white noise [85, 24]. Therefore, the total perturbations at reception, defined as the sum of noise and interference, is modeled as the sum the GG signals. Many other applications can be found in the literature to motivate the study of sum distribution of GG signals.

As a consequence, it is important to study the statistics and the density of the SGG distribution. The PDF was not derived before and so the CDF. Actually, the approach used in this work is based on the CHF which was investigated in [86] for $\alpha > 1$. However in our case we are studying the CHF for any value of α using another approach of calculation based on the properties of the FHF [55]. From the CHF of one GGRV, we get the CHF of the sum. Hence, the relation between the CHF and the distribution densities leads us to investigate the PDF and the CDF of such distribution and its statistics (moments, cumulant, kurtosis...).

B.1 GGD Statistics

B.1.1 Characteristic Function

Let $\alpha > 0$, and X be random variable following a GGD with mean μ, variance σ^2 and shape parameter α, i.e. $X \sim GGD(\mu, \sigma, \alpha)$. Starting from the definition of the CHF and the PDF of the GGD (2.1), the CHF can be expressed in integral form as

$$\varphi_\alpha(t) = \mathbb{E}[e^{itX}] = \int_{\mathbb{R}} e^{itx} f_X(x) dx = \frac{\alpha\Lambda}{2\Gamma(1/\alpha)} e^{it\mu} \int_{\mathbb{R}} e^{itx} \exp\left(-\Lambda^\alpha |x|^\alpha\right) dx. \tag{B.1}$$

Since $|x|$ is an even function, the integral in (B.1) is the cosine transform of the exponential component

$$\varphi_\alpha(t) = \frac{\alpha\Lambda}{\Gamma(1/\alpha)} e^{it\mu} \int_0^\infty \cos(tx) \exp\left(-(\Lambda x)^\alpha\right) dx. \tag{B.2}$$

Alternative expressions of $\cos(x)$ and e^{x^α} in terms of the FHF are available in [55, Eq. (2.9.8) & Eq. (2.9.4)] and described in (5.5) and (5.6) as

$$\cos(x) = \sqrt{\pi}\ \mathrm{H}^{1,0}_{0,2}\left[\frac{x^2}{4}\,\middle|\,\overline{}_{(0,1),(\frac{1}{2},1)}\right] \tag{B.3}$$

$$e^{-x^\alpha} = \frac{1}{\alpha}\mathrm{H}^{1,0}_{0,1}\left[x\,\middle|\,\overline{}_{(0,\frac{1}{\alpha})}\right] \tag{B.4}$$

Hence the integral identity defined in (2.21), solves the integral of the product of two FHF function over the positive real numbers. As a consequence the CHF of X, $\mathbb{E}[e^{itX}]$, is given by

$$\begin{aligned}\varphi_\alpha(t) &= \frac{\sqrt{\pi}\Lambda}{\Gamma(1/\alpha)} e^{it\mu} \int_0^\infty \mathrm{H}^{1,0}_{0,2}\left[\frac{t^2}{4}x^2\,\middle|\,\overline{}_{(0,1),(\frac{1}{2},1)}\right] \mathrm{H}^{1,0}_{0,1}\left[\Lambda x\,\middle|\,\overline{}_{(0,\frac{1}{\alpha})}\right] dx \\ &= \frac{\sqrt{\pi}}{\Gamma(1/\alpha)} e^{it\mu} \mathrm{H}^{1,1}_{1,2}\left[\frac{\sigma^2\Gamma(1/\alpha)}{4\Gamma(3/\alpha)}t^2\,\middle|\,\begin{matrix}(1-\frac{1}{\alpha},\frac{2}{\alpha}) \\ (0,1),(\frac{1}{2},1)\end{matrix}\right].\end{aligned} \tag{B.5}$$

Note that the result proved in (B.5) is valid for all positive shape parameter $\alpha > 0$.

A previous demonstration was derived in [86] but only for $\alpha > 1$, while the authors provided an expression of the CHF of GGD in terms of the Fox-Wright generalized hypergeometric function ${}_p\Psi_q(\cdot)$, which is a special case of the FHF [55, Eq. (2.9.29)].

B.1.2 Moment Generating Function

The moment generating function (MOGF) can be directly concluded from the CHF by the relation $M_\alpha(t) = \varphi_\alpha(-it)$, so the MOGF is obtained by

$$M_\alpha(t) = \frac{\sqrt{\pi}e^{t\mu}}{\Gamma(1/\alpha)} \mathrm{H}_{1,2}^{1,1}\left[\frac{-\sigma^2\Gamma(1/\alpha)}{4\Gamma(3/\alpha)}t^2 \,\middle|\, \begin{matrix}(1-\frac{1}{\alpha},\frac{2}{\alpha})\\(0,1),(\frac{1}{2},1)\end{matrix}\right]. \tag{B.6}$$

In some special cases, the MOGF can be expressed in terms of elementary functions. For example for Gaussian case, i.e. $\alpha = 2$, and using the special case of the FHF in [55, Eq. (2.9.4)], the MOGF of Gaussian is

$$M_2(t) = e^{t\mu}\mathrm{H}_{0,1}^{1,0}\left[\frac{-\sigma^2}{2}t^2 \,\middle|\, \begin{matrix}\\(0,1)\end{matrix}\right] = e^{t\mu+\frac{1}{2}\sigma^2t^2}. \tag{B.7}$$

Another special case appears interesting is the Laplacian distribution (i.e. $\alpha = 1$). Using the identity [55, Eq. (2.9.5)], the MOGF of Laplacian distribution is given by

$$\begin{aligned} M_1(t) &= \sqrt{\pi}e^{t\mu}\mathrm{H}_{1,2}^{1,1}\left[\frac{-\sigma^2}{8}t^2 \,\middle|\, \begin{matrix}(0,2)\\(0,1),(\frac{1}{2},1)\end{matrix}\right] \\ &= e^{t\mu}\mathrm{H}_{1,1}^{1,1}\left[-\frac{1}{2}\sigma^2t^2 \,\middle|\, \begin{matrix}(0,1)\\(0,1)\end{matrix}\right] \\ &= \frac{e^{t\mu}}{1-\frac{1}{2}\sigma^2t^2}. \end{aligned} \tag{B.8}$$

B.1.3 Moments and Cumulants

Without loss of generality, we are focusing our study to zero mean random variables (i.e. $\mu = 0$). Due to the symmetry of the PDF of GGD, the odd moments vanish

and the even moments obtained as follows

$$\begin{cases} m_{2n}(X) & = \mathbb{E}[X^{2n}] & = \sigma^{2n}\frac{\Gamma(1/\alpha)^n}{\Gamma(3/\alpha)^n}\frac{\Gamma(\frac{2n+1}{\alpha})}{\Gamma(1/\alpha)} \\ m_{2n+1}(X) & = \mathbb{E}[X^{2n+1}] & = 0. \end{cases} \tag{B.9}$$

Once the MOGF and the moments are obtained, one can investigate the expression of the cumulant generating function (CGF) and the cumulants of the GGD. Actually the CGF, $K_X(t)$ (or $K_\alpha(t)$), is defined as

$$\begin{aligned} K_\alpha(t) &= \log M_\alpha(t) \\ &= \log\left(\frac{\sqrt{\pi}}{\Gamma(1/\alpha)}\right) + \log \mathrm{H}^{1,1}_{1,2}\left[\frac{-\sigma^2\Gamma(1/\alpha)}{4\Gamma(3/\alpha)}t^2 \,\middle|\, \begin{matrix}(1-\frac{1}{\alpha},\frac{2}{\alpha}) \\ (0,1),(\frac{1}{2},1)\end{matrix}\right]. \end{aligned} \tag{B.10}$$

By definition, the n-**th cumulant**, noted $k_n(X)$, is the n-th term in the Taylor series expansion of $K_\alpha(t)$ at 0

$$k_n(X) = \left.\frac{d^n K_\alpha(t)}{dt^n}\right|_{t=0} = \frac{d^n K_\alpha(0)}{dt^n}.$$

Since the CGF appears as the composite of two functions, we may use the Faà di Bruno's formula [87, Eq. (2)] that computes the n-th derivative of composite functions

$$\frac{d^n K_\alpha(t)}{dt^n} = -\sum_{m_1,\ldots,m_n} \frac{n!(m_1+\cdots+m_n-1)!}{m_1!m_2!\ldots m_n!}\prod_{1\le j\le n}\left(-\frac{M^{(j)}_\alpha(t)}{j!M_\alpha(t)}\right)^{m_j}, \tag{B.11}$$

the sum is over $m_1, m_2, \ldots, m_n$ such that $\sum_{j=1}^{n} jm_j = n$. Thereby, evaluating (B.11) at zero and replacing the moments by their expressions, the even cumulants of a zero mean GG random variable X can be expressed in terms of the even moments of

X by

$$k_{2n}(X) = -\sum_{m_1+2m_2+\ldots nm_n=n} \frac{(2n)!(m_1+\cdots+m_n-1)!}{m_1!m_2!\ldots m_n!} \prod_{1\le j\le n} \left(-\frac{\sigma^{2j}\Gamma(1/\alpha)^j\Gamma(\frac{2j+1}{\alpha})}{\Gamma(3/\alpha)^j\Gamma(1/\alpha)(2j)!} \right)^{m_j}, \tag{B.12}$$

and the odd cumulants are equal to zero.

The cumulants of low order are easy to express

$$\begin{aligned} k_2(X) &= \sigma^2 \\ k_4(X) &= \sigma^4 \left(\frac{\Gamma(1/\alpha)\Gamma(5/\alpha)}{\Gamma(3/\alpha)^2} - 3 \right) \\ k_6(X) &= \sigma^6 \left(\frac{\Gamma(1/\alpha)^2\Gamma(7/\alpha)}{\Gamma(3/\alpha)^3} - 15\frac{\Gamma(1/\alpha)\Gamma(5/\alpha)}{\Gamma(3/\alpha)^2} + 30 \right). \end{aligned} \tag{B.13}$$

Another statistics appears interesting to evaluate, in occurrence the kurtosis. The kurtosis, $Kurt(X)$, is defined as the fourth cumulant divided by the square of the second cumulant of the distribution. In the GGD case the kurtosis is equal to

$$Kurt(X) = \frac{k_4(X)}{k_2(X)^2} = \frac{\Gamma(1/\alpha)\Gamma(5/\alpha)}{\Gamma(3/\alpha)^2} - 3. \tag{B.14}$$

One can easily check that (B.14) confirms that the Gaussian kurtosis is equal to 0 and the Laplacian kurtosis is equal to 3.

At this stage, the statistics of one GGRV are expressed in closed form. The next section considers the densities and statistics of the SGG distribution.

B.2 Sum of Two GG Random Variables

As known the CHF of the sum of two independent RV is the product of their CHFs. Since the CHF of the GGD is defined in the previous section, the CHF of the sum can be easily obtained and so the densities by inverse Fourier transform of the CHF.

In fact, let $X \sim GGD(\mu_1, \sigma_1, \alpha)$ and $Y \sim GGD(\mu_2, \sigma_2, \beta)$ two independent random variables following a GGD, and let $Z = X + Y$ be their sum. It is clear that the first and second moment of Z are easy to find

$$\begin{aligned} \mathbb{E}[Z] &= \mu = \mu_1 + \mu_2 \\ \mathbb{E}[(Z-\mu)^2] &= \sigma^2 = \sigma_1^2 + \sigma_2^2. \end{aligned} \tag{B.15}$$

B.2.1 PDF of the SGG

The PDF of a random variable is known as the inverse Fourier transform of the CHF. The CHF of Z is given by

$$\begin{aligned} \varphi_Z(t) &= \varphi_X(t)\varphi_Y(t) \\ &= \frac{\pi e^{it\mu}}{\Gamma(1/\alpha)\Gamma(1/\beta)} \mathrm{H}_{1,2}^{1,1}\left[\frac{\sigma_1^2\Gamma(1/\alpha)}{4\Gamma(3/\alpha)}t^2 \,\middle|\, \begin{matrix}(1-\frac{1}{\alpha},\frac{2}{\alpha}) \\ (0,1),(\frac{1}{2},1)\end{matrix}\right] \\ &\qquad \times \mathrm{H}_{1,2}^{1,1}\left[\frac{\sigma_2^2\Gamma(1/\beta)}{4\Gamma(3/\beta)}t^2 \,\middle|\, \begin{matrix}(1-\frac{1}{\beta},\frac{2}{\beta}) \\ (0,1),(\frac{1}{2},1)\end{matrix}\right]. \end{aligned} \tag{B.16}$$

Let $A = \frac{\sigma_1^2\Gamma(1/\alpha)}{4\Gamma(3/\alpha)}$ and $B = \frac{\sigma_2^2\Gamma(1/\beta)}{4\Gamma(3/\beta)}$. The inverse Fourier transform of the CHF (B.16) of Z gives the PDF as

$$\begin{aligned} f_Z(z) &= \frac{1}{2\pi}\int_{\mathbb{R}} e^{-itz}\varphi_Z(t)dt \\ &= \frac{1}{2\Gamma(1/\alpha)\Gamma(1/\beta)}\int_{\mathbb{R}} \mathrm{H}_{1,2}^{1,1}\left[A\,t^2 \,\middle|\, \begin{matrix}(1-\frac{1}{\alpha},\frac{2}{\alpha}) \\ (0,1),(\frac{1}{2},1)\end{matrix}\right] \\ &\qquad \times \mathrm{H}_{1,2}^{1,1}\left[B\,t^2 \,\middle|\, \begin{matrix}(1-\frac{1}{\beta},\frac{2}{\beta}) \\ (0,1),(\frac{1}{2},1)\end{matrix}\right] e^{it(\mu-z)}dt. \end{aligned} \tag{B.17}$$

The first two FHFs are even functions, so the integral becomes a cosine transform of the product of these two FHFs

$$f_Z(z) = \frac{1}{2\Gamma(1/\alpha)\Gamma(1/\beta)} \int_0^\infty \mathrm{H}_{1,2}^{1,1}\left[A\ t^2 \left| \begin{matrix} (1-\frac{1}{\alpha},\frac{2}{\alpha}) \\ (0,1),(\frac{1}{2},1) \end{matrix} \right.\right] \times \mathrm{H}_{1,2}^{1,1}\left[B\ t^2 \left| \begin{matrix} (1-\frac{1}{\beta},\frac{2}{\beta}) \\ (0,1),(\frac{1}{2},1) \end{matrix} \right.\right] \cos\left(t(\mu - z)\right) dt. \quad \text{(B.18)}$$

As seen before, the cosine has a representation in terms of the FHF (B.3). So we are facing an integral that involves the product of three FHFs over the positive real numbers. Such integral was solved (2.48) and it is expressed in terms of the BFHF. Thereby, the PDF of the sum of two independent GG random variable can be expressed in terms of the bivariate FHF

$$f_Z(z) = \frac{\sqrt{\pi}}{\Gamma(1/\alpha)\Gamma(1/\beta)|z-\mu|} \quad \text{(B.19)}$$
$$\times \mathrm{H}_{2,0;1,2;1,2}^{0,1;1,1;1,1}\left[\frac{\sigma_1^2\Gamma(1/\alpha)}{\Gamma(3/\alpha)(z-\mu)^2}, \frac{\sigma_2^2\Gamma(1/\beta)}{\Gamma(3/\beta)(z-\mu)^2} \left| \begin{matrix} (\frac{1}{2},1,1),\underline{(0,1,1)} \\ - \end{matrix} \right| \begin{matrix} (1-\frac{1}{\alpha},\frac{2}{\alpha}) \\ (0,1),(\frac{1}{2},1) \end{matrix} \left| \begin{matrix} (1-\frac{1}{\beta},\frac{2}{\beta}) \\ (0,1),(\frac{1}{2},1) \end{matrix} \right.\right].$$

B.2.2 CDF of the SGG

The CDF of Z is the primitive of $f_Z(\cdot)$ that vanishes at $(-\infty)$. Back to (B.18), it appears that the CDF is expressed in terms of an integral involving the product of two FHFs and sine function. The latter can be expressed in terms of the FHF for positive argument (5.9). Thereby, the CDF of the sum of two independent GGRV becomes the integral of the product of three FHFs which is evaluated in terms of the BFHF as

$$F_Z(z) = \frac{1}{2} + \frac{\sqrt{\pi}\ sign(z-\mu)}{2\Gamma(1/\alpha)\Gamma(1/\beta)} \quad \text{(B.20)}$$
$$\times \mathrm{H}_{2,0;1,2;1,2}^{0,1;1,1;1,1}\left[\frac{\sigma_1^2\Gamma(1/\alpha)}{\Gamma(3/\alpha)(z-\mu)^2}, \frac{\sigma_2^2\Gamma(1/\beta)}{\Gamma(3/\beta)(z-\mu)^2} \left| \begin{matrix} (\frac{1}{2},1,1),\underline{(1,1,1)} \\ - \end{matrix} \right| \begin{matrix} (1-\frac{1}{\alpha},\frac{2}{\alpha}) \\ (0,1),(\frac{1}{2},1) \end{matrix} \left| \begin{matrix} (1-\frac{1}{\beta},\frac{2}{\beta}) \\ (0,1),(\frac{1}{2},1) \end{matrix} \right.\right].$$

In (B.20), $sign(x)$ gives the signum of the real number x. The results in (B.19) and (B.20) represent new results and they were not investigated before.

B.2.3 Statistics of Z

In the following analysis, the zero mean case is considered, while the non zero mean random variable can be obtained from the zero mean random variable by a simple shift $Z = Z_0 + \mu$.

B.2.3.1 MOGF

As mentioned before the MOGF of Z can be obtained from the CHF by the relation $M_Z(t) = \varphi_Z(-it)$ which gives the MOGF of Z as

$$M_Z(t) = \frac{\pi}{\Gamma(1/\alpha)\Gamma(1/\beta)} \mathrm{H}_{1,2}^{1,1}\left[\frac{-\sigma_1^2\Gamma(1/\alpha)}{4\Gamma(3/\alpha)}t^2 \,\middle|\, \begin{matrix}(1-\frac{1}{\alpha},\frac{2}{\alpha})\\(0,1),(\frac{1}{2},1)\end{matrix}\right] \mathrm{H}_{1,2}^{1,1}\left[\frac{-\sigma_2^2\Gamma(1/\beta)}{4\Gamma(3/\beta)}t^2 \,\middle|\, \begin{matrix}(1-\frac{1}{\beta},\frac{2}{\beta})\\(0,1),(\frac{1}{2},1)\end{matrix}\right].$$

B.2.3.2 Moments

The moments of Z can be obtained from the binomial formula that describes the integer power of the sum of two numbers. Hence known the moments of X and Y (B.9), it appears that the odd moments of Z, $m_{2n+1}(Z)$, vanish while the even moments are given by

$$m_{2n}(Z) = \frac{\sigma_2^{2n}\Gamma(\frac{1}{\beta})^n}{\Gamma(\frac{1}{\alpha})\Gamma(\frac{1}{\beta})\Gamma(\frac{3}{\beta})^n} \sum_{k=0}^{n} \binom{2n}{2k} \left(\frac{\sigma_1^2}{\sigma_2^2}\frac{\Gamma(\frac{1}{\alpha})\Gamma(\frac{3}{\beta})}{\Gamma(\frac{3}{\alpha})\Gamma(\frac{1}{\beta})}\right)^k \Gamma\left(\frac{2k+1}{\alpha}\right)\Gamma\left(\frac{2n-2k+1}{\beta}\right).$$

B.2.3.3 Cumulant and Kurtosis

From the MOGF, it is easy to get the CGF by applying the logarithm to the MOGF $M_Z(t)$. Thereby the CGF of Z is the sum of the CGF of X and the CGF of Y, $K_Z(t) = K_X(t) + K_Y(t)$. Moreover, the cumulant of Z is expressed also as the sum of the cumulant of X and the cumulant of Y. Note that the odd cumulant are

equal to zero while the even ones are given by

$$\begin{aligned} k_{2n}(Z) &= k_{2n}(X) + k_{2n}(Y) \\ &= - \sum_{m_1+2m_2+\ldots nm_n=n} \frac{(2n)!(m_1+\cdots+m_n-1)!}{m_1!m_2!\ldots m_n!} \\ &\times \left[\prod_{1\le j\le n} \left(-\frac{\sigma_1^{2j}\Gamma(\frac{1}{\alpha})^j\Gamma(\frac{2j+1}{\alpha})}{\Gamma(\frac{3}{\alpha})^j\Gamma(\frac{1}{\alpha})(2j)!} \right)^{m_j} + \prod_{1\le k\le n} \left(-\frac{\sigma_2^{2k}\Gamma(\frac{1}{\beta})^k\Gamma(\frac{2k+1}{\beta})}{\Gamma(\frac{3}{\beta})^k\Gamma(\frac{1}{\beta})(2k)!} \right)^{m_k} \right]. \end{aligned} \tag{B.21}$$

Once the cumulant expression is evaluated, the kurtosis of Z can be expressed, per definition, in terms of the fourth and second moments as

$$Kurt(Z) = \frac{k_4(Z)}{k_2(Z)^2} = \frac{k_4(X)+k_4(Y)}{\left(k_2(X)+k_2(Y)\right)^2}.$$

Note that $k_2(X)+k_2(Y) = \sigma_1^2+\sigma_2^2 = \sigma^2$. Thus a relation between the kurtosis of Z, X and Y appears as

$$Kurt(Z) = \frac{\sigma_1^2}{\sigma^2}Kurt(X) + \frac{\sigma_2^2}{\sigma^2}Kurt(Y). \tag{B.22}$$

The final expression of the kurtosis of Z is thus given by

$$Kurt(Z) = \frac{\sigma_1^4}{\sigma^4}\frac{\Gamma(\frac{1}{\alpha})\Gamma(\frac{5}{\alpha})}{\Gamma(\frac{3}{\alpha})^2} + \frac{\sigma_2^4}{\sigma^4}\frac{\Gamma(\frac{1}{\beta})\Gamma(\frac{5}{\beta})}{\Gamma(\frac{3}{\beta})^2} + 6\frac{\sigma_1^2\sigma_2^2}{\sigma^4} - 3. \tag{B.23}$$

B.3 Approximation of the PDF of SGG

The expression of the PDF of the sum of two independent GGRV (B.19) is quite high complex since it is expressed in terms of the BFHF. Therefore, an approximation of the PDF is highly recommended to simplify the calculations and study, in simple way, the performance of systems in which the PDF of the sum is needed, like, for example, the evaluation of the SER of an MPSK over an GGN

channel. Such analysis needs the PDF and the CDF of the SGG distribution.
In this section we are investigating the approximation of the PDF of Z by the PDF of another GG random variable with shape factor λ to be determined. In [39], it has been proved that the PDF of the sum cannot be a PDF of one GGRV. However the authors proved that both PDFs have the same properties (symmetric, convexity, monotonicity...), from that analysis, an approximation of the PDF of Z by the PDF of GGD is needed and worth pursuing. In fact, as shown in (2.1), 3 parameters are needed to characterize a GGD, namely, the mean, the variance and the shape factor. The mean and the variance are given in (B.15). Therefore, we need to find a method to get the shape factor λ. In what follows, three approaches are presented.

B.3.1 Kurtosis Approach

The first method to estimate λ is by using the kurtosis of the distributions. Since the kurtosis of the sum is already known, the shape factor can be obtained by equalizing both kurtosis. Thereby, we get the following equation to solve

$$\begin{gathered} Kurt(Z_\lambda) = Kurt(Z) \\ \Longleftrightarrow \\ \frac{\Gamma(\frac{1}{\lambda})\Gamma(\frac{5}{\lambda})}{\Gamma(\frac{3}{\lambda})^2} = \frac{\sigma_1^4}{\sigma^4}\frac{\Gamma(\frac{1}{\alpha})\Gamma(\frac{5}{\alpha})}{\Gamma(\frac{3}{\alpha})^2} + \frac{\sigma_2^4}{\sigma^4}\frac{\Gamma(\frac{1}{\beta})\Gamma(\frac{5}{\beta})}{\Gamma(\frac{3}{\beta})^2} + 6\frac{\sigma_1^2\sigma_2^2}{\sigma^4}, \end{gathered} \tag{B.24}$$

while $Z_\lambda \sim GGD(\mu, \sigma, \lambda)$ is the approximated RV of Z with parameter λ.
Let us define the ratio between the variance of X and Y as $\omega = \frac{\sigma_1^2}{\sigma_2^2}$, so the equation on λ can be written in terms of ω as

$$\frac{\Gamma(\frac{1}{\lambda})\Gamma(\frac{5}{\lambda})}{\Gamma(\frac{3}{\lambda})^2} = \frac{1}{(1+\omega)^2}\left(\omega^2\frac{\Gamma(\frac{1}{\alpha})\Gamma(\frac{5}{\alpha})}{\Gamma(\frac{3}{\alpha})^2} + \frac{\Gamma(\frac{1}{\beta})\Gamma(\frac{5}{\beta})}{\Gamma(\frac{3}{\beta})^2} + 6\omega\right). \tag{B.25}$$

By knowing α, β, and ω, (B.24) is written as $h(\lambda) = C$, where $h(\lambda)$ is a function on λ, and C is a known positive constant. In Fig. B.1, the function h is drawn versus λ

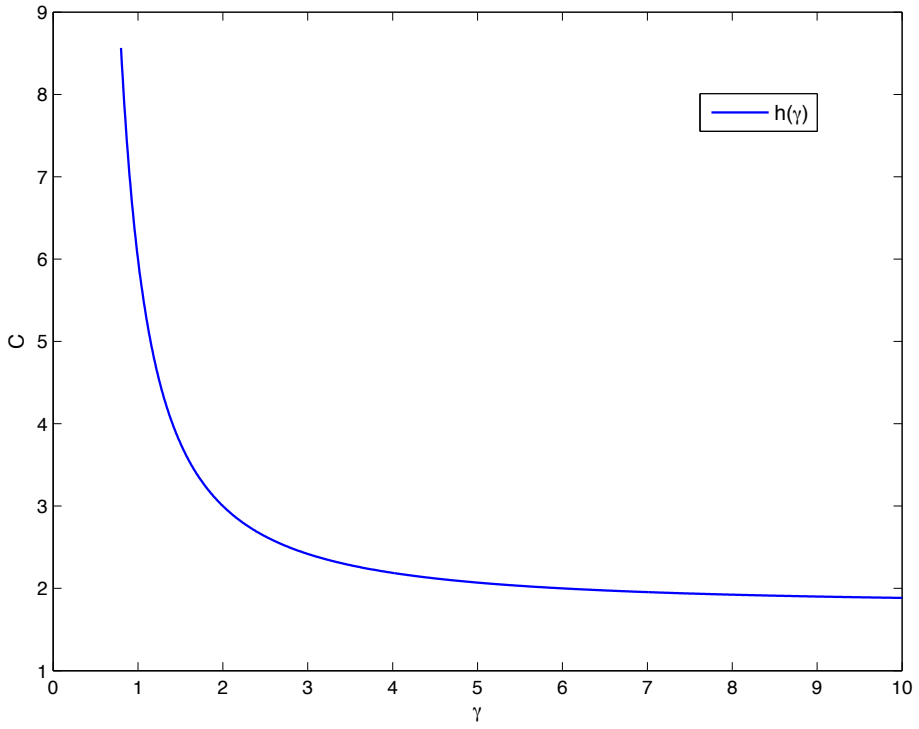

Figure B.1: Curve of $h(\lambda)$ for positive values of λ.

to analyze its behavior. Therefore, it appears that the function $h(\cdot)$ is a bijection. As such the equation $h(\lambda) = C$ has only one solution in the positive real axis. Which means that λ exists and it is unique, the value of λ is given as λ_{Kurt} in Table B.1 for some scenarios along with other values of λ obtained from other approaches that are discussed later on.

B.3.2 Best Tail Approximation

Another method to estimate λ consist of taking the best choice of λ that minimizes the square error of the tail. In other words λ is chosen so the error between the exact PDF, $f_Z(z)$, and the approximated PDF, $f_\lambda(z)$, at the tail is minimal. The

tail is defined so z is above some level $z \geq n\sigma$

$$\lambda_{Tail} = \arg\min_{\lambda>0} \int_{n\sigma}^{\infty} \left(f_\lambda(z) - f_Z(z)\right)^2 dz, \tag{B.26}$$

where n is chosen to define the desired region of the tail of the distribution. The minimization in (B.26) cannot be solved analytically by the available tools since it contains a shifted integral of a BFHF and FHF which is not known yet. An illustration of numerical values of λ_{Tail} is given in Table B.1 for some values of ω, α, and β.

B.3.3 CDF Approximation

This method is used to obtain the shape parameter that minimizes the error between the CDF of Z and the approximated CDF. Such approximation will give an asymptotic approximation of the complementary CDF (CCDF) which is needed in the computation of the probability of error. Mathematically, the shape parameter is given by

$$\lambda_{CDF} = \arg\min_{\lambda>0} \int_{0}^{\infty} \left(F_\lambda(z) - F_Z(z)\right)^2 dz. \tag{B.27}$$

In Table B.1 some numerical values of λ_{CDF} are given and a comparison between three methods of shape parameter estimation is available too.

An overview from Table B.1 shows that the optimal value of λ_{Tail} is near the value given by the kurtosis for any value of n. It is clear also that λ_{Tail} approaches closely to λ_{Kurt} specially for $n = 2$ for all values of ω. This analysis confirms the use of the kurtosis to approximate the PDF of the sum of two independent GGRV by another GGD to get a good tail approximation, this may also confirms that the kurtosis measures the heavy tail. Unlike this observation, the λ obtained by minimizing the CDF error is a little bit far from outcomes of the kurtosis method. To conclude,

Table B.1: Shape parameter for the approximated PDF using kurtosis, minimum CDF error, and minimum tail error for $\sigma_1 = 1$ and different values of $(\alpha,\ \beta,\ \omega)$

(α, β, ω)	λ_{Kurt}	λ_{CDF}	λ_{Tail}			
			$n = 0$	1	2	3
$(0.5, 0.5, 1)$	0.626	0.467	0.768	0.673	0.624	0.642
$(0.5, 0.5, 2)$	0.604	0.492	0.762	0.656	0.603	0.584
$(0.5, 0.7, 2)$	0.633	0.501	0.861	0.741	0.636	0.834
$(0.5, 1.2, 1)$	0.779	0.602	1.160	1.053	0.757	1.165
$(1.5, 1.5, 2)$	1.673	1.373	1.738	1.702	1.683	1.664
$(1.5, 2.5, 1)$	1.908	1.391	1.979	1.959	1.952	1.887
$(1.5, 2.5, 2)$	1.753	1.443	1.842	1.799	1.771	1.741
$(2.5,\ 3\ , 3)$	2.295	1.941	2.226	2.261	2.267	2.335

these three methods can be used according to the situation we are facing.

B.3.4 PDF and CDF Simulations

The illustrations in this section are made for $\beta = 1.5$, $\omega = 2$, and $\sigma_1 = 1$. In Fig. B.2, the PDF of the sum distribution is drawn for two values of α (0.5 and 2.5) and μ takes two values to split the curves of both cases. The exact and simulated PDF of Z are drawn in the same figure among with the approximated PDF. The latter is computed using the kurtosis and the optimal CDF methods. It is clear that the exact PDF matchs perfectly the simulated PDF. Far from the mean, the approximated PDF appears close to the exact PDF and both methods have a good tail approximation. For $\alpha < 2$, the kurtosis and the optimal CDF method are close to each other and match only the exact PDF at the tail with huge difference at the mean as mentioned in [39]. However, for $\alpha > 2$, the kurtosis method presents a good

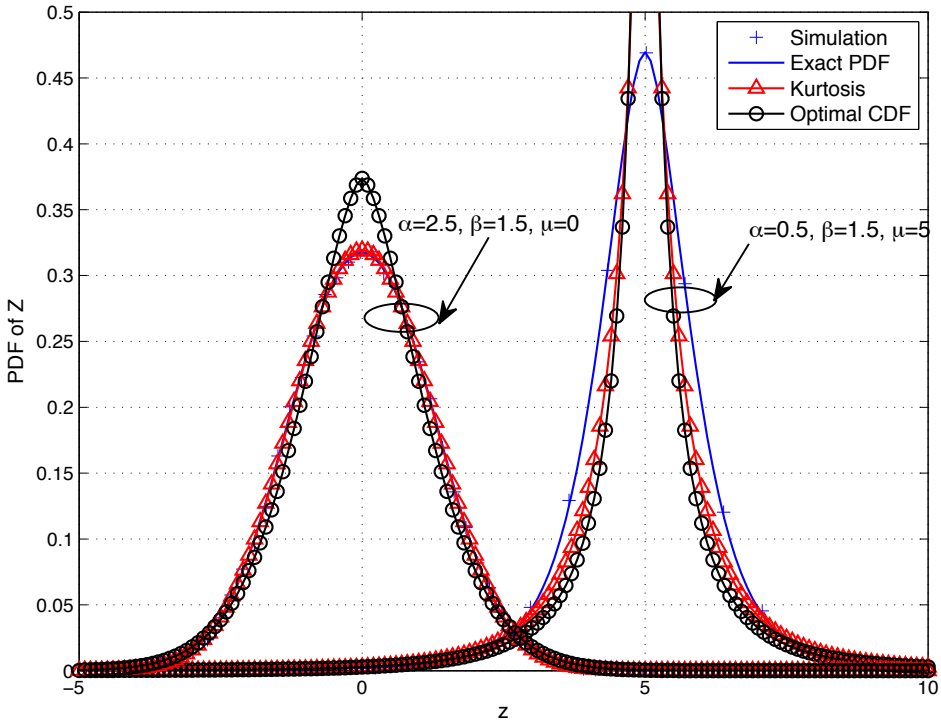

Figure B.2: Exact and approximated PDF of the sum of two GGRV, for $\beta = 1.5$, $\omega = 2$, $\sigma_1 = 1$, and two values of α.

approximation of the PDF even around the mean, while the optimal CDF method represents a good approximation of the CDF as it will be seen later. We omit the optimal tail method here because it is close to the kurtosis method as shown in Table B.1. However one can draw it easily using the values available in Table B.1. The second illustration is highlighted in Fig. B.3, and consists of drawing the CDF of the sum for $\alpha = 2.5$, $\beta = 1.5$, $\omega = 2$, and $\sigma_1 = 1$ using all three methods to approximate the CDF in linear scale. It is noticed that the results obtained from the optimal tail method (for $n = 3$) are very close to those issued from the kurtosis method. Another observation is that all the methods are close to each other and close to the exact CDF at the saturation region, i.e. $F_Z(z) \approx 1$. This result is more detailed in the next figure which shows the complementary CDF in Log scale.

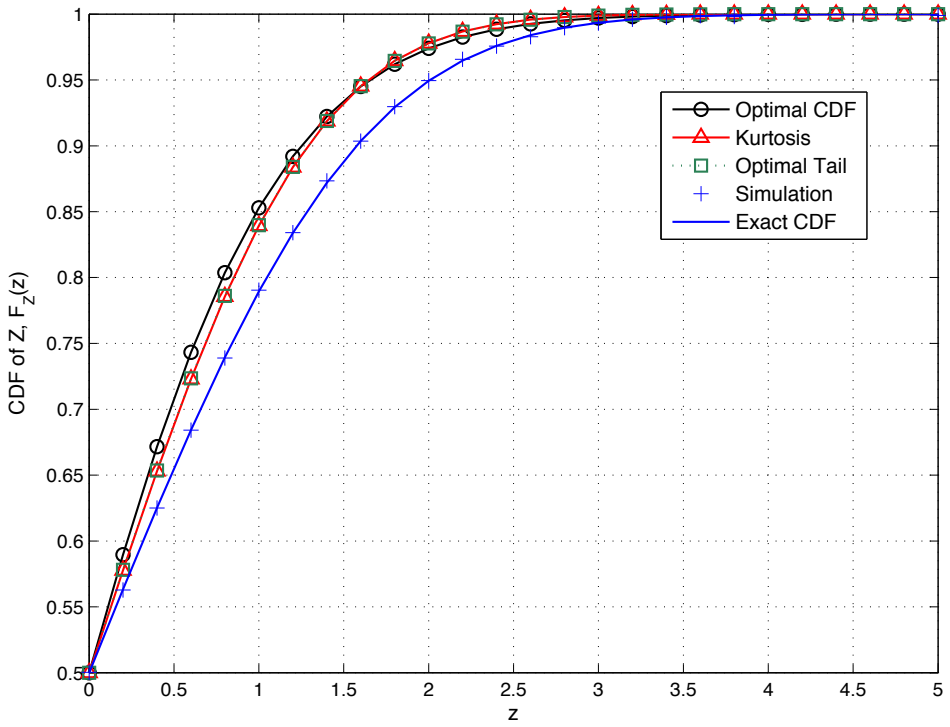

Figure B.3: CDF of the sum of two GGRV using the Kurtosis, optimal tail, and optimal CDF approximations methods, for $\alpha = 2.5$, $\beta = 1.5$, $\omega = 2$, and $\sigma_1 = 1$

In Fig. B.4, the complementary CDF of the distribution of the sum is drawn for two values of α (2.5 and 0.5). For both cases, the approximated CCDF using the optimal CDF method matches the exact CCDF. However, as seen in Fig. B.2, for $\alpha < 2$, the CCDF obtained from the kurtosis and optimal tail methods is not too close to the exact CCDF. While, for $\alpha > 1$, they are close to each other and asymptotically close to the exact CCDF.

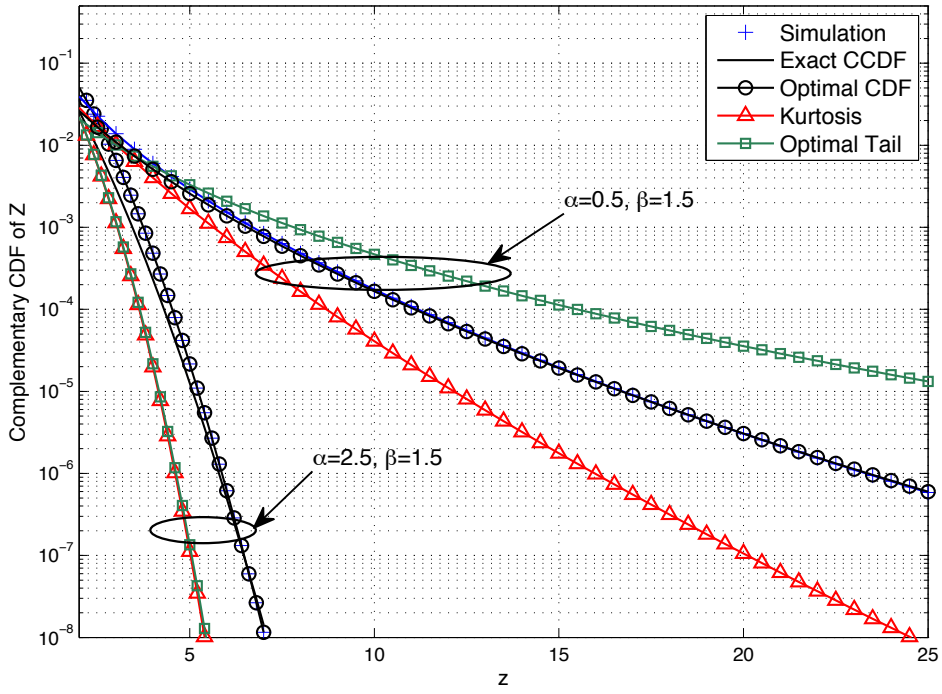

Figure B.4: Complementary CDF of the sum of two GGRV for two values of α.

Appendix C: Accepted and Submitted Publications

Accepted Publications

Journal Papers

• Emna Zedini, **Hamza Soury**, and Mohamed-Slim Alouini, "On the Performance Analysis of Dual-Hop Mixed FSO/RF Systems", *to appear in IEEE Transactions on Wireless Communications*, Feb. 2016.

• **Hamza Soury** and Mohamed-Slim Alouini, "Symbol error rate of MPSK over EGK channels perturbed by a dominant additive Laplacian noise", *IEEE Transactions on Communications*, vol. 63, no.7, pp. 2511-2523, July 2015.

• **Hamza Soury**, Faouzi Bader, Musbah Shaat, and Mohamed-Slim Alouini, "Joint sub-carrier pairing and resource allocation for cognitive networks with adaptive relaying", *EURASIP Journal on Wireless Communications and Networking*, vol. 2013, no. 1, pp. 259, November 2013.

• **Hamza SOURY**, Ferkan Yilmaz, and Mohamed-Slim Alouini, "Error rates of M-PAM and M-QAM in generalized fading and generalized Gaussian noise environments", *IEEE Communications Letters*, vol. 17, no. 10, pp. 1932-1935, Oct. 2013.

• **Hamza SOURY**, Ferkan Yilmaz, and Mohamed-Slim Alouini, "Average bit error probability of binary coherent signaling over generalized fading channels subject to additive generalized Gaussian noise", *IEEE Communications Letters*, vol. 16, no. 16, pp. 785-788, Jun. 2012.

Conference Papers

• **Hamza Soury** and Mohamed-Slim Alouini, "On the Symmetric alpha-Stable Distribution with Application to Symbol Error Rate Calculations", *Accepted in Proc. of the IEEE International Symposium on Personal, Indoor, and Mobile Radio Communications (PIMRC'2016)*, Sep. 2016.

• Emna Zedini, **Hamza SOURY**, and Mohamed-Slim Alouini, "Outage Probability of Dual-Hop FSO Fixed Gain Relay Transmission Systems", *Accepted in Proc. of the IEEE International Symposium on Personal, Indoor, and Mobile Radio Communications (PIMRC'2016)*, Sep. 2016.

• **Hamza Soury** and Mohamed-Slim Alouini, "New results on the sum of two generalized Gaussian random variables", *IEEE Global Conference on Signal and Information Processing (GlobalSIP'2015)*, Orlando, FL, USA, December 2015.

• Emna Zedini, **Hamza Soury**, and Mohamed-Slim Alouini, "On the performance of dual-hop FSO/RF systems", *in Proc. of the International Symposium on Wireless Communication Systems (ISWCS'2015)*, Brussels, Belgium, Aug. 2015, .

• **Hamza Soury**, Karim Abed-Meraim, and Mohamed-Slim Alouini, "Reduced rank adaptive filtering in impulsive noise environments", *in Proc. of the 48th Asilomar Conference on Signals, Systems and Computers (ASILOMAR'2014)*, Pacific Grove, CA, USA, Nov. 2014.

• **Hamza Soury** and Mohamed-Slim Alouini, "On the symbol error rate of M-ary MPSK over generalized fading channels with additive Laplacian noise", *in Proc. of the IEEE International Symposium on Information Theory (ISIT'2014)*, Honolulu, HI, USA, Jun. 2014.

• **Hamza SOURY**, Ferkan Yilmaz, and Mohamed-Slim Alouini, "Exact symbol error probability of square M-QAM signaling over generalized fading channels subject to additive generalized Gaussian noise", *in Proc. of the IEEE International Symposium on Information Theory (ISIT'2013)*, Istanbul, Turkey, Jul. 2013.

• **Hamza Soury**, Faouzi Bader, Musbah Shaat, and Mohamed-Slim Alouini, "Near optimal power allocation algorithm for OFDM-based cognitive using adaptive relaying strategy", *on Proc. of the 7th International ICST Conference on Cognitive Radio Oriented Wireless Networks and Communications (CROWNCOM'2012)*, Stockholm, Sweden, June 2012.

Submitted Publications

Journal Papers

• **Hamza SOURY** and Mohamed-Slim Alouini, "On the Performance of Communication Systems Perturbed by Symmetric alpha-Stable Noise", *In preparation*, July 2016.

• **Hamza SOURY**, Hesham ElSawy, and Mohamed-Slim Alouini, "Error Rates and Throughput of Half-duplex Users in Full-duplex Cellular Networks", *Submitted to IEEE Transactions on Wireless Communications*, May 2016.

• Emna Zedini, **Hamza SOURY**, and Mohamed-Slim Alouini, "Dual-Hop FSO Transmission Systems over Gamma-Gamma Turbulence with Pointing Errors", *Submitted to IEEE Transactions on Wireless Communications*, Apr. 2016.

Conference Papers

• **Hamza SOURY**, Hesham ElSawy, and Mohamed-Slim Alouini, "Error Rates and Throughput in Full-duplex Cellular Networks with Laplacian Intra-Cell Interference", *Submitted to the IEEE Global Telecommunication Conference (GlobeCom'2016)*, Dec. 2016.